A Mass Transfer Model for Structured Packing

by

David Mukuma Kawesha

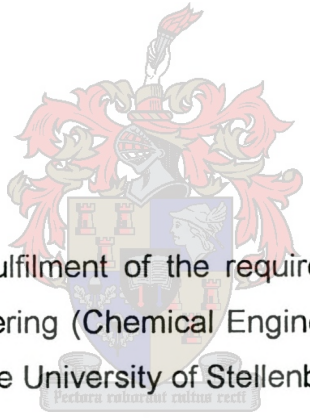

Thesis submitted in partial fulfilment of the requirements for the degree of Master of Science in Engineering (Chemical Engineering) in the Department of Chemical Engineering at the University of Stellenbosch.

Supervisor: Prof. Izak Nieuwoudt

Stellenbosch

December 2002

DECLARATION

I, the undersigned, hereby declare that the work contained in this thesis is my own original work and that I have not previously in its entirety or in part submitted it at any university for a degree.

David Mukuma Kawesha 20 May 2002

ABSTRACT

The distillation process is the most widely used separating process in the chemical process industry. The optimal design of the distillation units can lead to reduced capital costs and improved energy utilisation. This is particularly the case for structured packed distillation column where design methods tend to over-predict the column efficiency. This work seeks to contribute to the development of a reliable mass transfer model for structured packing.

A gas phase mass transfer correlation was developed based on the evaporation of pure components into an air stream. The mass transfer rates were measured in a short triangular wetted wall channel with a corrugated surface wall. The influence that the geometric configuration as well as surface structure has on the mass transfer rates was investigated. The channel geometry and surface wall structure resembled that of the structured packing (Flexipac 350Y). The influence of the channel geometry on the gas mass transfer rates was not significant except at low flow conditions. The liquid phase resistance was investigated for binary mixtures in the triangular wetted wall channel. It was found that the overall mass transfer rate decreased with increasing composition of the volatile component. The enhancement of the gas phase mass transfer rate masked the presence of the liquid resistance.

The gas phase mass transfer correlations were used in the mass transfer model to predict the separation efficiency of a structured packed distillation column. The structured packing used to validate the mass transfer model was high-capacity Flexipac 350Y and normal Flexipac 350Y. The binary distillation experiments were done at total reflux conditions for the pressure range 0.33-1atm. The accuracy of the separation efficiencies of the mass transfer model improved with increasing pressure for both materials. The mass transfer model was able to predict the variation of separation efficiencies with column loadings.

OPSOMMING

Distillasie is die skeidingsmetode wat die meeste in die chemiese industrie gebruik word. Die optimale ontwerp van distillasie eenhede kan lei tot verlagings in kapitaalkostes en 'n verbeterde gebruik van energie. Dit is veral waar in die geval van kolomme met gestruktureerde pakking waar huidige ontwerpsmetodes, die kolomeffektiwiteit nie akkuraat beskryf nie. Hierdie studie het ten doel om 'n bydrae te lewer tot die ontwikkeling van 'n betroubare massa-oordragsmodel vir gestruktureerde pakking.

'n Gasfase massa-oordragskorrelasie is ontwikkel gebaseer op metings van die verdampingstempo van suiwer komponente in 'n lugstroom. Die massa-oordragstempos is gemeet in 'n kort driehoekige benatte wand kanaal waarin die wand 'n bepaalde oppervlakprofiel het. Die invloed van beide die kanaalgeometrie en die oppervlakprofiel is ondersoek. Die geometrie en oppervlakprofiel is soorgelyk aan die van Flexipac 350Y gestruktureerde pakking. Die invloed van die kanaalgeometrie op die gasfase massa-oordragstempos is slegs beduidend by lae vloeitempos. Die vloeistoffase weerstand vir binêre mengsels is ondersoek in die driehoekige kanaal. Dit is gevind dat die algehele massa-oordragstempo verlaag met 'n verhoging in die konsentrasie van die vlugtige komponent. Die verhoging in die gasfase massa-oordragstempo verberg die invloed van die vloeistoffase weerstand.

Die gasfase massa-oordragskorrelasies is in 'n massa-oordragsmodel gebruik om die skeidingseffektiwiteit van gestruktureerde pakking in 'n kolom te voorspel. Metings op hoë-kapasiteit Flexipac 350Y en normale Flexipac 350Y is gebruik om die modelvoorspellings te evalueer. Die binêre distillasies is by totale terugvloei gedoen in die drukbereik 0.33 – 1.0 atm. Daar is gevind dat die model meer akkuraat is by hoër drukke. Die massa-oordragsmodel is in staat om die variasie in skeidingseffektiwiteit met veranderende kolomlading te voorspel.

ACKNOWLEDGEMENTS

I would like to express my sincere thanks to each and every individual who assisted me throughout the project.

Profound thanks goes out to my supervisor, Prof. Izak Nieuwoudt for his guidance and encouragement throughout the project.

A special thanks to Mr Andre Erasmus and Dr. Christo Crause for the invaluable assistance rendered throughout the project.

Last but not least I would like to thank the University of Stellenbosch for the financial support and Koch for providing the structured packing used in this project.

TABLE OF CONTENTS

LIST OF FIGURES

LIST OF TABLES

CHAPTER 1. Introduction

1.1 Distillation in Chemical Engineering

The chemical process industries are driven by the requirement of purer products combined with improved efficiency for processing equipment. Distillation is amongst the core processes in achieving the former, through the separation of liquid mixtures. Of all the separating processes employed in industry, distillation is by far the most widely used, {Bennett, 2000; Humphrey, 1995}, primarily because pure products can be obtained by direct separation without further separation. To illustrate its applicability, in the USA alone about 90-95% of all the separating columns in the chemical industries are distillation based {Humphrey, 1995}. Mass separating agents drive all separating processes, i.e. solvent in solvent extraction, membrane material in membrane separation processes and in the case of distillation, heat. Consequently from its extensive use in industry, distillation accounts for a significant portion of capital and operating costs. A study carried out on the chemical industries in the UK, revealed that distillation accounted for about 13% of total energy usage, whilst for certain sectors such as organic chemicals it accounted for up to 23% of total consumption {Grant, 1988}. It is therefore incumbent upon design engineers that efforts are made to reduce the use of energy in view of the economics and conservation. Through improved correlations for design parameters energy saving of up to 20% on capital expenditure is achievable {Porter, 1995}.

1.2 Distillation – Brief Description

Distillation separates liquid mixtures by the difference in composition between a liquid phase and the vapour formed from it due to the difference in boiling points of the components in the mixture. Three steps are involved in instituting the distillation separation principle:

- creation of a two-phase system,
- mass transfer between the phases,
- separation of the phases.

Distillation analysis can be broken down into areas that are paramount in the design namely: vapour-liquid equilibrium, stage calculations, separating devices, mass transfer (efficiency) and control. More often than not counter-current flow is applied to maximise the driving force for mass transfer. In a traditional fractionating column for binary mixtures, vapour rising through the column becomes richer in the more volatile component, whilst liquid flowing down enriched with the less volatile component. The separating devices i.e. column internals, play a significant role in promoting intimate contact between the phases and thus facilitating mass transfer. Mass transfer zones in plate columns are created by the hold-up of liquid on the plates due to the weir and downcomer, whilst rising vapour allowed to come into contact with this liquid through the nature of the openings i.e. valve or bubble caps. In the case of packed columns the packing material provides the area available for contact between the phases. Furthermore in the promotion of improved mass transfer the column internals should avail as large a transfer area as possible, as well as offering minimal flow resistance.

Not so long ago the predominately encountered column internals were sieve trays and bubble caps, but recently random and structured packings have found uses in distillation where they offer advantages over traditionally used caps or sieve trays.

1.3 Distillation and Structured Packing

A marked increase has been noted in the application of structured packing in the past two decades. Amongst the principle reasons behind this has been the advantages that structured packing offers in low pressure distillation, where it has marked capacity and efficiency advantages over either trays or random packing. Furthermore the scale-up problem for packed columns was solved in the early eighties {Porter, 2001}. Structured packing are replacing either trays or random packing in conditions of vacuum to atmospheric distillation where revamping of columns required. Laso et al. {1995} estimated that 25% of all refineries vacuum towers worldwide are fitted with structured packing. This is further enhanced by the fact that for vacuum distillation the column size is largely determined by the pressure drop per theoretical stage {Strigle, 1994}. In the separation of thermally sensitive mixtures, vacuum conditions usually have to be employed to avoid decomposition of the components. The smaller liquid hold-up and lower pressure drop per theoretical stage that structured packing offers at these conditions, makes it the desirable column internal to use.

Typically most widely encountered kinds of structured packing are made from sheet metal, though other materials employed as well e.g. plastic for corrosive systems. It has generally been agreed that structured packing under-perform when being employed in high-pressure distillation. It is speculated that vapour backmixing which stems from initial liquid maldistribution is excessive in high-pressure distillation columns with structured packing, therefore accounting for the decline in performance, {Nooijen et al., 1997}. Some investigators {Bravo, 1997} do indicate that structured packing can be applied at these conditions to certain systems, but these should be employed when all essential factors have been accounted for.

Below are some of the advantages and disadvantages of structured packing.

Advantages:

High vapour capacity at low liquid flow parameters.

High volumetric efficiency at low pressures.

Low entrainment.

Very low pressure drop.

Good performance in foaming system.

For small diameter columns (< 0.7m), packings are usually cheaper than plates.

Disadvantages:

Low vapour capacity at high liquid flow parameters.

Low efficiency at high pressures.

Low resistance to corrosion.

Sensitive to fouling.

High volumetric cost.

1.4 Mass transfer correlations and structured packing

More often than not the performance data of structured packing is presented in terms of HETP (height equivalent to a theoretical plate). Seader and Henley, {1998} are of the opinion that though the HETP concept may lack a sound theoretical basis, its use with equilibrium stage calculations has made it a convenient way of expressing efficiency data of packed columns. It is essential that current laboratory and pilot plant based models replicate industrial scale conditions thus countering scale up errors. The bulk of the models for evaluating performance of structured packing are empirically based, {Billet and Schultes, 1993; Rocha et al., 1993; Olujic et al., 1999}. These have proved to be extremely useful, though an alternative approach has been postulated by Shetty and Cerro {1997}, which estimates design parameters from the flow patterns and velocity parameters.

The favoured models in estimating the HETP are based on the two-film theory primarily because of its simplicity and separation of resistances. The resistances to mass transfer in either phase can be calculated from various correlations. In distillation applications the liquid-side resistance is at times assumed to be negligible {Spiegel et al., 1987} or estimated from Higbie's penetration theory {Billet and Schultes, 1993; Rocha et al., 1996; Shetty and Cerro, 1997; Olujic et al., 1999}. Though some empirical correlations have been obtained for liquid-side resistance, these have been developed from absorption experiments, which do not represent the distillation process in its entirety.

Since the pioneering work by Gilliland and Sherwood {1934} in correlating gas-side mass transfer, use of wetted wall columns to correlate this resistance has proved to be more than adequate. Based on this principle and to improve the correlation in applicability to structured packing certain changes were inevitable, shortening of the column {Crause, 1998} to account for entrance and end effects as would be experienced in a structured packed column. To further improve on this, Erasmus {1999} investigated the influence of the surface profile in corrugated sheet metal packing. This involved lining the short wetted wall column with a corrugated surface, thus replicating the flow structure as well as short contact times encountered in structured packing.

1.5 Aims of Study

Since distillation is the predominant separating process the chemical industries' quest to improve energy utilisation, reduce capital costs and boost-operating flexibility has put focus on the optimal design of distillation columns {Bennett, 2000}. Therefore, in order to improve on current designs a sound understanding of the fundamentals is of vital importance, which should curb over-compensation in designs. This work seeks to improve the design of structured packed columns through modelling of mass transfer mechanism using a short triangular wetted wall channel. It is a continuation of the work incepted by Crause {1998} and improved on by Erasmus {1999}. The mass

transfer process is modelled on the basis of fluid physical properties and flow parameters.

In more specific terms the main objectives of this work are:

- Extension of the database for the correlation of gas-side mass transfer resistance using a short triangular wetted wall channel.
- Investigating the geometric configuration effect of structured packing on the gas-side mass transfer resistance.
- To measure the liquid-side mass transfer resistance and to establish to what extent the geometric profile will affect this resistance.
- Development of a model to predict the performance of structured packed columns in conventional distillation applications.

CHAPTER 2. Mass Transfer in the Gas phase

2.1 Introduction

The two-film theory as postulated by Whitman {Coulson and Richardson, 1997} enables addition of resistances in series, consequently facilitating the separation of resistances of the different phases. Therefore, in order to determine single-phase coefficients for the liquid or gas phase, the experimental system has to be arranged such that one of the resistances is either negligible or can be calculated. Evaporation of pure liquids into an insoluble gas is used as the investigating method for evaluating gas side mass transfer resistance. In this case liquid phase resistance can be considered to be negligible. The geometric profile of structured packing defines a triangular flow channel for fluid flow and thus mass transfer. Therefore, based on this, this chapter seeks to establish to what extent the triangular flow channel as well as the corrugated surface effects the gas side mass transfer resistance.

2.2 Literature Review

Up to now, no specific studies investigating mass transfer from a falling liquid film flowing over corrugated surface in a triangular flow channel could be found in literature. Compared to mass transfer in smooth circular geometry, which has been extensively studied, little is known about the effect of corrugated surface in non-circular geometry on mass transfer. Granted that some models do account for geometrical and surface changes through certain parameters, these have not been developed fundamentally or verified experimentally. Consequently the following literature review will be split into three parts, firstly will be a review of wetted wall column work, then secondly liquid film flow over complex surface and finally liquid film flow in non-circular channels. The last two parts of the literature review do not involve mass transfer investigations but rather liquid flow hydrodynamics. These are

included because they will lead to a better understanding of how the factors i.e. geometrical configuration and complex surface, affect the mass transfer process.

2.2.1 Mass transfer in wetted wall columns

Numerous studies have been carried out for determining gas-side resistance. Amongst the first well-documented studies is that of Gilliland and Sherwood {1934}. They used a vertical pipe, 2.67cm inside diameter and 117cm long, to investigate evaporation of pure liquids into cocurrent and countercurrent air streams. The ranges of some of the dimensionless groups were; $2000 < Re_g < 20000$, constant Re_l and $0.6 < Sc_g < 2.17$. Nearly 400 tests were used to correlate their data using the following equation:

$$Sh_g\,(P_{BM}/P) = 0.023\,\mathrm{Re}_g^{\,0.83}\,Sc_g^{\,0.44} \qquad (2.1)$$

Chilton and Colburn {1934}, used the empirical j-factor developed from the Reynolds analogy for heat transfer and said that if two processes i.e. mass and heat transfer are analogous, then the j-factor for mass transfer should equal that of heat transfer. Taking data from various authors including that of Gilliland and Sherwood they correlated this data in the following way {Crause, 1998}:

$$Sh_g = 0.0296\,Re_g^{\,0.8}\,Sc_g^{\,0.33} \qquad (2.2)$$

Barnet and Kobe {1941} used similar wetted wall column to that of Gilliland et al. {1934} and measured evaporation rates of water into an air stream. The only difference between their set up and that of Gilliland et al. {1934} was the length of the column; the latter's being slightly shorter. The data was correlated by:

$$Sh_g = 0.02\,Re_g^{\,0.83}\,Sc_g^{\,0.44} \qquad (2.3)$$

Jackson and Ceaglske {1950} carried out both vaporisation and rectification experiments in a wetted wall column. They evaporated three liquids including water into an air stream and found that upon plotting the results their data generally fell below that of Gilliland et al. {1934}, though it did concur with that of Barnet and Kobe {1941}. It should be noted that they only presented their data in the form of logarithmic plots of the j-factor for mass transfer against the gas Reynolds number. They used the relative velocity in evaluating the Reynolds number.

Cairns and Roper {1954} measured evaporation rates of water in an air stream at different humidities, in an adiabatic wetted wall column with a length of 0.95m and 22.86mm internal diameter. They found an appreciable influence of liquid rate on mass transfer as well as slight pressure dependency and their results were correlated as follows:

$$Sh_g\,(P_{BM}/P)^{0.83} = 0.021\,Re_g^{\,0.83}\,Sc_g^{\,0.44} \qquad (2.4)$$

McCarter and Stutzman {1959} investigated the evaporation of a number of organic liquids. They found no appreciable difference in the correlation, when wetted wall height was varied (35-100cm). In calculating the Reynolds number they used the velocity relative to the liquid surface. They represented the data with the following correlation:

$$Sh_g = 0.024\,Re_{g,r}^{\,0.8}\,Sc_g^{\,0.4} \qquad (2.5)$$

Kafesjian et al. {1961} conducted wetted wall experiments on water evaporating into a counter flow air stream, in order to establish the effect of rippling and liquid rate on mass transfer rate. The use of the liquid Reynolds number in the correlation accounted for the rippling effect. In the non-rippling case use of the velocity relative to the liquid surface was sufficient in correlating the data. The results were presented separately for the rippling and non-rippling cases, and correlated as follows:

Non-rippling water films: $Sh_g\,(P_{BM}/P) = 0.013\,Re_{g,r}^{\,0.83}$ (2.6)

Rippling water films: $Sh_g\,(P_{BM}/P) = 0.0065\,Re_g^{\,0.83}\,Re_l^{\,0.15}$ (2.7)

Strumillo and Porter {1965} evaporated carbon tetrachloride into an air stream, in a temperature range of 16-35°C, in a wetted wall column of length 0.61m and 25.4mm internal diameter. Their results showed a marked influence of liquid rate on mass transfer. The liquid rate effect was attributed to the relative velocity effect and rippling. They correlated their data with:

$$Sh_g\,(P_{BM}/P) = 0.0093\,Re_g^{\,0.68}\,Re_l^{\,0.34} \qquad (2.8)$$

Reker et al. {1966} found that the most significant effect of surface rippling would be increased surface area. They derived an equation theoretically relating fractional area increase to flow conditions and physical properties. The relationship for the percentage increase in area was given as:

$$\Delta S = 0.721\,Re_l^{\,5/3}\,(g\,\nu_l)^{1/3}\,\mu_l/\sigma \qquad (2.9)$$

Their mass transfer experiments were conducted with methanol and carbon tetrachloride and the data correlated as follows:

$$Sh_g\,(P_{BM}/P) = 0.163 Re_{g,r}^{\,0.83}\,Sc_g^{\,0.5} S^{\varepsilon} \qquad (2.10)$$

where ε is a function of the system

Spedding and Jones {1988} conducted humidification experiments of air in wetted wall columns where the height was varied from 0.72-3.54m. It was found that rippling occurred on the liquid film, but this did not affect the mass transfer rates. The liquid rate was found to have a definite influence on the mass transfer rate. They also incorporated end effects in their data by catering for the height due to the end effect in the effective column height. The height due to the end effect was determined graphically. Their results were correlated as follows:

$$Sh_g = 0.02\ Re_{g,r}^{\ 0.83}\ Sc_g^{\ 0.44} \qquad (2.11)$$

Dudukovic {1996} obtained the data from Gilliland et al. {1934} and Barnet, et al. {1941} and correlated it in the following manner:

$$Sh_g = 0.031\ Re_g^{\ 0.79}\ Sc_g^{\ 0.5} \qquad (2.12)$$

Nielsen et al. {1998} used gas absorption experiments to measure gas-side and liquid-side mass transfer rates at high Reynolds values. The experimental work was conducted in a long wetted-wall column with cocurrent flow. The transfer rates were measured for systems where one of the transfer resistances could be considered to be negligible. A highly soluble system, SO_2 in H_2O, was used to measure the gas-side mass transfer rates. For liquid-side resistance measurements they used a sparingly soluble system i.e. O_2 in H_2O. The data was represented with the following correlations:

$$Sh_g = 0.00031\ Re_g^{\ 1.05}\ Re_l^{\ 0.207}\ Sc_g^{\ 0.5} \qquad (2.13)$$

$$Sh_l = 0.01613\ Re_g^{\ 0.664}\ Re_l^{\ 0.426}\ Sc_l^{\ 0.5} \qquad (2.14)$$

Ranges: $4000 < Re_l < 12000$ and $7500 < Re_g < 18300$

Crause {1998} investigated gas-side mass transfer rates of a variety of organic liquids as well as water in a short wetted wall column. A similar set-up is used in the current study with variations in the geometry and column wall surface. The data was correlated as follows:

$$Sh_g = 0.00283\ Re_g\ Re_l^{\ 0.08}\ Sc_g^{\ 0.5} \qquad (2.15)$$

Ranges: $2000 < Re_g < 8000$ and $50 < Re_l < 480$

Erasmus {1999} used the same wetted wall column as Crause, {1998} to determine the gas-side mass transfer rate. The wetted wall column height was 0.1m. His investigations also included measuring the transfer rate with the liquid film flowing down a complex surface. This aspect will also be

investigated in the current study. He correlated the data as follows for columns with and without a complex surface structure:

Smooth surface: $Sh_g = 0.0044\, Re_g\, We_l^{0.111}\, Sc_g^{0.5}$ (2.16)

Complex surface: $Sh_g = 0.0036\, Re_g^{0.76}\, Re_l^{0.41}\, Bo_l^{-0.13}\, Sc_g^{0.5}$ (2.17)

For smooth surface, $1800 < Re_g < 7000$ and $6 < Re_l < 330$

For complex surface, $1650 < Re_g < 6050$ and $50 < Re_l < 200$

Almost all but the last two experimental studies used wetted wall columns of the range 0.5 - 5m in length, with mostly the water-air system. These as illustrated by Crause {1998}, are not indicative of the flow path lengths encountered in structured packed columns, which are significantly shorter. The influence of certain variables is not well understood, such as liquid rate, which in some cases was not varied at all and in others found to affect the transport process but not included in the correlation. Furthermore only Erasmus {1999} found a surface tension effect, (i.e. Weber number) on the mass transfer rate. Other variations included Schmidt number exponent 0.33-0.5, and gas Reynolds number exponent 0.68-1.05. It has been found that an exponent of 0.5 for the Sc_g number describes gas-liquid mass transfer more accurately than an exponent of 0.33, {Dudukovic, 1996}. The exponent of 0.33 for the Sc_g number applies to gas-solid mass transfer {Dudukovic, 1996}. In the wetted wall columns mass transfer occurs between the gas and liquid phase. Therefore, gas-liquid mass transfer could be described more accurately with an exponent of 0.5 for the Sc_g number.

2.2.2 Complex surface

As stated by Erasmus {1999} available literature has not dealt with mass transfer from a liquid flowing over a complex surface, but rather on the evaluation of the velocity and surface profiles. There is a recent numerical model by Negny et al. {2001}, which incorporates the flow pattern for a wavy

column into heat and mass transport rates. They theoretically investigated the transport rates for film flow over a complex surface into a stagnant gas phase. In the wetted wall experiments the gas phase is not stagnant, therefore it is doubtful that the model would be expected to predict the transport rates accurately. It is important that more studies are done to improve the understanding of the characteristics of the velocity and free surface profiles. This would then enable investigators predict more accurately the transfer rates for liquid film flow over complex surfaces. Following is a survey of literature for liquid flow over complex surfaces.

Wang {1981} developed a theoretical three-dimensional model of liquid film flow along a wavy incline at low Reynolds numbers. It was found that at these liquid rates the corrugation amplitude is small in comparison to the film thickness. On the assumption of small disturbances due to the wavy surface, the results indicated that amplitude and phase shift of the free surface are a function of surface tension, wavelength and orientation of wavy undulations.

Dassori et al. {1982} analysed two-phase flow in a sinusoidal channel at low Reynolds numbers. Regular perturbation analysis was used to evaluate the velocity field of the stratified two-phase flow and its interfacial shape. The investigations focused on the effect of the non-wetting phase on the shape of the fluid–fluid interface. They discovered that there was a phase shift between the wavy shaped fluid-fluid interface and the sinusoidal solid-fluid interface.

Pozrikidis {1988} theoretically investigated liquid film flow along an inclined periodic wall at low flow rates. In application of the method, results showed that for a sinusoidal wall at low flow rates, the liquid surface profile mirrored closely that of the wall. It was found that the free surface profile is a function of flow rate, inclination angle, wave amplitude and surface tension. It was indicated that the onset of re-circulating fluid regions could have inhibiting effects on the transfer rates from the liquid film. The results also showed that the surface tension had a significant influence on the surface profile of the liquid interface.

Zhao and Cerro {1992} experimentally characterised viscous film flow over a variety of complex surfaces. For the various surfaces they measured the film thickness profiles, free-surface velocities as well as streamline patterns. The liquid film thickness was measured with a precision translator whilst the free surface velocities were measured with a particle image velocimeter. The streamline patterns were generated visually using the streak image of particles in the liquid films. The experimental data was correlated with the Nusselt film thickness for a flat surface, the Reynolds number and the capillary number. They found that where the Nusselt film thickness was comparable to the surface amplitude the free-surface profile was almost flat. They also discovered that due to larger film thicknesses over complex surfaces, films were less likely to break up than those over flat vertical surfaces. They concluded that on average the film thicknesses for complex surfaces were larger, whilst the free surface velocities were smaller than those of a smooth surface. Therefore for complex surfaces larger liquid hold-up and longer residence times are expected.

Shetty and Cerro {1993} theoretically developed a perturbation solution for small film thickness profiles. They used a two-dimensional streamline function to evaluate the velocity field and reduce the equation of motion to a single non-linear ordinary differential equation. The results showed good agreement between the experimental and theoretical film thickness when the ratio of Nusselt film thickness to solid surface amplitude was small. At larger values of this particular ratio their theoretical approach was inaccurate, this being attributed to inertial and capillary effects.

Kang and Chen {1995} did a theoretical study of gravity driven two-layer steady flow down a periodic incline. They were also of the opinion, as was Pozrikidis {1988}, that characterisation of wall shear stress distribution, could be important to the mass transfer process. The results showed that the interfacial and surface tensions reduced the amplitudes of the interfacial and free surfaces as well as increasing the perturbation wall shear stress.

Bontozoglou and Papaolymerou {1997} theoretically studied laminar liquid flow down an inclined wall with sinusoidal corrugations. They used linear analysis to characterise the liquid film flow. This analysis, which was valid for small amplitude perturbations, led to a differential equation with non-homogenous boundary conditions. For certain conditions results indicated an amplification of the wall corrugation at the free surface. The variation of the amplification ratio with the liquid rate suggested the existence of a resonance phenomenon.

Trifonov {1998} carried out a theoretical analysis of viscous liquid film flow down a vertical one-dimensional periodic surface, based on both Navier-Stokes and integral equations. The theoretical results were compared with the experimental work of Zhao and Cerro {1992}. The results showed as with the latter, that the average film thickness was greater than the Nusselt film thickness. It was concluded that at moderate Reynolds numbers, surface tension forces control the flow, whilst inertial forces dominated the flow at higher Reynolds numbers. For low viscosity liquids it was found that stagnation zones formed at certain Reynolds numbers.

Erasmus {1999} experimentally investigated mass transfer rates from a complex surface, by evaporating organic liquids into a counter flow air stream. He used smooth surface hydrodynamics to characterise the flow. The results showed that the measured mass transfer rates were higher for a complex surface column as compared to a smooth surface column. It was also found that the transfer rates were more dependent on the liquid rate for the complex surface. The complex surface data was correlated by equation 2.17. A similar surface structure is employed in the present study.

Negny et al. {2001} theoretically investigated the flow pattern and heat and mass transfer characteristics for an isothermal liquid film over a sinusoidal wall column. They separated the analysis of the flow pattern and transfer rates, with the velocity field developed from the former, being the linked parameter. The hydrodynamic model showed that with the onset of the recirculation zones, a corresponding increase in the liquid film thickness is

observed. For the case of mass transfer they used absorption of CO_2 into water as a test case. The results showed only a slight enhancement of mass transfer over a wavy wall in comparison to that over a smooth surface. They concluded that for the range of Reynolds numbers investigated the recirculation zones did not interfere with the gas-liquid interface. Therefore, the enhancement was primarily from the increased transfer area.

Further in a subsequent paper the above authors {Negny et al., 2001} experimentally characterise the liquid film flow over a sinusoidal wall column at liquid Reynolds numbers less than 300. It was found that above $Re_l > 150$, the formation of waves was observed on the gas-liquid interface, which increased in amplitude and decreased in velocity with increasing Reynolds number. It was found that viscosity had an effect on the observed wave formation, with waves appearing at higher flow rates for increasing viscosity. They concluded that the mass transfer enhancement in their first paper was underestimated because of:

- the theoretical model not accounting for wave formation at the gas-liquid interface,
- the assumption of a stagnant gas phase, therefore no shear stress at the interface.

From the above review most of the complex surface work has been theoretical with few experimental studies. As illustrated by Negny et al. {2001} the theoretical model developed can grossly underestimate the transfer process. This can therefore, lead to significant under-prediction of the efficiencies in mass transfer equipment.

2.2.3 Non-circular channels

As with measurements of mass transfer rates from complex surfaces, there is no literature available at present looking at determining mass transfer rates from liquid film flow in non-circular channels. From the current literature it can

be gathered that research is focused on understanding two-phase flow patterns in non-circular channels, {Sadatomi et al., 1982; Wolk et al., 2000}. Furthermore even less literature is available specifically studying two-phase flow patterns for triangular flow channels, {Zhao and Bi, 2001}. Therefore, improved understanding of flow patterns in two-phase flow would enable investigators to predict the possible geometrical effect on the mass transfer rate. This can then be adapted to certain structured packing, which define triangular flow channels for gas-liquid flow. Below is a short literature summary of vertical two-phase flow in triangular flow channels.

Sadatomi et al. {1982} experimentally studied vertical two-phase flow in several non-circular channels, including a triangular channel with a hydraulic diameter of 16.3mm. They determined flow pattern transitions for various flow regimes including bubble to slug flow and slug to annular flow. It was found that channel geometry had no remarkable influence on flow pattern transition in non-circular channels, where hydraulic diameter is greater than 10mm.

Triplett et al. {1999} experimentally investigated gas-liquid two-phase flow patterns for an air-water system in circular and semi-triangular (triangular with one corner smoothened) channels with small hydraulic diameters. The flow patterns were mapped using gas and liquid superficial velocities as the coordinates for the graphical plots. They found that the results for the flow patterns were similar to that of existing data. The difference in their results and that of the existing models was attributed to the confusion of identifying the flow patterns.

Wolk et al. {2000} experimentally studied cocurrent two-phase flow in circular and non-circular geometry's each with approximately 6mm hydraulic diameter. This work is primarily a comparison between the two-phase flow patterns in circular and non-circular channels. Their results indicated that cross–sectional geometry did affect flow pattern transition. The superficial gas and liquid velocities also had an influence on the transition between flow patterns. The transition between the flow patterns occurred at different velocities in non-circular channels as compared to that of circular channels. The reason for the

shift in the transition regions was due to turbulent secondary flow that occurs in non-circular channels and the steeper radial distribution of the phases and velocities.

Zhao and Bi {2001} experimentally characterised gas-liquid two-phase flow patterns for an air-water system in vertical equilateral triangular channels with small hydraulic diameters. In comparison to previously developed models for circular geometry certain discrepancies occurred in the mapping of the flow patterns. They put this down to geometrical differences, surface tension forces and meniscus effects induced by the sharp corners. In conclusion they were of the opinion that previous theories cannot be extended to predict flow patterns in the non-circular channels studied.

It is important to note that all the above researchers used air-water systems to model the two-phase flow patterns. This is obviously done from the aspect of familiarity of the system and the ease of prediction of the physical properties. It is possible that the wetting of metal with water may have caused experimental problems.

2.3 Theory

Stemming from the complexity of describing flow over a corrugated surface, smooth surface hydrodynamics will be used in describing the liquid film flow.

The vaporisation of liquid film into a gaseous stream can be described through the use of the two-resistance theorem as postulated by Whitman {Coulson and Richardson, 1997}. Assuming no mass transfer driving force in the liquid, this can be considered as a case of unimolecular diffusion where mass transfer of component A occurs through stagnant component B. The equation relating molar flux per unit area and the binary diffusion coefficient can be written as follows Treybal, {1980}:

$$N_A = \frac{D_{AB}}{\delta} \frac{P_t}{P_{BM} RT} (P_{Ai} - P_{Ab}) \tag{2.18}$$

where δ is the thickness of the diffusional sublayer, which is difficult to measure or correlate, therefore introduction of the mass transfer coefficient,

$$N_A = k_g \frac{P_t}{P_{BM} RT} (P_{Ai} - P_{Ab}) \tag{2.19}$$

P_{BM} is the log mean pressure difference of the non-diffusing gas B, and is given by:

$$P_{BM} = \frac{P_{Bi} - P_{Bb}}{\ln\left(\frac{P_{Bi}}{P_{Bb}}\right)} \tag{2.20}$$

In order to evaluate the mass transfer rate, one has to integrate over the surface of the channel, see figure 2.3.1.

$$n = N_A A = \int_0^l \int_0^w \left[k_g \frac{P_t}{P_{BM} RT} (P_{Ai} - P_{Ab}) \right] dz dy \tag{2.21}$$

Assuming that,

- The variables are independent of z-direction,
- The pressure drop is negligible in comparison to the system pressure, i.e. constant P_t, and
- The gas and liquid flow profiles are fully developed, i.e. k_g is independent of y.

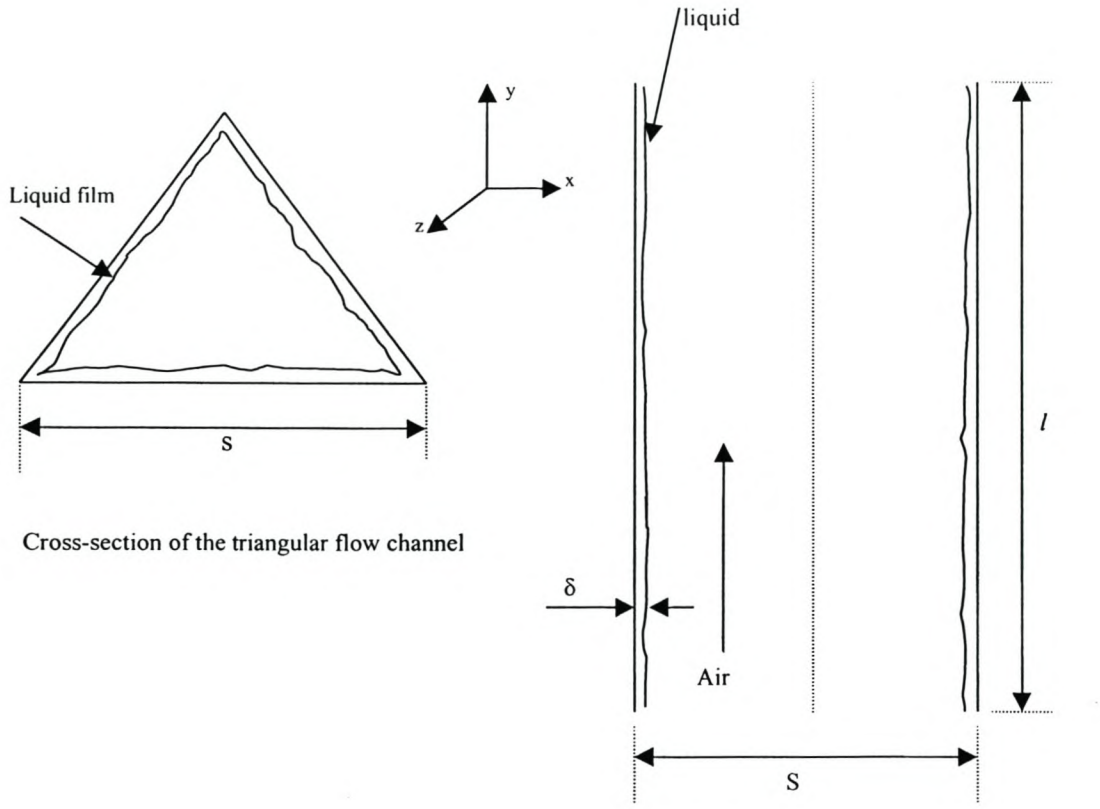

Figure 2.3.1 Liquid Film Flow in wetted wall channel

Then equation 2.21 reduces to:

$$n = 3sk_g P_t \int_0^l \frac{1}{P_{BM} RT}(P_{Ai} - P_{Ab})dy \qquad (2.22)$$

where s is the triangular channel side (see figure 2.3.1).

The partial pressure driving force and P_{BM} will vary along the length of the wetted wall channel due to evaporation and temperature gradients. If it can be assumed that low mass transfer rates and isothermal conditions apply, then evaporative cooling can be ignored. This would imply that the variation in P_{BM} between the top and bottom of the wetted wall channel could be considered to be small. Consequently the arithmetic mean of the top and bottom values can be used for the evaluation of P_{BM}. Based on these

assumptions the numerical integration of equation 2.22 is not necessary. The variation of the partial pressure driving force will be more than that of P_{BM} over the length of the wetted wall channel. Therefore, in evaluating the partial pressure driving force the logarithmic average of the inlet and outlet driving force will be used.

$$\Delta P_A = \frac{(P_{Ai} - P_{Ab})_{inlet} - (P_{Ai} - P_{Ab})_{outlet}}{\ln\left(\frac{(P_{Ai} - P_{Ab})_{inlet}}{(P_{Ai} - P_{Ab})_{outlet}}\right)} \tag{2.23}$$

By straightforward substitution of equation 2.23 into the equation 2.22 and integrating, the molar transfer rate can then be evaluated from:

$$n = A_i \frac{k_g P_t \Delta P_A}{R T P_{BM}} \tag{2.24}$$

The liquid film thickness is taken into account in evaluating the interfacial area. It should be noted that film thickness is assumed to be uniform on all the channel sides.

$$A_i = 3 s_f l \tag{2.25}$$

Where s_f is the channel side with the film thickness accounted for. The calculation of film thickness and interfacial velocity are done as described in Appendix 1.

2.4 Experimental

2.4.1 Experimental Set-up

This work is structured to ultimately develop a model for mass transfer in structured packed columns, therefore the length of wetted wall channel should reflect the flow path lengths encountered in these columns. Furthermore on

top of using a short wetted wall channel, the geometrical configuration was also designed to resemble the triangular flow channels defined by the packing. A flow channel with an equilateral triangular cross-section is used in this study. The entire wetted wall channel is operated at isothermal conditions. This is achieved by having the whole wetted wall assembly submerged in a water bath. Figure 2.4.1 shows the metallic triangular flow channel, which fits into the glass tube of the complete wetted wall assembly.

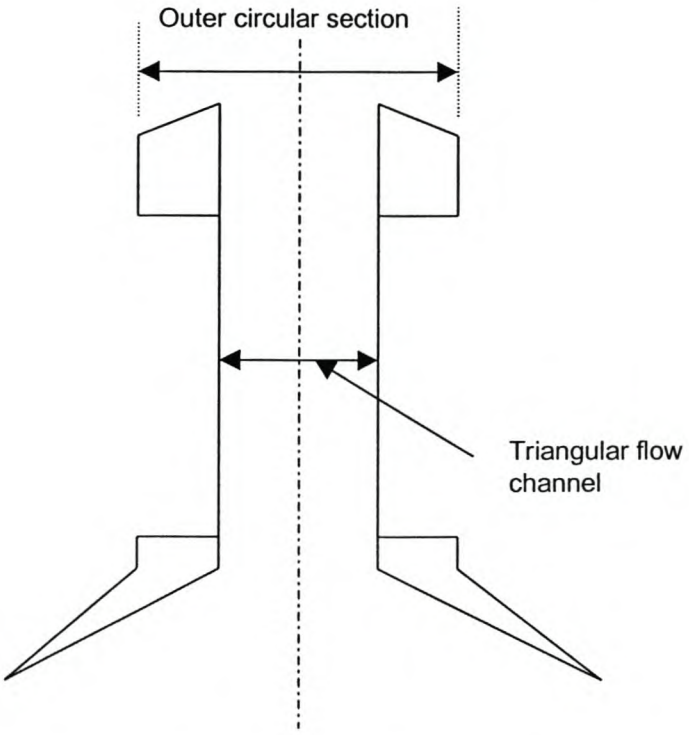

Figure 2.4.1 Machined metallic triangular flow channel

The above triangular stainless steel section is fitted into the inner glass tube, of the complete glass assembly (figure 2.4.3). The triangular section is machined out with each side of length 22.5mm and a longitudinal length of 110mm. The lower part of this section is machined at angle slightly more acute than the flared angle of the precision glass tube shown in figure 2.4.3. The reasoning behind this is to ensure continuity of the liquid film flow. Furthermore the metallic flared section only goes half way down the glass-flared part, this enables the visualisation of the continuous liquid film before the liquid drains out through the liquid exit. The metallic outer circular section

shown in figure 2.4.1 has a diameter of 38.2mm. This section is slanted upwards so that it protrudes above the glass tube. Silicone sealant is used to firmly attach the metallic section into the precision glass tube. The inner column walls of the triangular section are fitted with a thin corrugated surface sheet (see figure 2.4.2). This sheet metal made from packing material (Sulzer 350Y) without perforations is folded and fitted into all the sides of the flow channel. With the corrugated surface the side dimension of the flow channel is 21mm. Silicone sealant is used to bond the corrugated surface to the channel sides. The upper slanted section of the metallic piece, (figure 2.4.1) is grooved at the higher edges to encourage liquid flow to spread over the entire corrugated surface. The characteristic dimensions of the corrugated surface are:

Wavelength: 3.75mm

Amplitude: 0.6mm

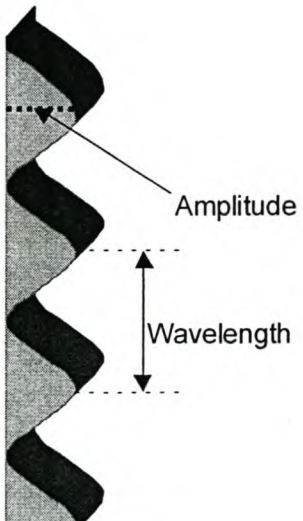

Figure 2.4.2 Corrugated surface

The triangular flow channel shown in figure 2.4.1 fits into the centre tube of the glass assembly shown in figure 2.4.3. This centre tube is a precision bore glass tube of inside diameter 39mm and of length 111mm. As mentioned earlier the diameter of outer circular metallic piece with the triangular channel

is 38.2mm, which allowed the section to fit into the glass tube. Metal expansion is also taken into account in determining the glass tube diameter. The bottom part of the centre tube is flared at an angle of 45° and fused to an outer glass tube of 100mm diameter, the enclosed section thus creating a reservoir for the fluid.

As the wetted wall channel describes a triangular flow channel, a triangular cross section channel is used for the gas inlet piece. This inlet piece, of length 182mm is welded onto the bottom flange, and allowed to form a drainage slot of approximately 3mm upon assembly of the whole unit. The top end of the inlet piece is smoothed out by filing. The channel sides used for the inlet piece are about 20mm, thus compensating for the liquid film thickness. The gas outlet piece of length 75mm has an inner bevel of 20^{o} and is allowed to form a drainage slot of approximately 2mm with the upper end of the wetted wall channel. The gas outlet piece has an internal diameter of 25mm.

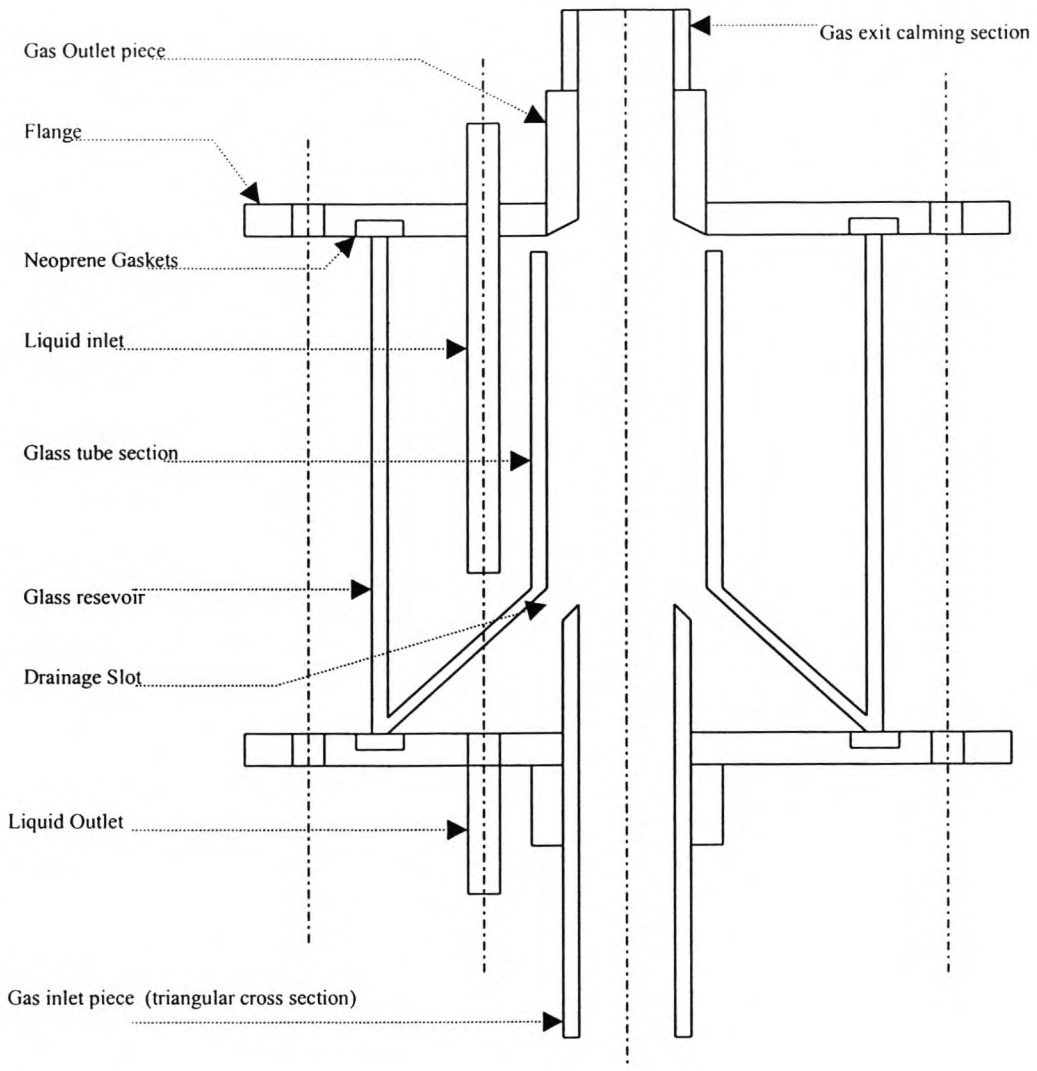

Figure 2.4.3 Wetted Wall Channel

Gas inlet and outlet calming sections are used, with 540mm and 205mm in length respectively. The gas inlet piece is made from stainless steel whilst the gas outlet calming section is made from phosphor bronze and the inlet calming section is made from copper tubing of internal diameter 18.75mm.

Two stainless steel flanges, 10mm thick, support the complete wetted wall arrangement. Three tie rods clamp the wetted wall channel and glass reservoir between the flanges. To seal between the glass section and the flanges, neoprene gaskets are used. Due consideration is given in ensuring

uniformity of distances between the flanges as well as alignment of gas inlet and outlet pieces, when assembling the complete wetted wall channel.

The flow diagram of the experimental set-up is shown in figure 2.4.4. As mentioned earlier the complete wetted wall section is submerged in metallic water bath with perspex windows on three viewing sides. During experiments, water in the bath was kept at a constant temperature. This is achieved by using a MGW Lauda constant temperature bath, which circulates and heats the water. The liquid feed to the wetted wall channel is pumped by a small centrifugal pump from a calibrated reservoir. At the pump outlet is a valve, which controls the liquid flow through the rotameter. From the rotameter the liquid flows through a heating coil submerged in the constant temperature bath. The heating coil is a quarter inch copper tubing of 6m in length. The liquid is allowed to fill the glass reservoir and overflow into the wetted wall channel as a thin liquid film. The liquid drains out of the channel and flows back to the calibrated reservoir under gravity through a level control valve. The liquid flow rotameter is calibrated for each of the working liquids with a stopwatch and measuring cylinder.

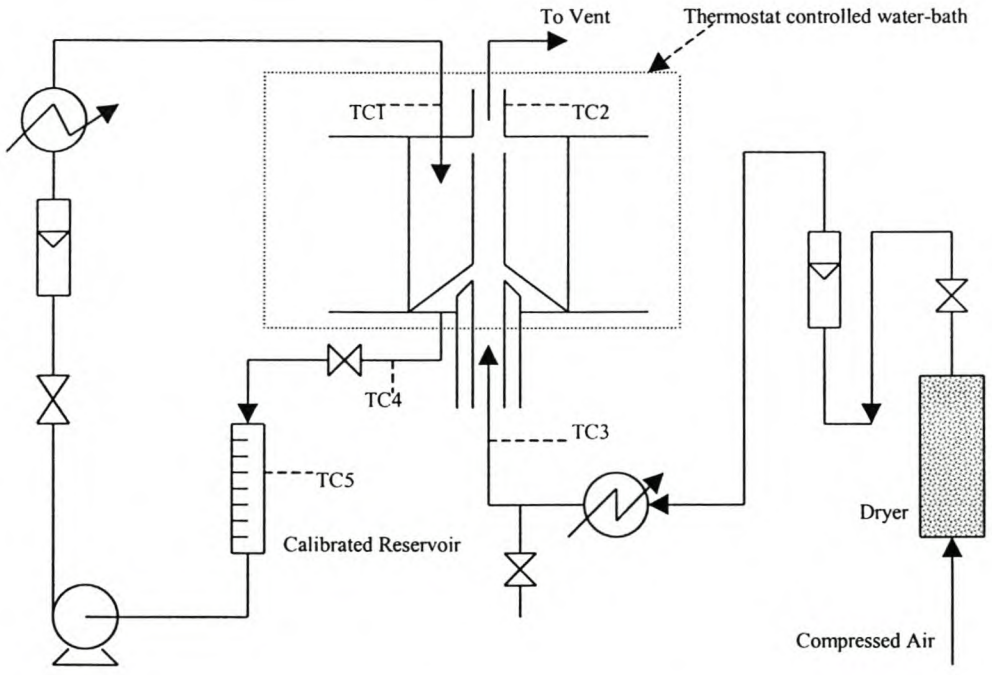

Figure 2.4.4 Flow diagram of experimental set-up

Compressed air is passed through an air dryer with silica gel. The air flows through a valve and then a rotameter before going through an electrical resistance heater. The resistance heater is used to heat up the air flowing through the wetted wall flow channel from the gas inlet section. Adjusting the power to the resistance heater with a variable transformer controls the temperature of the air entering the flow channel. The air exiting the wetted wall channel passes through the gas outlet calming section and is ultimately vented to atmosphere.

During the experimental runs, all the temperatures are measured using type K thermocouples and the temperature readings registered on a Yokogawa HR3100 hybrid recorder. The thermocouples have an accuracy of ± 0.2°C. The inlet air pressure to the rotameter is measured with a manometer.

Following are the temperature points that were measured during the experimental runs:

Temperature of liquid in calibrated reservoir	TC5
Liquid inlet and outlet to wetted wall channel	TC1 and TC4
Gas inlet and outlet to wetted wall channel	TC3 and TC2
Temperature of air before the rotameter	TC6

The temperatures measured in the experimental work are given in Appendix 3.

2.4.2 Experimental procedure

Before commencing any series of experimental runs the wetted wall channel is removed from the water bath and thoroughly cleaned and dried. The initial stage involved filling the calibrated reservoir with the working liquid; this is then pumped through piping to fill up the glass reservoir of the wetted wall channel, after which the pump is switched off. The air flow rate is adjusted to the desired rate and the resistance heater power varied to approximate the

operating temperature. The operating temperature is specified for the constant temperature bath and recirculation of water in the bath started. The apparatus is then left to stand until the temperatures stabilise at the operating conditions. Upon the system stabilising the liquid pump is switched back on and working liquid circulated until it reaches operating temperature, thereafter the apparatus is ready for operation.

Once the apparatus is ready for operation, evaporation rates were measured for varying liquid rates at a particular gas rate. This was done for a number of different gas rates. The desired liquid flow rate is achieved by adjusting the control valve on the liquid pump outlet line. The evaporation rates are evaluated from the volume change in the calibrated reservoir per unit time. The volume of liquid evaporated is obtained by noting the initial level in the calibrated reservoir and the final level reading after the run. It should be noted that the final level reading is taken once the liquid from the wetted wall channel has completely drained into the calibrated reservoir. The air inlet temperature is adjusted during the runs in order to obtain equivalent values of average liquid and gas temperatures. The experimental runs were allowed to run for a minimum of at least 5minutes, with the average evaporated liquid volumes of 40-60ml. During each run temperatures' were noted an average of 3 times.

2.5 Results

The experimental results obtained are illustrated graphically through the use of dimensionless numbers. Figure 2.5.1 below shows the variation of gas Sherwood numbers with the gas Reynolds numbers of the test liquids. A compilation of the experimental work results is given in Appendix 3.

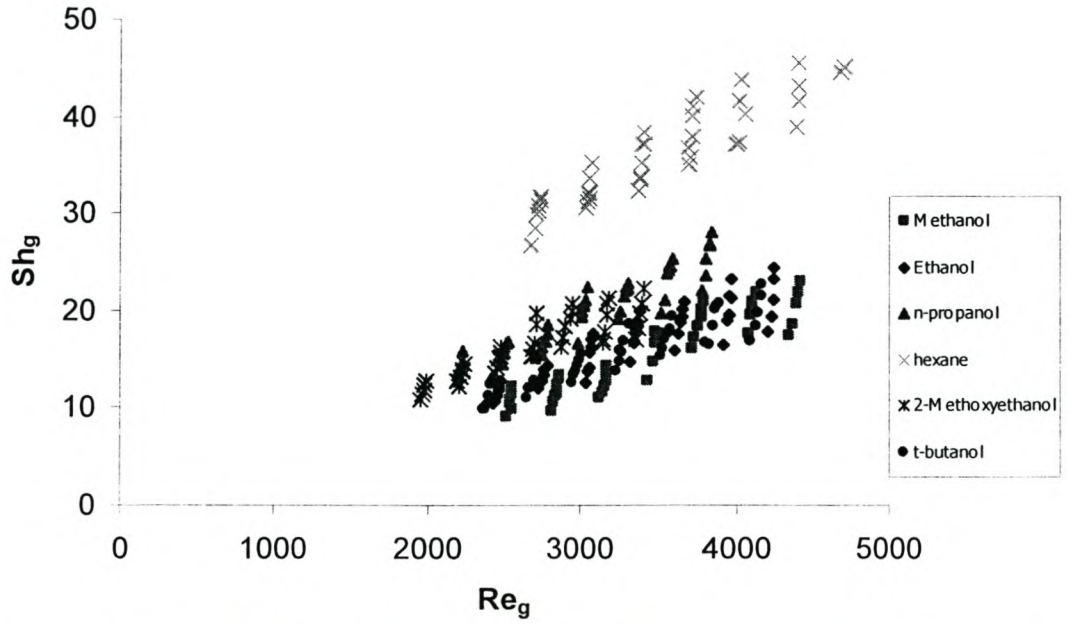

Figure 2.5.1 Graphical representation of Re_g vs. experimental Sh_g, for the different pure components investigated.

The following plots (Figures 2.5.2 – 2.5.4), show the variation of experimental Sherwood number with liquid Reynolds. This is shown for only three of the test liquids as all of them showed a similar trend, i.e. increasing experimental Sherwood number with increasing gas Reynolds number at a particular liquid rate.

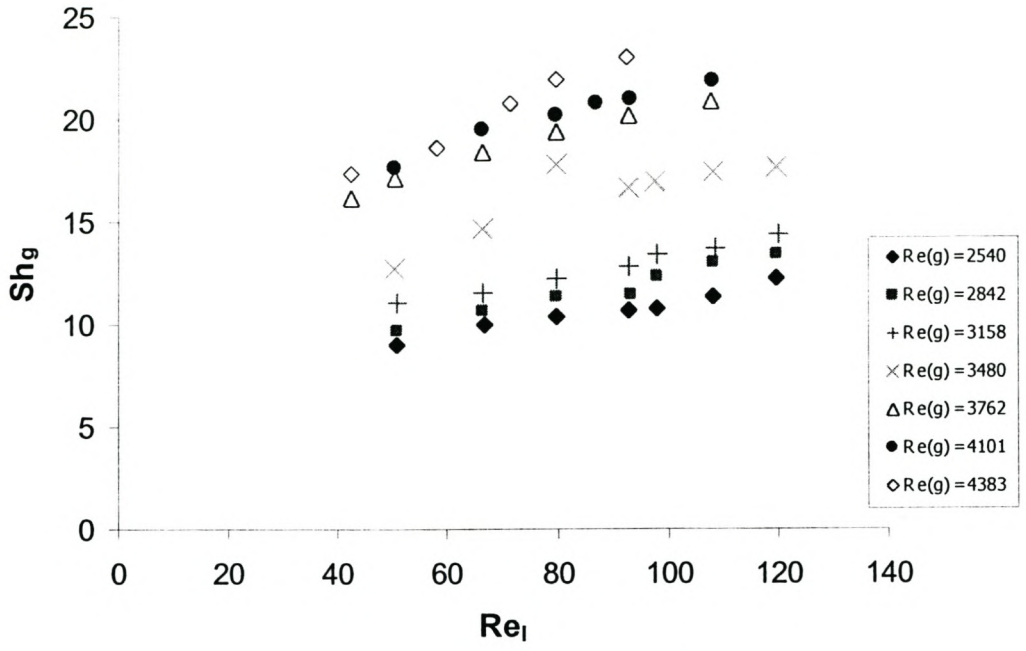

Figure 2.5.2 Sh_g vs. Re_l for Methanol, $42 < Re_l < 120$

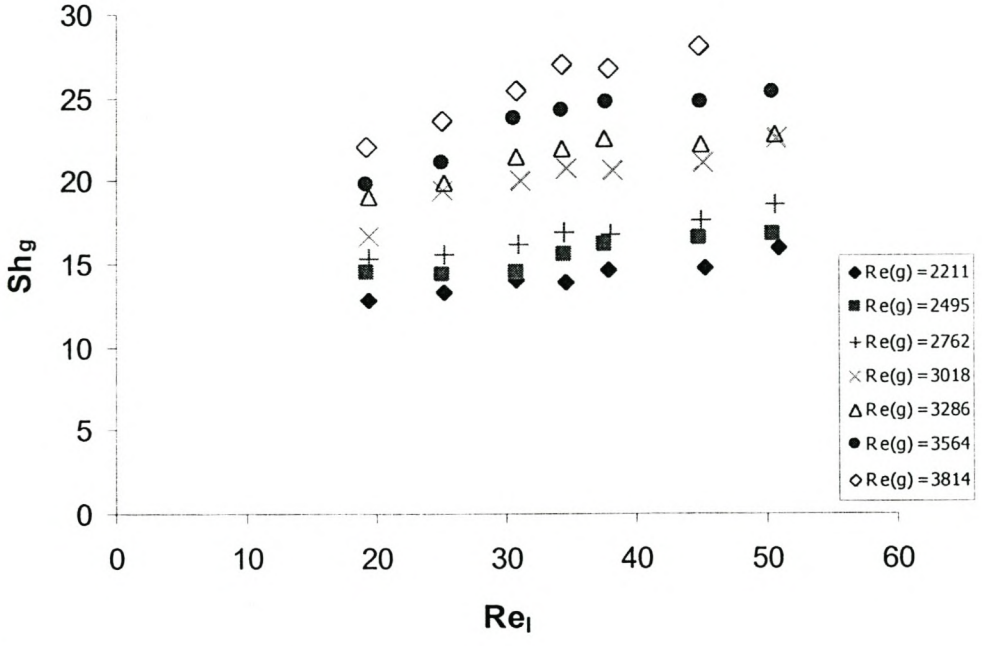

Figure 2.5.3 Sh_g vs. Re_l for n-propanol, $19 < Re_l < 51$

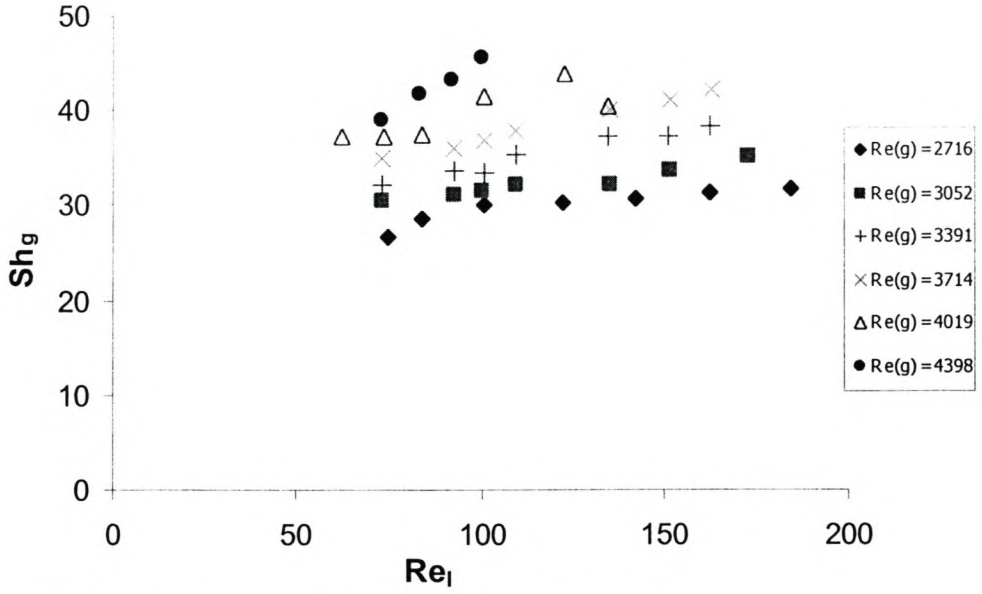

Figure 2.5.4 Sh_g vs. Re_l for hexane, $62 < Re_l < 184$

The experimental results obtained from the wetted wall channel were compared with correlations developed in earlier studies. It should be noted that all previous investigators used circular flow channels for their experimental work.

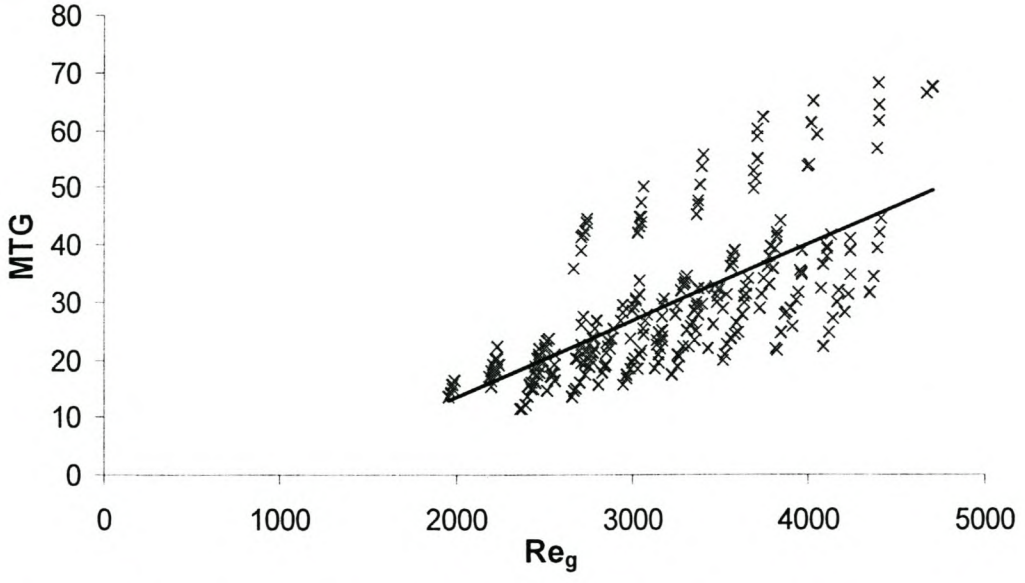

Figure 2.5.5 Comparisons: Gilliland & Sherwood correlation. Mass Transfer group (MTG) = $\left[\frac{Sh_g}{Sc_g^{0.44}}\right]^{\frac{1}{0.83}}$

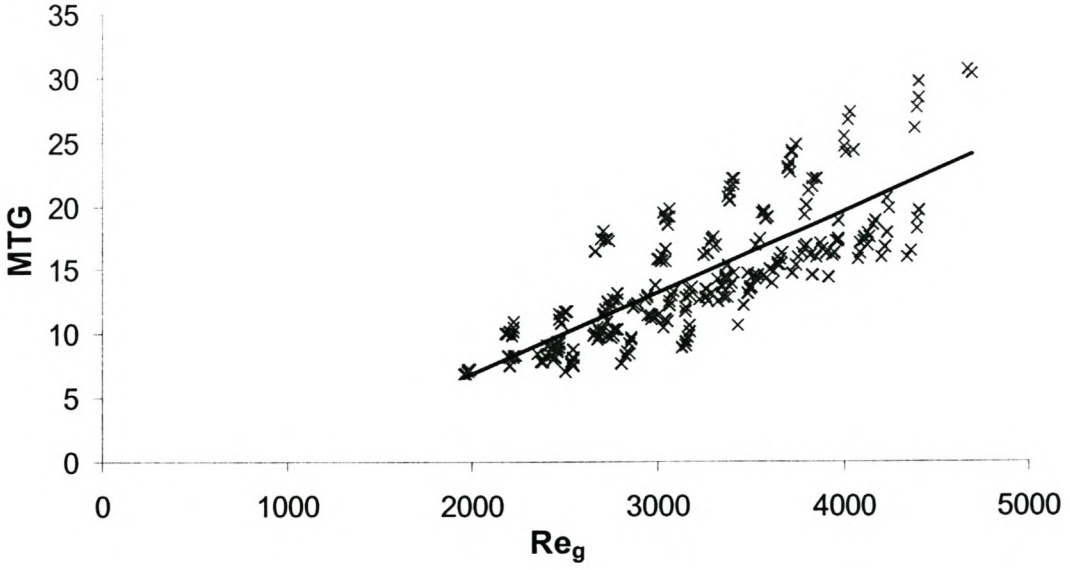

Figure 2.5.6 Comparisons: Kafesjian et al correlation. MTG = $\left[\frac{Sh_g}{Sc_g^{0.44}\,\mathrm{Re}_l^{0.15}}\right]^{\frac{1}{0.83}}$

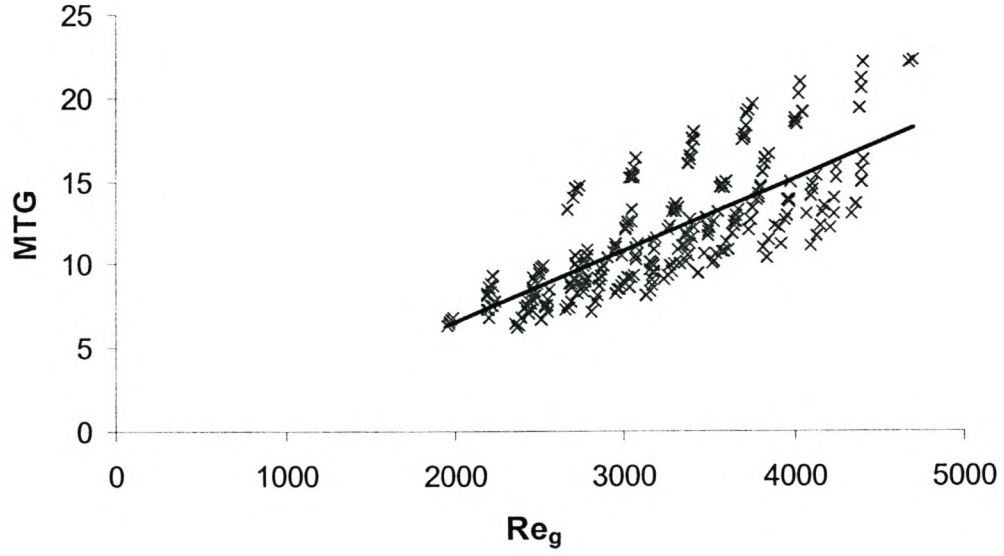

Figure 2.5.7 Comparisons: Crause correlation. MTG = $\left[\frac{Sh_g}{Sc_g^{0.5}\,\mathrm{Re}_l^{0.08}}\right]$

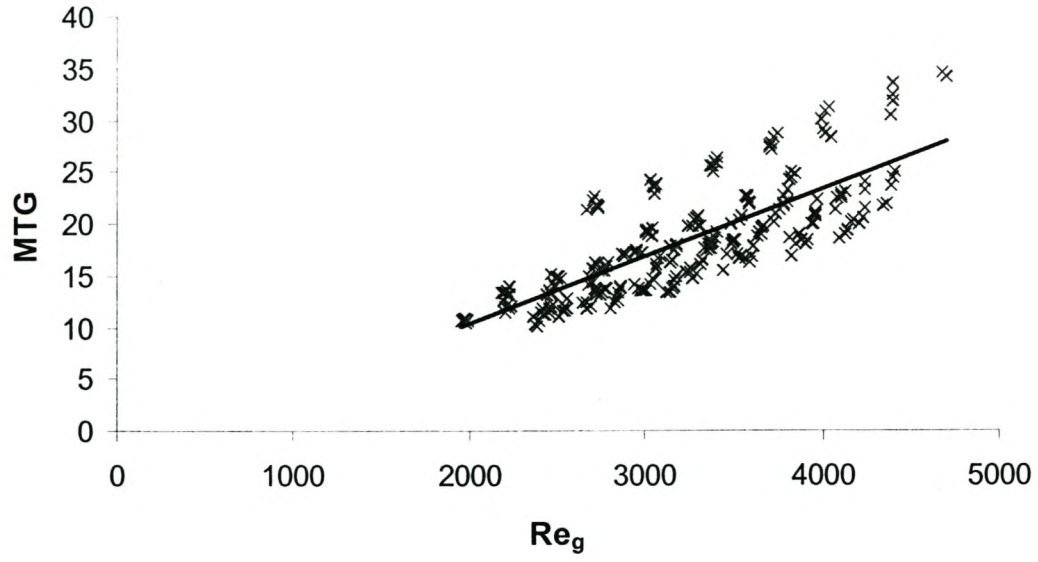

Figure 2.5.8 Comparisons: Erasmus (smooth surface) correlation. MTG = $\left[\frac{Sh_g}{Sc_g^{0.5} We_l^{0.111}}\right]$

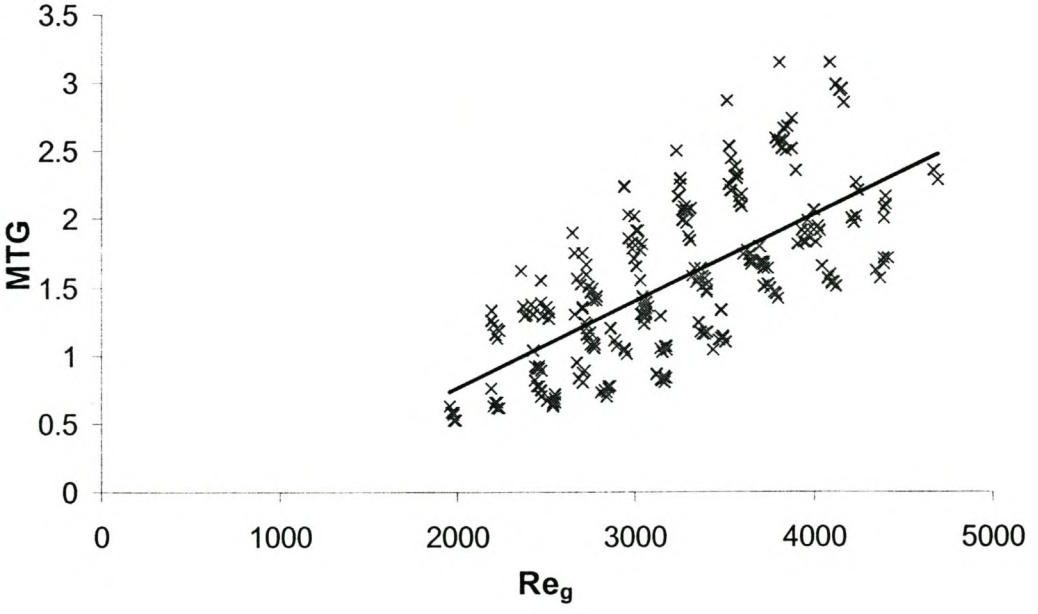

Figure 2.5.9 Comparisons: Erasmus (complex surface) correlation. MTG = $\left[\frac{Sh_g}{Sc_g^{0.5} \mathrm{Re}_l^{0.41} Bo_l^{-0.13}}\right]^{\frac{1}{0.76}}$

The general trend observed from the above comparisons (figures 2.5.5-2.5.9) is that the bulk of the experimental data lies below the regression lines, therefore indicating a general over prediction of the mass transfer rates by the above correlations. It can be observed that certain data points lie consistently above the correlation lines. These correspond to the hexane data, which is under predicted significantly by all the correlations, but this effect is less marked for the correlations with liquid terms than those without. A similar trend of under-prediction of the transfer rates by the above correlations observed with some n-propanol data as well. Granted this effect is not as significant as for hexane data but it is also consistent for all correlations.

The correlation developed by Gilliland and Sherwood {1934}, figure 2.5.5, tends to under predict mass transfer rate at low Re_g, but with increasing gas rate over predicts the transfer rate for bulk of the data. The correlation developed by Kafesjian et al. {1961}, figure 2.5.6, showed a similar trend to Gilliland and Sherwood, {1934}, though their correlation had a better fit at low Re_g values. As with the correlations just mentioned those developed by Crause {1998} and Erasmus {1999}, for smooth surfaces in a short wetted wall column showed more or less the same trend. That is a good estimate of the transfer rate at low Re_g with an over prediction of most of the data at higher gas rates except for hexane and some n-propanol data (as illustrated in figures 2.5.7 and 2.5.8, respectively). From the correlation developed by Erasmus, {1999} for flow down a circular channel with complex surface (see figure 2.5.9) no conclusive trend could be established. The correlation over predicts one half of the data set whilst under predicting the other half. As a consequence it can be observed that present correlations developed for flow in circular channels cannot accurately predict transfer rates in non-circular channels.

To model mass transfer based on all physico-chemical and hydrodynamic factors separately would require vast amounts of experimental data. Therefore, the use of dimensionless parameters enables the reduction of the independent variables for the correlation of the experimental data. These dimensionless parameters are developed from the knowledge of properties

affecting the desired quantity, in this case the mass transfer coefficient. From the present understanding of the process, it is assumed that the gas phase mass transfer coefficient will be affected by gas and liquid physical properties as well as geometric parameters. The list of the properties deemed to have an influence on the transfer coefficient are given as follows:

$$k_g = f\,(\,D_{AB},\,\rho_g,\mu_g,u_g,d_{eq},l,\rho_l,\mu_l,u_l,\delta,\sigma,g,u_{g,r}\,)$$

These symbols given above are defined in the nomenclature at the end of the chapter. The dimensionless groups are derived from these properties including the gas phase transfer coefficient.

Different methods are available in literature {Coulson and Richardson, 1997; de Nevers, 1991; Zlokarnik, 1991} indicating how the dimensionless numbers can be obtained from the properties. For this particular case the Buckingham π-theorem as illustrated in Coulson and Richardson, {1997} will be used in deriving the dimensionless groups. The maximum number of derivable groups is equal to the number of properties less the independent dimensions. The independent dimensions being mass, length and time in this case. It should be noted that the derived dimensionless groups might not be in a form generally encountered in literature. Consequently groups have to be transformed into suitable forms. The examples of how the dimensionless parameters are derived from the properties are given in Appendix 6. Table 2.1 indicates the relevant dimensionless numbers in the suitable form that can be derived from the dimensional analysis and used in the correlation of the data.

It should be noted that the dimensional analysis only enables the derivation of the dimensionless groups and gives no indication of the functional form between the desired quantity (Sh_g) and other dimensionless groups. Consequently, similar functional forms to that of previous investigators of correlating mass transfer data with dimensionless groups will also be employed in this study. It involves the application of the power law series to the dimensionless parameters in correlating the experimental transfer rates.

In the development of the correlations it is essential to ensure that no one group in the correlation is a combination of the remaining groups of that particular correlation.

The ranges of various dimensionless numbers as well as viscosity and surface tension ranges for the test liquids are given below:

Sh_g	: 8-46	Re_l	: 6-190
Re_g	: 1800-4700	σ (mN/m)	: 17-25
$Re_{g,r}$	: 1900-5200	μ_l (Pa.s)	: 2.65 -12.6 $\times 10^{-4}$
Sc_g	: 0.97-2.04		

The characteristic dimension for gas flow is based on the cross-section geometry of the flow channel with a liquid film of constant thickness on all channel sides. It is calculated as shown in Appendix 1. This characteristic dimension is used in the calculation of the gas phase Reynolds number. The liquid flow characteristic dimension is taken as the liquid film thickness. The calculation of the liquid film thickness is shown in Appendix 1. The formulae for the dimensionless terms are given in table 2.1.

Table 2.1 Dimensionless Groups

Name	Symbol	Formula	Physical Interpretation
Gas Reynolds number	Re_g	$\frac{\rho_g u_g d_{eq}}{\mu_g}$	$\frac{\text{inertial force}}{\text{viscous force}}$
Relative Reynolds number	$Re_{g,r}$	$\frac{\rho_g (u_g + u_i) d_{eq}}{\mu}$	$\frac{\text{inertial force}}{\text{viscous force}}$
Gas Schmidt number	Sc_g	$\frac{\mu_g}{\rho_g D_{AB}}$	$\frac{\text{Momentum force}}{\text{diffusion force}}$
Sherwood number	Sh_g	$\frac{k_g d_{eq}}{D_{AB}}$	concentration gradient at the interface
Liquid Reynolds number	Re_l	$\frac{\rho_l u_l \delta}{\mu_l}$	$\frac{\text{inertial force}}{\text{viscous force}}$
Weber number	We_l	$\frac{\rho_l u_l^2 \delta}{\sigma}$	$\frac{\text{inertial force}}{\text{surface tension force}}$
Froude number	Fr_l	$\frac{u_l^2}{g\delta}$	$\frac{\text{inertial force}}{\text{gravity force}}$
Capillary number	Ca_l	$\frac{\sigma}{\mu_l u_l}$	$\frac{\text{surface tension force}}{\text{viscous force}}$

In the dimensional analysis the selected properties of the recurring set will determine which dimensionless terms can exist in a particular correlation. The dimensionless parameters can then be used to correlate the experimental data according to these limitations. The different combinations of the dimensionless parameters will determine the relative influence of the physical properties. The correlation constants are evaluated from non-linear least square minimisation of the squared sum of the residues between experimental and predicted Sherwood numbers.

Results of the various correlations are given in table 2.2.

In the correlations the theoretical value of 0.5 was taken as the exponent for the Schmidt number. It has been shown that the mass transfer coefficient proportional to the square root of the diffusivity describes the transfer process accurately, {Dudukovic, 1996}. Furthermore, as postulated by Higbie's penetration theory {Sherwood et al. 1975}, gas-liquid contact times in

industrial equipment (such as columns with structured packing) are short and therefore do not allow for development of a steady concentration gradient in the liquid film. The theory shows a dependency of mass transfer coefficient on $D_{AB}^{0.5}$. It should also be noted that since the gas Schmidt number only varied from 0.97-2.04 in this work, the other dimensionless groups in the correlations might have a larger influence on the exponent of Sc_g due to this limited range.

Table 2.2 Correlation results

Correlations	a	b	c	d	e	rms error	r^2
2.26 $Sh_g=aRe_g^bSc_g^c$	0.000814	1.227	0.5	N/A	N/A	5.193	0.610
2.27 $Sh_g=aRe_{g,r}^bSc_g^c$	0.000159	1.415	0.5	N/A	N/A	4.289	0.734
2.28 $Sh_g=aRe_g^bSc_g^cRe_l^d$	0.000384	1.187	0.5	0.276	N/A	2.937	0.878
2.29 $Sh_g=aRe_{g,r}^bSc_g^cWe_l^d$	0.00101	1.220	0.5	0.213	N/A	2.745	0.891
2.30 $Sh_g=aRe_{g,r}^bSc_g^cFr_l^d$	0.00197	1.013	0.5	0.220	N/A	2.170	0.931
2.31 $Sh_g=aRe_g^bSc_g^cWe_l^d$	0.00230	1.139	0.5	0.272	N/A	3.020	0.868
2.32 $Sh_g=aRe_{g,r}^bSc_g^cCa_l^d$	0.000114	1.429	0.5	0.042	N/A	4.276	0.736
2.33 $Sh_g=aRe_{g,r}^bSc_g^cRe_l^d$	0.000328	1.224	0.5	0.215	N/A	2.658	0.902
2.34 $Sh_g=aRe_g^bSc_g^cRe_l^dFr_l^e$	0.00728	0.857	0.5	-0.106	0.350	2.241	0.925

$$\text{rms error} = \sqrt{\frac{\left(Sh_{experimental} - Sh_{predicted}\right)^2}{n}}$$

2.6 Discussion of results

Table 2.2 above shows the results of the correlations used in the regression of the experimental data. It is evident that the mass transfer rate in the gas phase is affected by the liquid properties. The correlation 2.26, similar to the Gilliland and Sherwood form was unable to correlate the data well. Correlations, (2.27, 2.29, 2.33) were the Reynolds number uses a velocity of

the gas relative to the moving liquid interface perform better than the ones with which the velocity is relative to the wall. Correlations (2.28, 2.33-2.34) where liquid Reynolds numbers were used correlated the data reasonably well but these did not show a reduction in the error compared to correlation 2.30.

The correlation (2.30), which best describes the data employs the relative velocity for the gas Reynolds term and further incorporates liquid effects through a term including liquid film thickness and velocity. The regression of data using the relative velocity is in contrast to earlier work done in a short wetted wall column by Crause {1998} and Erasmus {1999}. They found that their respective data sets could be regressed with the gas velocity relative to the wall. A possible explanation could be the nature of the flow over the complex surface. It has also been illustrated by McCarter and Stutzman {1959} that the liquid velocity can be expected to contribute to shear forces determining the film thickness. Most notably though is the difference in the liquid term, the Froude number in this case, where previous studies {Kafesjian et al., 1961; Crause, 1998} have characterised liquid effect through Re_l. Erasmus, {1999} for smooth surface work found a surface tension effect in the liquid term (We_l), whilst complex surface work was characterised by Re_l and Bo_l numbers. The reasoning behind this, the Fr number appearing in the correlation, could possibly be that not a wide enough range of physical properties were used in this work. This would therefore limit the effects of properties such as viscosity and surface tension. Furthermore, the majority of the experiments were conducted for Re_l less than 100. Therefore, the exact liquid influence outside this range might not be accounted for accurately. This therefore warrants for further experimental work. Continued discussion of results will apply to correlation 2.30, unless stated otherwise.

Earlier work ({Crause, 1998; Erasmus, 1999}) found that the transfer rate is independent of surface tension. However, figure 2.6.1 indicates a significant augmentation when the developed correlation is compared to the experimental data of a high surface tension liquid. The data for water was obtained from Crause {1998}. The experimental work was done in a smooth surface circular column at high liquid rates. Since there are differences in

geometric configuration, surface orientation and other properties, Re_l of 430, Sc_g = 0.62 and σ = 0.063 N/m (all out of working range) this enhancement cannot be completely attributed to surface tension effects. Correlation 2.30 was obtained for a low liquid rate range and this heavily influences it through relative velocity and Fr_l number. Furthermore considering the nature of flow (wavy) over complex surface this promotes development of interfacial turbulence at the interface. As a result, correlation 2.30 predicts significant augmentation of the transfer rate, which could be partly attributed to the increase in interfacial turbulence at these high flow conditions. Therefore the enhanced transfer rates as predicted by correlation 2.30 could be due various factors including surface tension effects and the interfacial turbulence. Furthermore the correlation is unable to accurately extrapolate outside the range of Sc_g numbers it was fitted for, as the Sc_g number of water (0.62) falls into this category.

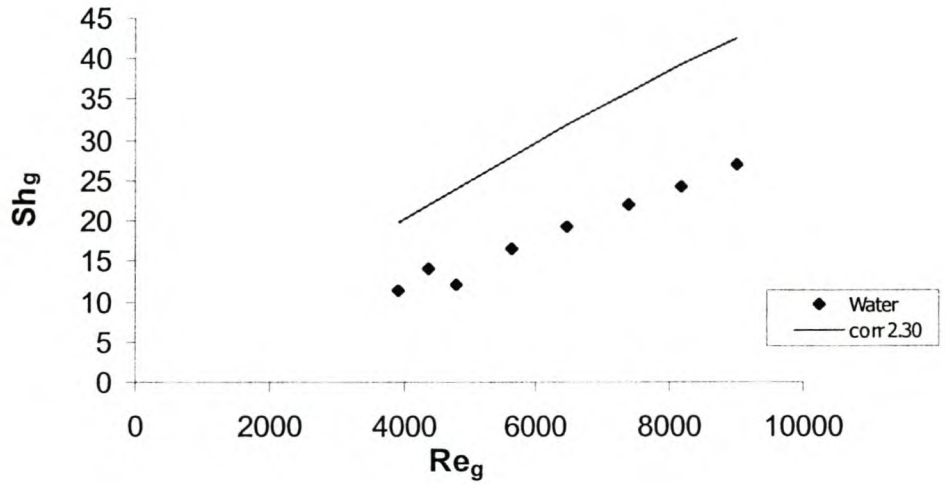

Figure 2.6.1 Experimental Water results {Crause, 1998} vs. Sh_g predicted.

A further comparison to better clarify the observed augmentation in figure 2.6.1 is done with ethylene glycol (data obtained from Crause {1998}) see figure 2.6.2.

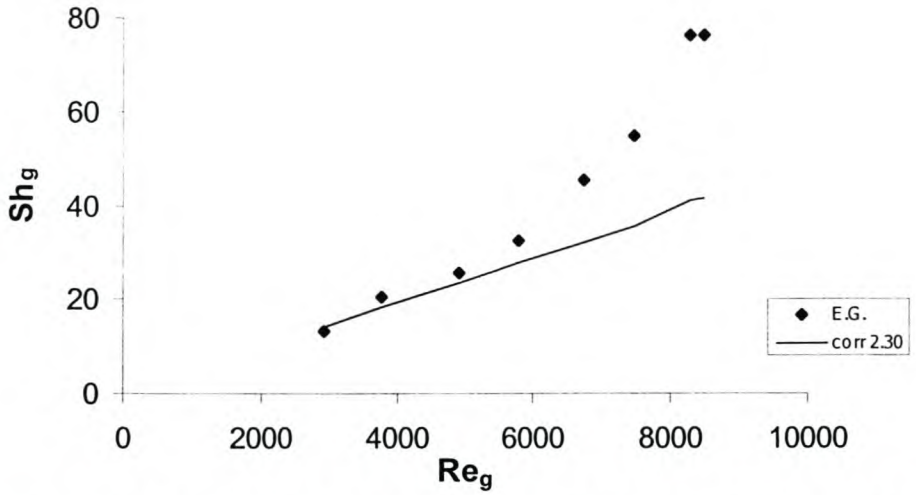

Figure 2.6.2 Experimental Ethylene glycol results {Crause, 1998} vs. Sh_g predicted.

It was found that for ethylene glycol the data for Re_l and Sc_g are within this working range whilst the viscosity and surface tension values are outside the operating range. From figure 2.6.2, it can be seen that no transfer rate enhancement is observed. The developed correlation shows good agreement at low gas rates but significantly under estimates the transfer rates at higher gas rates. Crause {1998} attributed the large differences between the predicted and experimental values at these high gas rates to larger experimental errors since the transfer rates were measured at extremely low evaporation rates. The surface tension of ethylene glycol (42mN/m) is outside the range of that of the tests liquids (17-25 mN/m). Then the observed enhancement in figure 2.6.1 could be due to viscosity, geometric configuration effect as well as increased transfer area and interfacial turbulence. It is most likely that the increased interfacial turbulence and increased transfer area are the dominant effects on the transfer rate. Ethylene glycol with its high viscosity is expected to form a thick film, which should flatten out the liquid film. A flatter liquid film may have less area for mass transfer and thus reduced transfer rates. Therefore, increased turbulence in the gas phase could be responsible for the observed transfer rates at the higher gas rates ($Re_g > 7000$) in figure 2.6.2. Based on the above observations one is inclined to perceive that surface tension doesn't affect the transfer rate significantly. From this particular case one is lead to deduce that there is no obvious

surface tension effect. However, it has been found that for decreasing surface tension values there is an increase in free-surface activity, thus inducing turbulence in the gas phase, which can then lead to enhanced transfer rates, {Peramanu, 1998}.

The developed correlation has shown a significant dependency on the liquid flow rate. To what extent geometric configuration will affect transfer rate will depend on how it describes flow through the channel. The developed correlation is used in predicting the transfer rates of a circular channel with complex surface and compared with experimental data (the data obtained from Erasmus {1999}), (see figure 2.6.3). It can be observed that the data is spread around the correlation within reasonable extremities. Simplistic comparison between the predicted and the experimental Sh_g values shows an average percentage error of less than 10%, for the whole data set. The predicted Sh_g are calculated from correlation 2.30. Erasmus {1999} found that transfer rates were markedly higher in a column with a complex surface than one without. Therefore, based on this and observed results in figure 2.6.3 it can be deduced that the nature of the surface over the wall has a significantly larger influence on transfer rate than the geometric configuration of the flow channel.

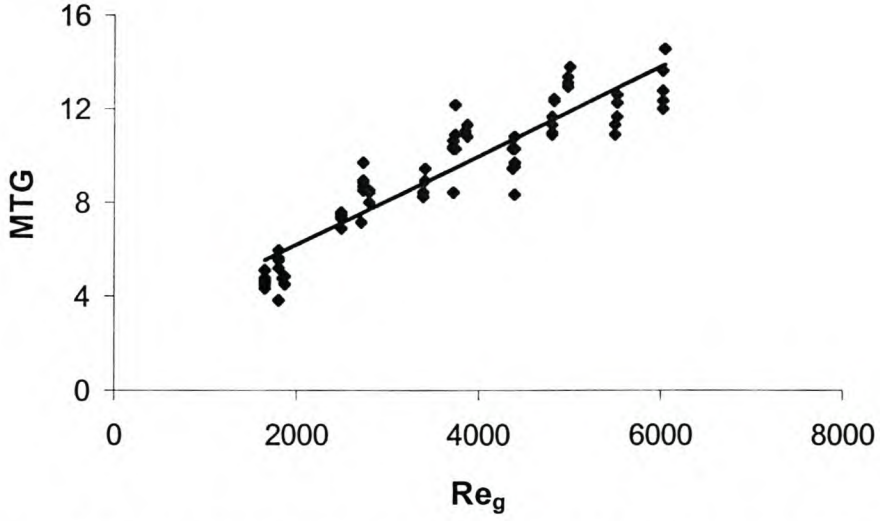

Figure 2.6.3 Comparison: correlation 2.30, Sh_g predicted and Sh_g experimental (♦). MTG = $\left[\frac{Sh_g}{Sc_g^{0.5} Fr_l^{0.220}}\right]^{\frac{1}{1.013}}$

To better understand the geometric effect on transfer rate a comparison of experimental Sh_g values for circular and triangular channels is made at similar gas and liquid rates. Figure 2.6.4 shows experimental Sh_g values at similar flow conditions.

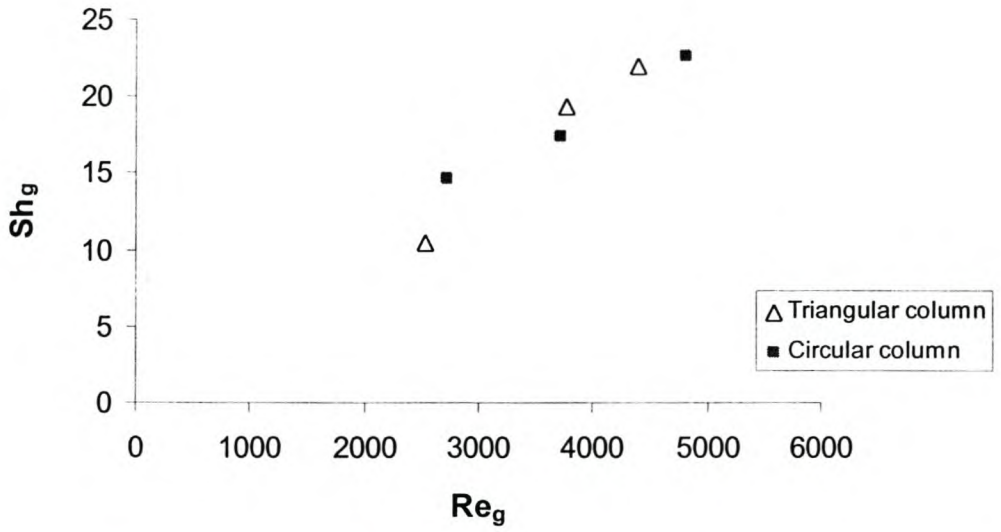

Figure 2.6.4 Methanol results: Comparison between circular (data from Erasmus {1999}) and triangular flow channels with complex surfaces. $Re_l \approx 78$

The observed variation of Sh_g number with Re_g number (figure 2.6.4) at the given liquid rate also obtained for different liquid rates. Similar graphs were obtained for ethanol, though it should be noted that due to limited fluid phase velocity range in this study, only a few data points are available for comparison. For the triangular flow channel at low Re_g values, lower Sh_g values were obtained, though these increased sharply with increasing Re_g. Assuming no significant experimental error in either case, then the following explanation can be put forward. It is possible that at lower Re_g values there is a lack of radial distribution of gas velocity in the triangular flow channel, and as the transfer rate is gas controlled the lack of a fully developed concentration driving force in the gas phase would lead to reduced transfer rates. At higher gas rates ($Re_g > 3500$) there is no appreciable difference in transfer rates. It is highly plausible that the geometric cross section impacts differently at higher flow rates ($Re_g > 5500$, outside this study's working range), but this flow rate range was not covered in this work.

It is proposed that correlation 2.30 gives the best fit for the experimental data of this work. This correlation is plotted with experimental data in figure 2.6.5 below.

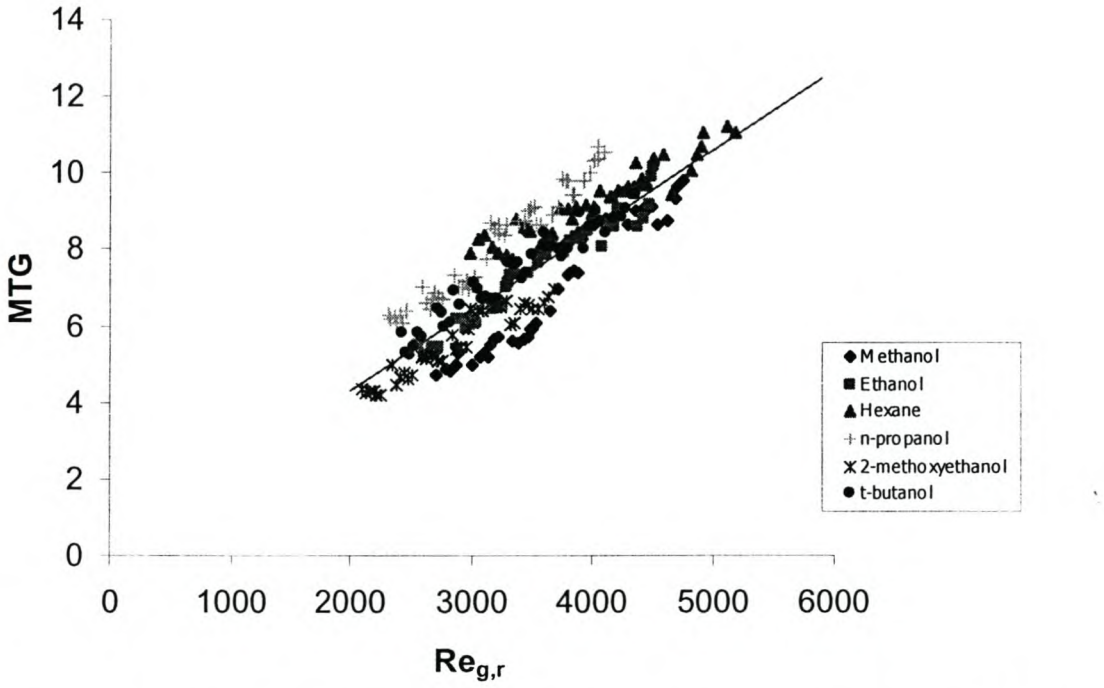

Figure 2.6.5 Graphical plot of experimental data and correlation 2.30. (–).

$$\text{MTG} = \left[\frac{Sh_g}{Sc_g^{0.5} Fr_l^{0.220}} \right]^{\frac{1}{1.013}}$$

The correlation results show that the exponent (1.013 ≈ 1) of the gas Reynolds term concurs with earlier work done on short wetted wall flow columns, {Crause 1998; Erasmus 1999}. Both found that the exponent of the gas Reynolds was approximately equal to 1. Though in this case the velocity relative to the liquid film is used in calculating the gas Reynolds number. The use of a shorter length column could explain as to why this exponent is higher than previously encountered values found in literature (0.8-0.83), {Crause 1998}. However, Nielsen et al., {1998} also found an exponent ≈ 1 (1.05), for absorption in a long wetted wall column, 5m in length. In structured packed columns entrance effects are expected to influence transfer rates due to the

short flow path length for mass transfer, {Erasmus, 1999}. Taking into consideration the ratio of channel height to equivalent diameter in this case, entrance effects are expected to have a significant influence on the transfer rate. This exponent is in agreement with the values obtained in literature for structured packed columns (Weiland et al. {1993} for Montz A2, Spiegel and Meier {1987} for Mellapak 125Y-500Y). Whilst for gauze packing the latter found a value of 0.8.

The exponent for the Schmidt number is fixed at 0.5 for the reasons mentioned earlier in section 2.5. Dudukovic {1996} has shown that a theoretical value of 0.5 describes gas-liquid mass transfer more accurately than the value of 0.33 adapted from mass transfer between gas-solid surfaces. This value, 0.33, therefore applies to a solid-fluid interface rather than a fluid –fluid interface.

The exponent of 0.220 on the liquid phase term (Fr_l) shows the considerable influence that liquid flow has on gas phase mass transfer considering that a liquid effect is incorporated through the relative velocity for $Re_{g,r}$. This increased liquid effect can probably be attributed to lower mass transfer rates investigated and mainly due to nature of flow over the complex surface. It is probable that film flow over this surface will impact transfer rate through variation of the liquid velocity, interfacial area as well as interfacial turbulence. It should be noted that the complex surface correlation by Erasmus {1999} also showed considerable liquid effect on transfer rate. The exponents of the liquid terms were found to be 0.41 on Re_l and –0.13 on Bo_l numbers. In the theoretical study by Trifonov {1998} it was found that viscous, surface tension and inertia forces had a significant influence on the liquid film flow over complex surfaces. The equations derived from the analyses included dimensionless terms accounting for these forces. This shows that the effect of liquid hydrodynamics on mass transfer may be described with terms accounting for these forces.

2.7 Summary

- The mass transfer rate in a wetted wall channel with an equilateral triangular cross section was found to be generally lower than that predicted by previous investigators. This applies to the flow conditions investigated in this work. The correlations developed in smooth circular channels {Gilliland and Sherwood, 1934; Kafesjian et al., 1961; Crause, 1998; Erasmus, 1999} all over predicted most of the data. The correlation developed for a complex surface column {Erasums, 1999} predicted widely varied data.
- The developed correlation showed significant augmentation of the transfer rates for high surface tension liquids. For high viscosity liquids the correlation was able to predict the transfer rate at lower Re_g values (< 6000), but significantly under-predicts the transfer rates at higher gas rates.
- It was found that the complex nature of surface wall has a considerable influence on the transfer rate through the liquid surface profile, thus determining interfacial turbulence and available effective mass transfer area. The extent of these effects will differ depending on fluid properties.
- Geometric configuration, triangular in this case, did not show any considerable effect on mass transfer rate. Minimal influence at low gas rates tended to decrease the transfer rate.
- The exponent ($1.013 \approx 1$) of the relative gas Reynolds numbers concurs with earlier work on short wetted wall columns, {Crause, 1998; Erasmus, 1999} as well as that for structured packed column, {Weiland et al., 1993}.
- The exponent for Schmidt number was fixed at the theoretical value of 0.5.
- A significant liquid phase effect was found on the gas phase mass transfer rates. This effect brought about by the liquid flow rate range and complex nature of the wall surface, thus influencing velocity profile. The liquid influence in the correlation characterised by the relative velocity in the gas Reynolds number and the Fr_l as the liquid term with an exponent of 0.22.

- Proposed correlation for gas phase mass transfer given as follows with the gas Reynolds term exponent rounded off to 1:

$$Sh_g = 0.00219 Re_{g,r}\ Sc_g^{0.5} Fr_l^{0.220} \qquad (2.30a)$$

within the bounds of $6 < Re_l < 190$ and $1800 < Re_g < 4700$

Nomenclature

Symbol	Description	Unit
A	Area	[m^2]
Bo	Bond number	
Ca	Capillary number	
D_{AB}	Diffusion coefficient of A in B	[m]
d_{eq}	Equivalent diameter	[m]
Fr	Froude number	
g	Gravitational acceleration, 9.81	[m/s^2]
k	Mass transfer coefficient	[m/s]
l	length	[m]
MTG	Mass transfer group	
n	Molar transfer rate	[mol/s]
N	Molar flux	[$mol/(s.m^2)$]
P	Pressure	[Pa]
P_{BM}	Mean pressure of B	[Pa]
r^2	Correlation coefficient	
R	Universal gas constant, 8.314	[J/(mol.K)]
Re	Reynolds number	
s	side length of triangular channel	[m]
s_f	side with liquid film	[m]
Sc	Schmidt number	
Sh	Sherwood number	
T	Temperature	[K]
u	Velocity	[m/s]

w	width	[m]
We	Weber number	

Greek symbols

Symbol	Description	Unit
Δ	Difference	
δ	Liquid film thickness	[m]
ρ	Density	[kg/m^3]
μ	Viscosity	[Pa.s]
σ	Surface tension	[N/m]

Subscripts

b	bulk
eq	equivalent
f	liquid film
g	gas phase
i	interfacial
l	liquid phase
r	relative
t	total

CHAPTER 3. Mass Transfer in the Liquid Phase

3.1 Introduction

The appropriate quantification of liquid side resistance in the distillation process is still a matter of debate. In conventional distillation it is appreciated that there is a finite resistance in the liquid phase, though be it small. Consequently it is at times considered as having a negligible effect. In the case of extractive distillation, inadequate information is available to predict the extent of the liquid phases resistance. Therefore, in the case of extractive distillation it would be difficult to assume that the liquid phase resistance is negligible. The following chapter seeks to show the extent of the liquid phase resistance or whether it is masked by enhancement in the gas phase resistance.

3.2 Literature Review

A large number of papers are available in the literature looking at the estimation of liquid phase resistance in wetted wall columns. It should be noted though that the bulk of the investigators were concerned with the evaluation of this resistance for gas absorption, {Emmert et al., 1954; Vivian et al., 1956; Striba et al., 1955; Lamourelle et al., 1972; Henstock et al., 1979}. Experimental procedures involved the absorption or desorption of a sparingly soluble gas from a liquid film. Results indicated that mass transfer rate enhancement occurred when rippling and wave formation occurred on the liquid surface. Consequently the commonly employed Higbie's penetration theory for estimating liquid phase resistance was found to over-estimate this resistance where rippling occurred {Emmert et al., 1954; Vivian et al., 1956; Striba et al., 1955}. It is generally agreed that the observed enhancement, which occurred when rippling was present can be attributed to bulk mixing caused by the ripples as well as increased interfacial area.

Stemming from the experimentally observed transfer rate enhancement, subsequent papers focused on attempting to model the wave formation thus better predicting liquid phase resistance in wavy films, {Javdani, 1974; Banerjee et al., 1967; Imaishi et al., 1982; Wasden et al., 1990; Yoshimura et al., 1996}. Banerjee et al. {1967} and Yoshimura et al. {1996} use surface renewal models to illustrate the gas absorption in liquid films, with the latter incorporating wave characteristics in the model whilst the former took account of eddy formation in their model. Javdani {1974} and Wasden et al. {1990} used the convective-diffusion equation to model the absorption rate with the former including wave characteristics in the model. In their conclusion, Yoshimura et al. {1996} noted that evaluation of transfer rates from irregular three-dimensional waves still awaits a solution.

Portalski and Clegg {1971} experimentally observed in a wetted wall column that the rippling of the liquid film caused an increase in the interfacial area. The resultant increase in the interfacial area was small when the countercurrent air flow was below a particular critical value. An appreciable area rise was observed when the gas rate exceeded this value. It is believed that the hydrodynamic instability brought about by the rippling/wavy liquid film is responsible for the induction for interfacial turbulence {Sternling and Scriven, 1959}. It is this effect i.e., interfacial turbulence through the Marangoni effect, which influences the liquid phase mass transfer rate. A number of investigators have studied how the Marangoni effect impacts on the liquid phase transfer rate {Imaishi et al., 1982; Semkov et al., 1991; Vazquez et al., 1994}. The Marangoni effect as illustrated by Sternling et al. {1959} is caused by longitudinal variation of the interfacial tension on the interface. It has been found that depending on how the interfacial tension varies with surface concentration, this can lead to either significant mass transfer enhancement or no change in transfer rate at all.

Certain experimental work, {Jackson and Ceaglske 1950; Spiegel and Meier 1987} has shown that liquid phase resistance in mass transfer for conventional distillation can be considered to be negligible. Fair and Bravo

{1990} are of the opinion that in certain instances the resistance should be taken into account.

Crause {1998} and Erasmus {1999} both experimentally investigated the presence of liquid phase resistance in extractive distillation. Experimental work involved evaporation of binary liquid mixtures consisting of volatile and non-volatile components as well as cases were both components were volatile. A similar wetted wall column was used in every case, though Erasmus {1999} also included work were the column was lined with complex surface. Results obtained by Crause {1998} indicated that no liquid side resistance could be observed. Further, he observed enhancement in the overall mass transfer coefficients for most of the systems. He attributed the observed enhancement to the surface tension gradients present in the liquid film. Similarly Erasmus {1999} also found virtually no liquid side resistance in most of the systems investigated, though one of the systems did show some liquid side resistance. The observed resistance was much less than that predicted by the Higbie's penetration theory. He also observed the enhancement in the overall mass transfer coefficient, which in this case seemed to be coupled to the difference in surface tension between solute and solvent. Crause {1998} and Erasmus {1999} found that the observed enhancement could not be correlated with the Marangoni number.

There is no conclusive evidence in present literature affirming the argument that the liquid phase resistance can be assumed to be negligible in extractive distillation applications. Further investigation of liquid side resistance for different binary mixtures will have to be carried out.

3.3 Theory

The theory explaining mass transfer across a phase boundary when both phase resistances are non-negligible is given by Sherwood {1975}. The equation relating the individual phase resistances to the overall gas phase transfer resistance is given below:

$$\frac{1}{k_{og}} = \frac{1}{k_g} + \frac{m}{k_l} \tag{3.1}$$

where m is the slope of the equilibrium line and is defined as {Nieuwoudt, 1994}:

$$m = \frac{y_A}{x_A}\left(\frac{M_{r,l}}{M_{r,g}}\right)\left(\frac{\rho_g}{\rho_l}\right) \tag{3.2}$$

Where y_A is evaluated as P_{Ai}/P_t. P_{Ai} is the partial pressure of component A corresponding to the mole fraction of x_A in the liquid phase. The overall mass transfer coefficient can be calculated from {Crause, 1998}:

$$N_A = \frac{k_{og} P_t \Delta P_A}{RTP_{BM}} \tag{3.3}$$

In determining the experimental overall mass transfer coefficients, the molar flux is evaluated in a similar manner to the gas phase measurements in chapter 2. The molar flux is based on the total mass evaporated. This is assumed to be appropriate as only one of the binary mixture components is volatile. The mass transfer driving force for equation 3.3 in terms of the partial pressures is given as follows:

$$\Delta P_A = \frac{\left(P_{Ai} - P_{Ab}\right)_{inlet} - \left(P_{Ai} - P_{Ab}\right)_{outlet}}{\ln\left(\frac{\left(P_{Ai} - P_{Ab}\right)_{inlet}}{\left(P_{Ai} - P_{Ab}\right)_{outlet}}\right)} \tag{3.4}$$

P_{Ai} as mentioned is the partial pressure of component A at the interface and is calculated from the NRTL equation using the bulk liquid composition. It is assumed that there is no mass transfer driving force in the liquid phase. P_{Ab} is the free stream partial pressure of component A.

As mentioned earlier, interfacial turbulence may occur due to the Marangoni effect, believed to be brought about by surface tension gradients in the liquid film. This effect has been used to correlate observed enhancement through the Marangoni number {Imaishi et al., 1982; Semkov et al., 1991}. The Marangoni number has been defined in various forms, (see Semkov et al. {1991}), though the most convenient form for practical applications is:

$$Ma = \frac{\Delta\sigma}{\mu_l k_l} \tag{3.5}$$

where $\Delta\sigma$ is the difference between the interfacial tension and bulk phase surface tension, and given as:

$$\Delta\sigma = \sigma_i - \sigma_l \tag{3.6}$$

The interfacial surface tension σ_i is evaluated from the interfacial concentration C_{li}, and calculated from the following equation, {Imaishi et al., 1982}:

$$C_{li} = \frac{C_l}{(1+B)} \tag{3.7}$$

with B as the ratio of the separate mass transfer resistances and defined as follows:

$$B = \frac{mk_g}{k_l} \tag{3.8}$$

The gas phase mass transfer coefficient is evaluated from the correlation developed in chapter 2, namely equation 2.30a. Liquid phase transfer coefficient as defined by Vivian and Peaceman {1956} for a wetted wall column will be calculated from:

$$k_l = 2\sqrt{\frac{D_{AB}\, u_i}{\pi\, l}} \qquad (3.9)$$

Where l is defined as the height of the wetted wall column.

3.4 Experimental

Experimental work was conducted in the same wetted wall channel as described in section 2.4.1. A number of binary mixtures consisting of one volatile and one non-volatile component were evaporated in the triangular channel. Experimental work was performed for relatively low evaporation rates, thus minimising the liquid composition change as well as simplifying the analysis. The apparatus was operated at a temperature where the evaporated vapour consisted almost exclusively of the volatile component. Total volume in the experimental set-up is about 1350ml. To avoid large composition change in the binary mixture the average evaporated liquid volume was about 45ml. To ensure an almost constant liquid concentration throughout a series of experimental runs, the liquid reservoir was topped up with the volatile component of the liquid mixture after each run. Average liquid concentrations of the start and end of each series of experimental runs were used in the calculations.

3.5 Experimental Results

The experimental results are listed in Table A3-2 of Appendix 3. The binary liquid mixtures investigated are n-tridecane/cyclohexane, 1-octanol/n-hexane and n-decane/cyclohexane. The experimental overall mass transfer resistances are compared to the predicted values evaluated from equation 3.1. The gas phase coefficient is calculated from the correlation developed in chapter 2, whilst the liquid side transfer coefficient is calculated from Higbie's penetration theory given by equation 3.9. The experimental overall mass transfer coefficients are calculated from equation 3.3, from the measured

molar flux and the mass transfer driving force at the prevailing operating conditions. Experimental overall mass transfer coefficients are also compared to the gas phase mass transfer coefficients.

To illustrate the experimental results two diagrams are given for each binary system that was investigated (see figures 3.5.1- 3.5.3). Parts (a), of these figures indicate comparisons between the measured overall mass transfer coefficients and the predicted gas phase mass transfer coefficients. In these figures (3.5.1- 3.5.3 parts (a)) the Mass Transfer Group (MTG) is defined as:

$$= 0.00219\, Re_{g,r}$$

for correlation 2.30a, and

$$= \frac{Sh_{og}}{Sc_g^{0.5}\, Fr_l^{0.22}}$$

for the experimental data. Where Sh_{og} is calculated for k_{og} as determined from equation 3.3.

The second parts of figures 3.5.1-3.5.4, i.e. parts (b), compare the overall experimental transfer coefficients as evaluated from equation 3.3 to the overall transfer coefficients as predicted by equation 3.1. The individual phase transfer coefficients used in equation 3.1 are calculated from correlation 2.30a for the gas phase coefficients and equation 3.9 for the liquid phase coefficients.

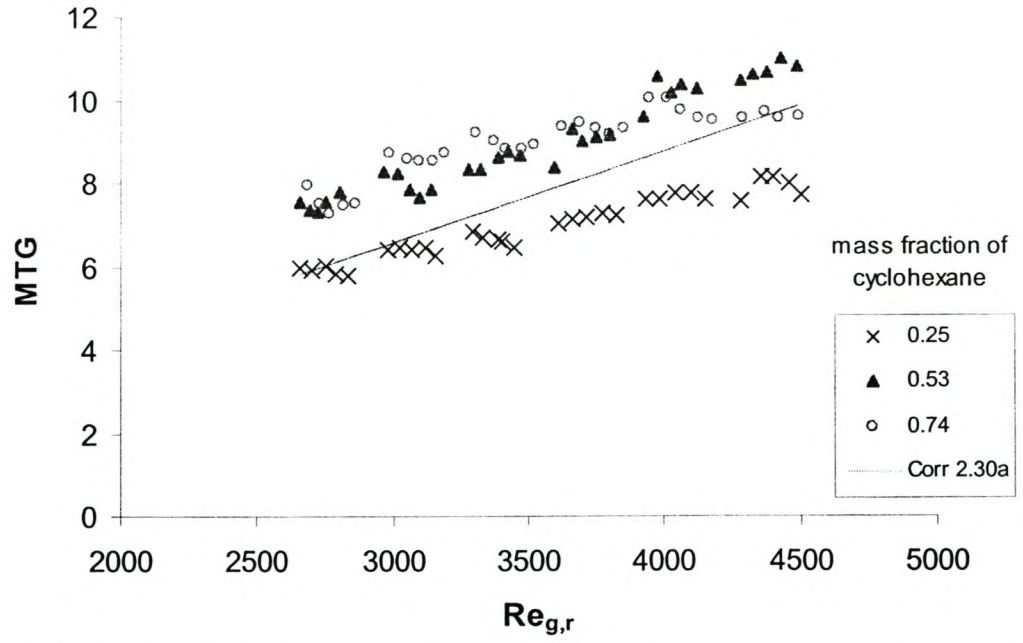

Figure 3.5.1(a) Graphical illustration of experimental mass transfer with correlation 2.30a for n-tridecane/cyclohexane. $11<Re_l<50$; $2520<Re_g<4180$

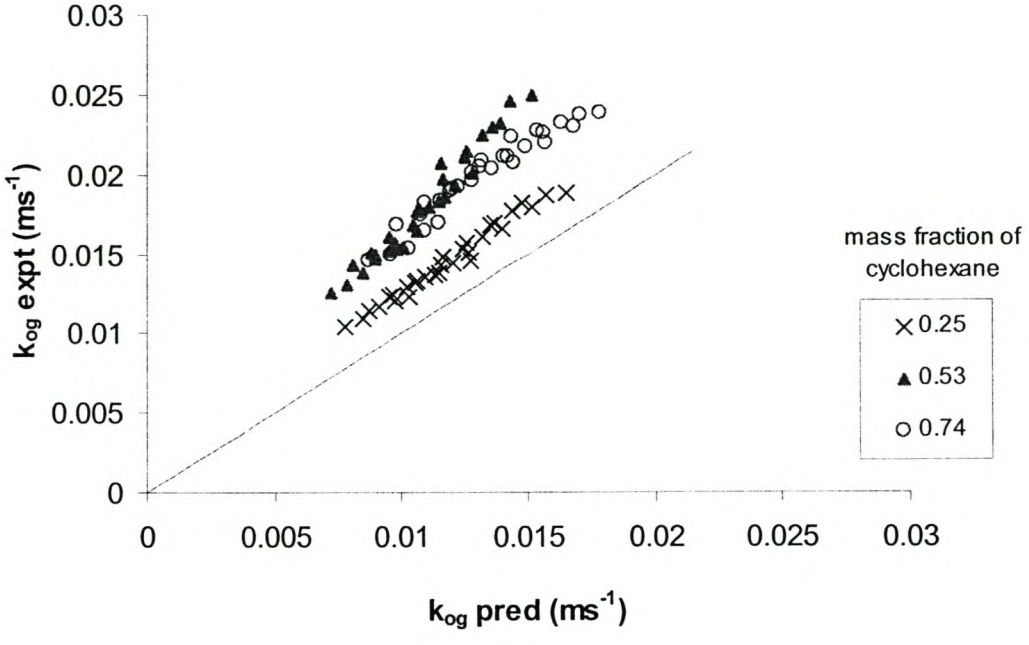

Figure 3.5.1(b) Graphical illustration of the experimental k_{og} and predicted k_{og} for n-tridecane/cyclohexane. The predicted k_{og} values are calculated from equation 3.1.

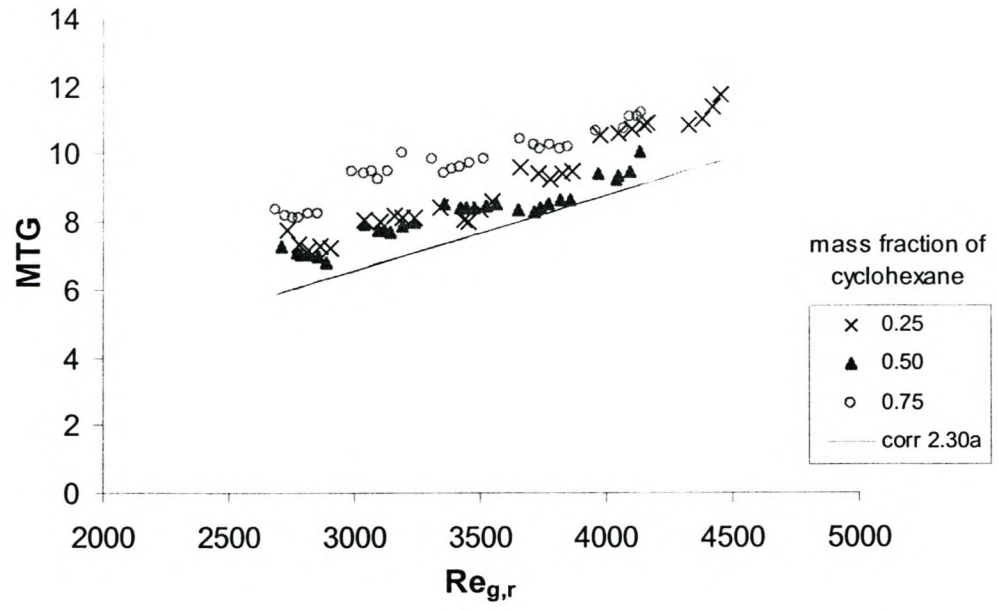

Figure 3.5.2(a) Graphical illustration of experimental mass transfer with correlation 2.30a for n-decane/cyclohexane. $27<Re_l<65$; $2500<Re_g<4110$

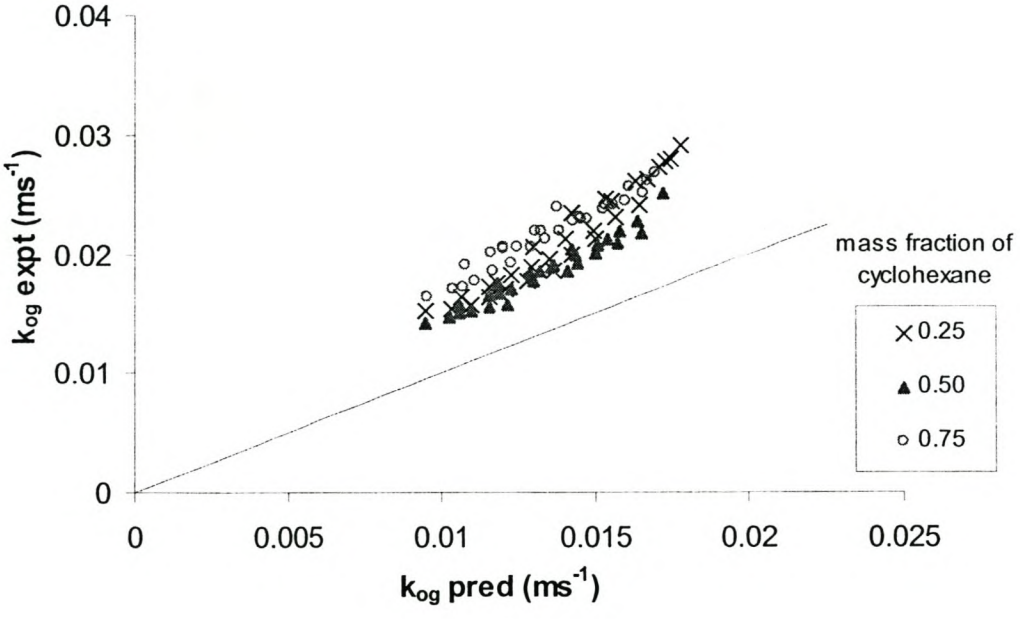

Figure 3.5.2(b) Graphical illustration of experimental k_{og} and predicted k_{og} for n-decane/cyclohexane. The predicted k_{og} values are calculated from equation 3.1.

Figures 3.5.1-3.5.2, parts (a) and (b) show comparisons between experimental and predicted mass transfer coefficients for n-tridecane/cyclohexane and n-decane/cyclohexane respectively. For both the systems no VLE data could be found in literature to calculate m in equation 3.2. Consequently interaction parameters used in the NRTL model were estimated from UNIFAC group contribution method in the Pro II simulation package. The n-tridecane used in experiments was distilled from a mixture of heavy cut paraffins and ethanol. The distilled product consisted of n-tridecane with an approximate purity of 95% whilst the remainder of the distillate constituted non-volatile long chain paraffins.

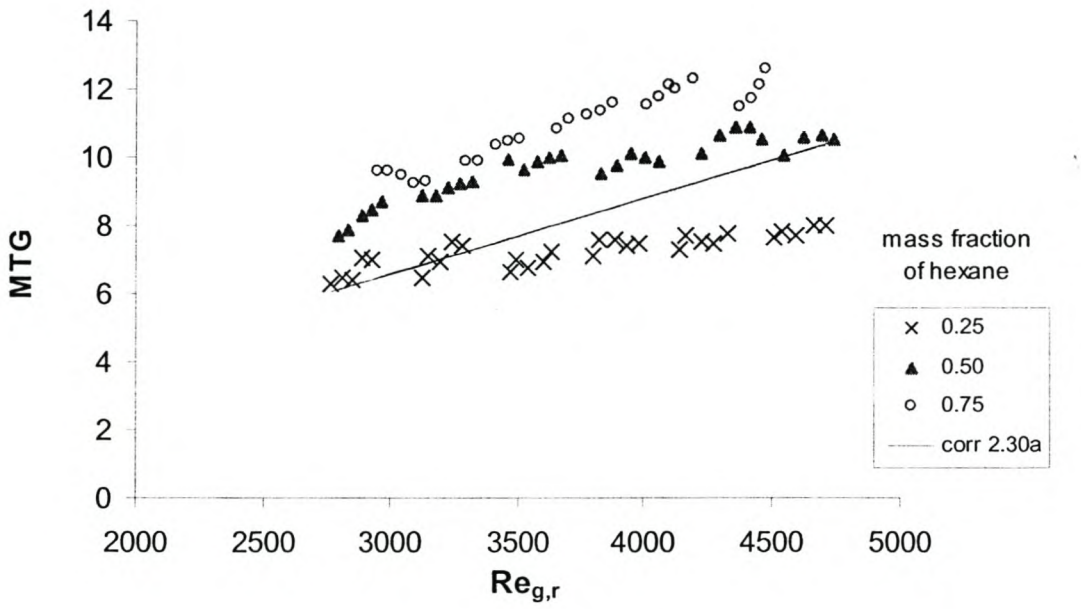

Figure 3.5.3(a) Graphical illustration of experimental mass transfer with correlation 2.30a for 1-Octanol/n-hexane. $6 < Re_l < 82$; $2640 < Re_g < 4490$

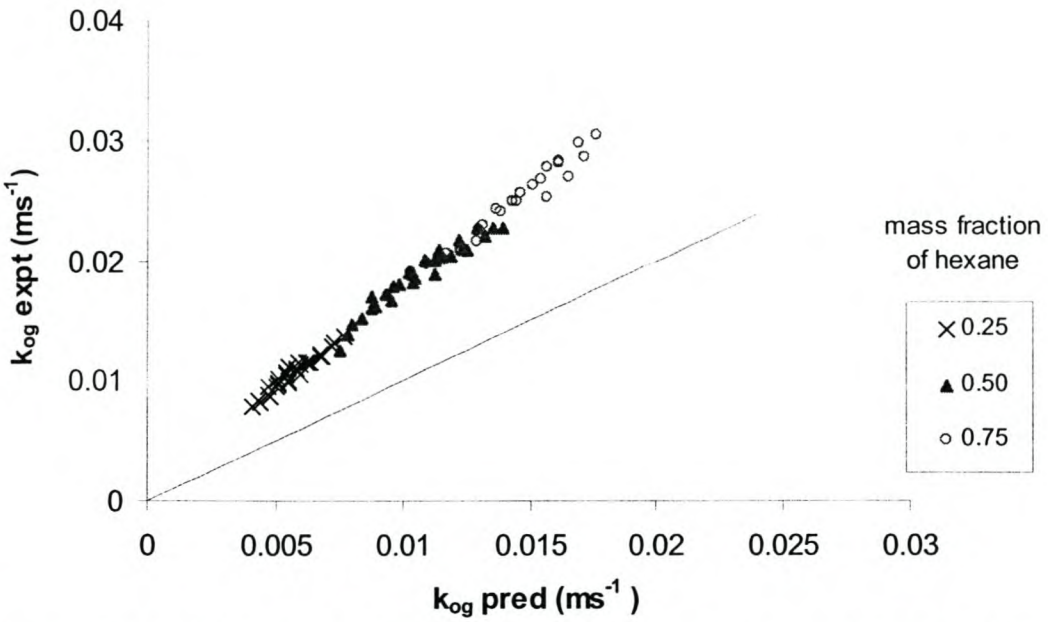

Figure 3.5.3(b) Graphical illustration of experimental k_{og} and predicted k_{og} for 1-Octanol/n-hexane. The predicted k_{og} values are calculated from equation 3.1.

3.6 Discussion of Results

It is observed that for the systems, n-tridecane/cyclohexane, n-decane/cyclohexane and 1-octanol/hexane the experimental overall transfer resistance is less than the gas phase resistance {see figure 3.5.1-3.5.3 parts (a)}. Therefore the experimental overall transfer coefficients are actually greater than the predicted gas phase coefficients from correlation 2.30a. It can be seen that at certain mass fractions of the volatile component for both n-tridecane/cyclohexane and 1-octanol/hexane a quantifiable liquid side resistance is observed which seems to increase with increasing gas flow rate. Parts (b) of figures 3.5.1-3.5.3 show comparisons between experimental transfer coefficient and the predicted value as evaluated from equation 3.1. It can be observed that the experimental coefficient is greater than the overall coefficient predicted by equation 3.1, as the data points lie above the x=y line.

From figures 3.5.1-3.5.3 a general trend seems to emerge showing that with decreasing mass fraction of the volatile component there is a corresponding decrease in the overall mass transfer coefficient. This trend indicates the presence of some liquid resistance, which gets progressively larger resulting in a decreasing overall mass transfer coefficient. To appropriately quantify the liquid resistance would be difficult as the evaluation of the gas phase mass transfer coefficient is not accurate. It can be observed from the graphs that there is no quantifiable liquid resistance for almost all the cases. This can probably be attributed to a significant enhancement in the gas phase mass transfer coefficient. The enhancement of the gas phase coefficient could result from various factors, including increased effective area as well as increased interfacial turbulence.

Previous studies have been conducted in wetted wall columns with smooth surfaces, {Crause, 1998; Erasmus, 1999}, for binary systems with one volatile component. It was found that for most of the mixtures investigated the overall mass transfer coefficients were larger than the predicted gas phase coefficients. Similar results have been obtained in this work (see figures 3.5.1-3.5.3 (a)) where most of the experimental k_{og} data points lie above correlation 2.30a. The mechanism responsible for the transfer rate enhancement is deemed to result from the flow instabilities that are brought about by the evaporation of the volatile component from the binary mixture. This effect would probably be among the reasons as to why the measured k_{og} values are higher than the predicted k_g values for both smooth surface and complex surface wetted wall channels. The extent of the transfer rate enhancement will to a large degree depend on the particular binary system. The flow instabilities brought about by a mixture are thought to induce turbulence in the gas phase and thus enhancement of the transfer rate, Erasmus {1999}. Therefore, as this instability will depend on the interactions of a particular binary mixture, it then follows that the enhancement will to an appreciable degree depend on the particular mixture.

From the results of the binary mixture n-tridecane/cyclohexane it can be observed that the measured transfer rate decreases with decreasing mass fraction of the volatile component, (see figures 3.5.1(a) and (b)). For this particular mixture a quantifiable liquid resistance can be observed at the lowest mass fraction of the volatile component, see figure 3.5.1(a). The binary interaction parameters used in the evaluation of the component vapour pressures of the mixture, were estimated from the UNIFAC group contribution method. The experimental determination of these parameters will confirm whether or not the observed liquid resistance is as significant as obtained in the results.

The n-decane/cyclohexane system shows enhancement at various volatile component mass fractions, see figure 3.5.2(a) and (b). The observed enhancement of the measured transfer rates for this particular mixture seems to be independent of the composition.

For 1-octanol/hexane results seem to show, figure 3.5.3(a) that mass transfer enhancement is related to composition, as enhancement is seen to increase with increasing volatile composition. It should be noted that experimental interaction parameters used in evaluating the vapour pressures are from the NRTL equation, as obtained from Gmehling et al. {1990}. This should give credence to the observed liquid phase resistance.

Results generally seem to show a trend of enhancement of the overall mass transfer coefficient. To illustrate this enhancement of mass transfer, a factor describing this enhancement is defined as follows:

$$F = \frac{Sh_{og}\ measured}{Sh_{g}\ predicted} \qquad (3.10)$$

The enhancement factor is averaged over a particular mass fraction of the volatile component for each of the mixtures (see table 3.1).

Table 3.1 Binary mixture enhancement factors

Mass fraction: component 1	Viscosity (Pa.s) x 10^{-4}	Surface tension difference $\sigma_{mix} - \sigma_1$ (mN/m)	F
cyclohexane (1)/n-tridecane (2)			
0.25	10.33	0.867	0.90
0.53	8.95	0.539	1.15
0.74	7.55	0.233	1.16
cyclohexane (1)/n-decane (2)			
0.25	6.50	-0.434	1.15
0.50	6.50	-0.310	1.09
0.75	6.53	-0.143	1.29
n-hexane (1)/1-octanol (2)			
0.25	18.35	6.60	0.90
0.50	7.71	3.85	1.18
0.75	4.59	2.02	1.33

A couple of reasons could be responsible for the augmentation of the overall transfer rate, these including increased interfacial turbulence and increased area for transfer. It has been found that in certain systems where interfacial turbulence occurs, a significant enhancement in the mass transfer rate can be observed, {Sherwood, 1975}. Interfacial turbulence could result from the random variation of interfacial tension at the interface that results from concentration variation as mass transfer occurs. This effect, which leads to the instability of the liquid film arising from formation of circulation cells, is generally termed the Marangoni effect.

It is believed that among the effects of the Marangoni effect is the enhancement of the transfer surface, {Dijkstra, 1990}. This is thought to occur for systems where the transferred component has a lower surface tension than the bulk phase. A number of investigators have observed that the

presence of waves on the liquid surface can lead to enhanced mass transfer rates, {Emmert et al., 1954; Striba et al., 1955}. These enhanced transfer rates are thought to result from various factors including the increased transfer area brought about by the wavy nature of the liquid surface. It is possible that the enhancement of the transfer surface resulting from the Marangoni effect could contribute to the observed enhanced mass transfer rates. This would apply to systems where the transferred component has a lower surface tension than the bulk phase.

For certain cases in table 3.1 no transfer rate enhancement was observed. It is known that liquid film flow over complex surfaces can at certain liquid rates form stagnation zones, {Zhao and Cerro, 1992}, which could possibly lead to a reduction in the transfer rates. Furthermore, due to the cross-section geometric configuration of the wetted wall channel there is a distinct possibility of the formation of rivulet like film flow at certain flow conditions. This could also lead to reduced transfer rates. If these effects did not influence the transfer rate, then it is possible that a significant liquid resistance was present for the cases where no transfer rate enhancement was observed.

It can be observed from table 3.1 that an increase in surface tension difference did not correspond to a simultaneous increase in the enhancement factor. It is thought that the enhancement of the gas phase mass transfer coefficient depends on surface tension gradients in the liquid phase {Crause, 1998}. Liquid film hydrodynamics can also be expected to have an affect on the mass transfer rates. It has been observed that the liquid interface is destabilised by the formation of intermittent waves {Negny et al., 2001}. The waves are thought to contribute to the enhancement of the mass transfer rates {Negny et al., 2001}. It is possible that the effect of the liquid film hydrodynamics may have a larger influence on the mass transfer rate than the surface tension gradients. This could be possible because the surface tension difference is small for the cases investigated in this work. Therefore, this could explain why an increase in the surface tension difference does not correspond to an increase in the enhancement factor.

The system n-decane/ cyclohexane included in experimental work so as to induce the negative Marangoni effect as the evaporated liquid is of a higher surface tension than the bulk phase. As can be seen from table 3.1 no reduction in the transfer rate is observed for this system. A plausible explanation for this could be the lack of a significant surface tension gradient at the interface. Surface tension difference between non-volatile and volatile component is only –0.8mN/m.

If the Marangoni effect is deemed as influencing the observed mass transfer enhancement, it would be appropriate to attempt to correlate the enhancement as a function of the Marangoni number. However, there is no proof supporting the argument that the mass transfer enhancement can be correlated in terms of the Marangoni number, {Imaishi et al., 1982}. Attempts at correlating the mass transfer enhancement with the Marangoni number are given by Imaishi et al., {1982} and Semkov et al., {1991}. They defined an equation of the form:

$$F = \left(\frac{Ma}{Ma_c} \right)^n \tag{3.11}$$

where n = 0.4 ± 0.1 and Ma_c (critical Marangoni number) taken as the value when F = 1.

Certain impediments do arise in estimating the Marangoni number as illustrated by Crause {1998}, these being:

- Accuracy of existing correlations for evaluating liquid diffusion coefficient has been found to questionable.
- No turbulent flow correlation for estimating liquid phase coefficient. k_l estimated from Higbie's penetration theory in evaluating predicted k_{og} for this work.
- Concentration gradient of the liquid phase required in evaluating interfacial surface tension.

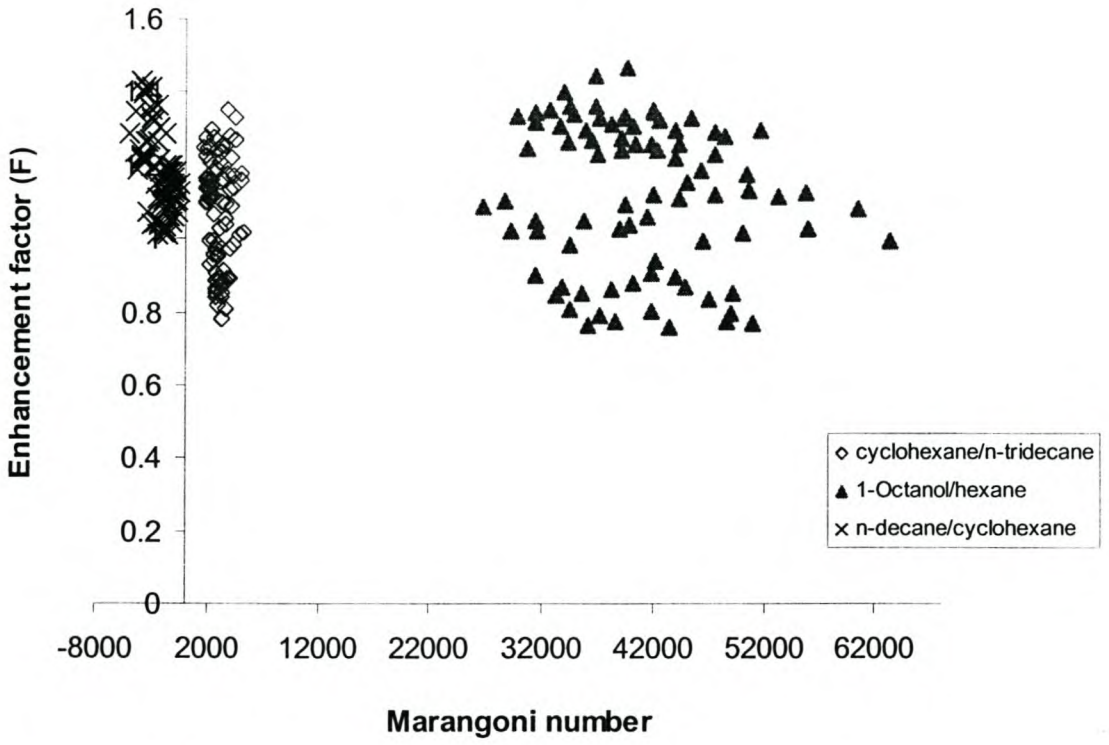

Figure 3.6.1 Graph of enhancement and Marangoni

From figure 3.6.1 it can be seen that no correlation exists between the mass transfer enhancement factor and the Marangoni number. As earlier mentioned, difficulty arises from the estimation of the Marangoni number, therefore this could possibly affect what is observed. The negative Marangoni numbers obtained for n-decane/cyclohexane binary mixture are expected, since the volatile component has a higher surface tension than the bulk phase.

Earlier work conducted in a smooth surface wetted wall column, {Crause, 1998 and Erasmus, 1999} show a similar trend of transfer enhancement where surface tension gradients are present. Of all the binary systems that were investigated in earlier wetted wall work with smooth surfaces, none are identical to those investigated in this work. Consequently no direct comparison can be made of the surface effect on the experimental mass transfer coefficients. It can be expected though that correlations developed in these studies would tend to predict higher enhancement factors. Reasoning

behind this is that correlations developed for the smooth surface tended to over predict experimental gas phase transfer coefficient for this work as is shown in chapter 2. Table 3.2 shows comparisons of enhancement factors predicted by this work and correlations developed by Crause {1998} and Erasmus {1999}.

Table 3.2 Comparison of enhancement factors

Mass fraction of (1)	This Work	Crause {1998} - smooth surface	Erasmus {1999} - smooth surface
cyclohexane(1)/n-tridecane(2)			
0.25	0.90	1.13	1.14
0.53	1.15	1.41	1.42
0.74	1.16	1.53	1.53
cyclohexane(1)/n-decane(2)			
0.25	1.15	1.56	1.60
0.50	1.09	1.45	1.50
0.75	1.29	1.71	1.77
n-hexane(1)/1-octanol(2)			
0.25	0.90	0.93	0.93
0.50	1.18	1.51	1.49
0.75	1.33	1.97	1.91

It can clearly be seen in table 3.2 that correlations developed in earlier wetted wall work predict higher enhancement factors. It is highly feasible that higher enhancement factors can occur in smooth surface columns as compared to complex surface columns. It has been observed that liquid films over smooth surface columns are not entirely wavy over the length of the column {Erasmus, 1999}. The presence of waves on the liquid surface is thought to induce interfacial turbulence {Crause, 1998}. It has also been attributed to the increase in the transfer area for mass transfer {Reker et al., 1966}. In a smooth surface column Crause {1998} observed visually the liquid surface to be more turbulent in binary mixture experiments as compared to single component evaporation experiments. The liquid surface in complex surface

columns is inherently wavy in both k_{og} and k_g experiments. Therefore, the expected enhancement factors in complex surface columns may not be as significant as those in smooth surface columns. This comparison would only be applicable if relative flow conditions were of similar magnitudes in both cases.

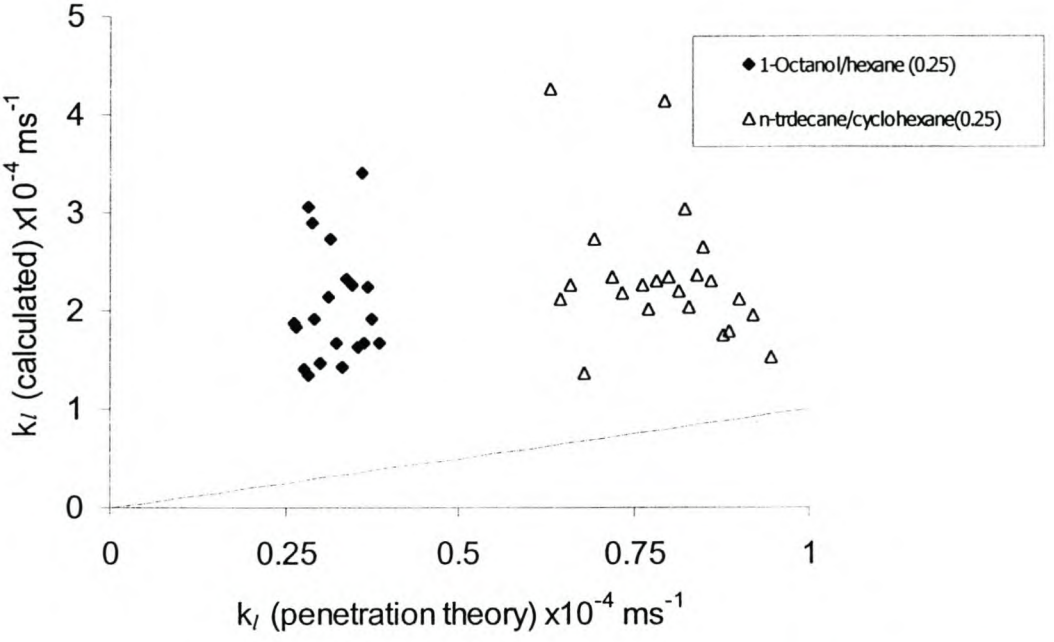

Figure 3.6.2 Plot of calculated k_l and predicted k_l. Predicted k_l evaluated from Higbie's penetration theory. Values in brackets indicate volatile component mass fraction.

Figure 3.6.2 above shows a plot of calculated k_l values against predicted values. The calculated k_l values are obtained from equation 3.1. The k_{og} values used in equation 3.1 are determined for the experimental measurements with equation 3.2. The k_g values used in equation 3.1 are calculated from equation 2.30a. The predicted k_l values are evaluated from Higbie's penetration theory (equation 3.9). It should be noted that k_l was only evaluated for the cases where a positive liquid resistance was found. This diagram gives an indication as is to be expected, that the calculated k_l values are much larger than the predicted ones. The penetration theory is estimated for laminar conditions therefore it only serves as an estimate for liquid side

resistance under turbulent conditions. Therefore, the penetration theory is unable to characterise liquid resistance for turbulent flow conditions, as is the case in this work.

3.7 Summary

- For the binary mixtures investigated, the general trend observed showed decreasing overall mass transfer rate with increasing non-volatile mass fraction. This indicates that there is some liquid resistance in the mixtures.
- The liquid resistance was not quantifiable for almost all cases except at the lowest volatile mass fractions of n-tridecane/cyclohexane and 1-octanol/hexane.
- For all the cases where a quantifiable liquid resistance was not observed, it was found that the measured overall mass transfer coefficient was larger than the predicted gas phase mass transfer coefficient.
- In the cases where mass transfer enhancement was observed it may be due to the enhanced turbulence at the interface and increased interfacial area.
- Increased turbulence could be affected by variation in liquid profile over the complex surface during mass transfer. A further effect could be through the Marangoni effect. No correlation could be found between enhancement and Marangoni number.
- No relationship between the surface tension difference and enhancement factor could be found for the systems investigated.
- For the cases where liquid side resistance was present it was found that Higbie's penetration theory under predicts the liquid side mass transfer coefficient.

The results seem to indicate that some liquid resistance would likely occur where components have similar surface tensions. The extent of the liquid resistance will definitely vary depending on the system; consequently further investigation would assist in quantifying this effect. The enhancement in the gas phase mass transfer rate completely masks the liquid phase resistance

that is present in the binary mixtures. In the development of the correlations in chapter 2 smooth surface hydrodynamics were used. It would be more appropriate that for future work, the hydrodynamic analysis should be based on the surface structure of the particular column wall.

Nomenclature

Symbol	Description	Unit
B	ratio of transfer resistances	
C	Concentration	[mol/m^3]
D_{AB}	Diffusion coefficient of A in B	[m^2/s]
F	Enhancement factor	
Fr	Froude number	
k	Mass transfer coefficient	[m/s]
l	length	[m]
m	slope of equilibrium line	
Ma	Marangoni number	
MTG	Mass transfer group	
M_r	Molecular mass	[g/mol]
N	Molar flux	[mol/(s.m^2)]
P	Pressure	[Pa]
P_{BM}	Mean pressure of B	[Pa]
R	Universal gas constant, 8.314	[J/(mol.K)]
Re	Reynolds number	
Sc	Schmidt number	
Sh	Sherwood number	
T	Temperature	[K]
u	Velocity	[m/s]
x	liquid mol fraction	
y	gas/vapour mol fraction	

Greek symbols

Symbol	Description	Unit
Δ	Difference	
ρ	Density	[kg/m^3]
μ	Viscosity	[Pa.s]
σ	Surface tension	[N/m]

Subscripts

c	critical
g	gas phase
i	interfacial
l	liquid phase
mix	mixture
og	overall gas phase
r	relative
t	total

Superscripts

n	exponent

CHAPTER 4. Distillation Modelling with Structured Packed Columns

4.1 Introduction

The process industry has in recent times seen a considerable increase in columns with structured packing especially in distillation, as it is the predominant separation process. The principle reasons behind this include the increased capacity, lower pressure drop and efficiency advantage of structured packing as compared to other column internals at similar conditions. The use of structured packing is limited somewhat as the performance of structured packed columns is not fully understood. The performance of structured packed columns may be described by the HETP or HTU, which include transfer resistances of both phases and effective transfer area. The HETP approach has been found to be a convenient way of describing column performance. The HETP values generally do not vary as widely with physical conditions as the mass transfer coefficients, {Seader and Henley, 1998}. To develop a more fundamental understanding of structured packing performance, reporting column efficiency in terms of separate transfer resistances could be seen as a step in the right direction.

4.2 Literature Review

In describing structured packed column performance certain works do include the hydraulic models as well. As this work is concerned with the development of a mass transfer model, the hydraulic modelling is not reported in the review below.

One of the earliest and most recognised works describing structured packing performance is that by Bravo et al. {1985}. This initial work was developed for gauze-type structured packing. This model is built on the view that a packed

element consists of a series of parallel inclined wetted wall columns. Consequently they employed a Gilliland and Sherwood {1934} type correlation to describe the gas phase mass transfer with the following relationship:

$$Sh_g = 0.00338\,\mathrm{Re}_{g,r}^{\ 0.8}\, Sc_g^{\ 0.333} \tag{4.1}$$

The liquid side mass transfer coefficient was modelled using Higbie's penetration theory as follows:

$$k_l = 2\left[\frac{D_L u_{l,eff}}{\pi S}\right]^{0.5} \tag{4.2}$$

They further assumed that effective area (a_e) is equal to surface area (a_p) as the gauze nature of the packing promotes capillary action even at low liquid rates. Thus the packing is essentially completely wetted at all liquid rates. The equivalent diameter was taken as the average between the triangular and rhombic cross-section geometry's and defined as follows:

$$d_{eq} = \frac{Bh}{\left(\frac{1}{2S} + \frac{1}{B+2S}\right)} \tag{4.3}$$

This initial model has undergone considerable changes to better represent efficiency of structured packing, not only for sheet metal packing but also for sheet packing of different materials. As the earlier model was developed for gauze packing, the model has been corrected to cater for sheet metal packing. Initial changes included catering for the fraction of wetted surface in sheet metal packing by the following equation, Fair and Bravo {1990}:

$$\frac{a_e}{a_p} = 0.5 + 0.0058(\%\,flooding) \tag{4.4}$$

Furthermore the characteristic length was changed and the equivalent diameter was set equal to the corrugation side, S, {Fair and Bravo, 1990}. This characteristic length was used in all subsequent papers to date. Rocha et al. {1996} carried out further work and they adjusted the correlations for evaluating transfer coefficients as follows:

$$Sh_g = 0.0054 \mathrm{Re}_{g,r}^{\ 0.8} Sc_g^{\ 0.333} \tag{4.5}$$

$$k_l = 2\left[\frac{D_L C_E u_{l,eff}}{\pi S}\right]^{0.5} \tag{4.6}$$

Where C_E is a correction factor accounting for parts of the packed bed that do not promote rapid surface renewal. The changes for the gas phase correlation were not supported by wetted wall work. Other modifications included a different correlation for evaluating the effective transfer area for gauze packing. The relationship is given by:

$$\frac{a_e}{a_p} = 1 - 1.203\left(u_{ls}^{\ 2} / Sg\right)^{0.111} \tag{4.7}$$

Rocha et al. {1996} also altered the correlation for evaluating the effective area for sheet metal packing and adopted the correlation developed by Shi and Mersmann {1985} for rivulet flow down an inclined plane. Using this same equation Gualito et al. {1997} adapted it to include adjustable parameters, which cater for variation of packing material. The final form as given by Gualito et al. {1997} is:

$$\frac{a_e}{a_p} = \frac{\left(We_l\, Fr_l\right)^{0.15} A_1 S^{A_2}}{\mathrm{Re}_l^{\ 0.2}\, \varepsilon^{\,0.6}\left(1 - 0.93\cos\gamma\right)\left(\sin\theta\right)} \tag{4.8}$$

Where parameters A_1 and A_2 are functions of packing material. It should be noted that these parameters were back calculated from experimental mass transfer and pressure drop work in structured packed distillation columns.

Gualito et al. {1997} do list the parameter values as t eet metal, ceramic and plastic structured packing.

Spiegel and Meier {1987} determined performance cha ent Mellapak structured packed columns in distillation. S al. {1985} their gas phase mass transfer model was bas wall analogy. Their graphical plot of gas Reynolds number ood number indicated a direct proportionality between the e a gradient of 1. For gauze packing, Bravo et al. {1985} to 0.8 from the Gilliland and Sherwood work and refitte itial constant. Spiegel and Meier {1987} explain the di nts between sheet metal and gauze packing by the wett uze packing it is assumed that the geometric surface is c For sheet metal packing it is thought that the interfacia with increasing liquid load. Based on these assumption eier {1987} gave a gas phase mass transfer relationship of t

$$Sh_g \alpha\ Re_g^{0.8}\ Sc_g^{1/3}$$

No proportionality constant was given.

For the effective transfer area for sheet metal pacl d a relationship in terms of liquid density and velocity in the

$$a_e \alpha \left(\rho_l u_{l,s}\right)^{0.2}$$

As with the mass transfer relationship no proportional ven for the transfer area relationship. They ignored the liqu sfer coefficients as it was found that $k_l > k_g$ always and often

Nawrocki et al. {1991} simulated the performance of by establishing a fluid flow mechanism model for liquid dis low over the packing surface. They employed the same n l as

that of Bravo et al. {1985}. They used a slightly different definition of the effective liquid velocity. In establishing the liquid distribution model, it was perceived that the liquid flowing on the surface of any channel would split into two at each intersection point. Using the simulated results of the liquid distribution they were able to determine liquid flow rates at each intersection in the packing element.

Weiland et al. {1993} measured the performance of two structured packings using absorption and desorption experiments for obtaining gas phase and liquid phase transfer coefficients respectively. The work also included the determination of the gas-liquid interfacial area. Goodloe and Montz A2 packing were investigated and the developed phase transfer correlations for the respective packing given as follows:

Goodloe packing:

$$Sh_g = 0.0567\,\mathrm{Re}_g^{\,1.10}\,Sc_g^{\,1/3} \tag{4.11}$$

$$Sh_l = 3.4\,\mathrm{Re}_l^{\,-0.08}\,Sc_l^{\,1/2} \tag{4.12}$$

Montz A2 packing:

$$Sh_g = 0.0373\,\mathrm{Re}_g^{\,1.02}\,Sc_g^{\,1/3} \tag{4.13}$$

$$Sh_l = 5.2\,\mathrm{Re}_l^{\,-0.04}\,Sc_l^{\,1/2} \tag{4.14}$$

With the interfacial area correlations given as:

Goodloe packing: $a_e = 356F^{-0.2}$ (4.15)

Montz A2 packing: $a_e = 265F^{-0.4}$ (4.16)

Where F is the F-factor as evaluated from gas velocity and gas density.

Billet and Schultes {1993} developed a model describing the performance of random packed columns as well as structured ones. The phase transfer coefficients evaluated from Higbie's penetration theory for either phase. Equations given as follows:

$$k_l = \frac{2}{\sqrt{\pi}} \sqrt{D_l \frac{1}{\tau_l}} \tag{4.17}$$

$$k_g = \frac{2}{\sqrt{\pi}} \sqrt{D_g \frac{1}{\tau_g}} \tag{4.18}$$

with,

$$\tau_l = h_l l_\tau \frac{1}{u_l} \tag{4.19}$$

$$\tau_g = (\varepsilon - h_l) l_\tau \frac{1}{u_g} \tag{4.20}$$

τ_l is the time necessary for renewal of the interfacial area

τ_g is the time of contact corresponding to flow path length, l_τ

The effective transfer area is evaluated from the following equation:

$$\frac{a_e}{a_p} = 1.5\left(a_p d_{eq}\right)^{-0.5} \mathrm{Re}_l^{-0.2} We_l^{0.75} Fr_l^{-0.45} \tag{4.21}$$

with the equivalent diameter being evaluated from:

$$d_{eq} = 4\frac{\varepsilon}{a_p} \tag{4.22}$$

Further developments of this model are given in Billet and Schultes {1999}. The significant change was the inclusion of the Marangoni number in the

effective transfer area equation (see equation 4.23). It was primarily included to cater for distillation systems that show a reduction in surface tension as mass transfer occurs, i.e. negative systems. The equation as applies to the distillation of negative systems was given as follows:

$$\left(\frac{a_e}{a_p}\right)_{neg.\ sys.} = \left(\frac{a_e}{a_p}\right)_{Equ\ 4.21} \left(1 - 2.4\times10^{-4}\ |Ma_L|^{0.5}\right) \qquad (4.23)$$

The effective transfer area is evaluated from equation 4.21 for the distillation of neutral and positive surface tension systems. Finally it has be noted that for evaluating packing performance in terms of HETP or HTU, specific packing constants are required. Unfortunately neither the initial nor the updated paper gives constants for Mellapak or Flexipac packing.

Shetty and Cerro {1997} theoretically estimated design parameters in structured packing based on fluid flow patterns over a periodic complex surface. In evaluating the gas phase mass transfer coefficient they adopted the correlation as given by Rocha et al. {1996}, i.e. equation 4.5. For estimating the liquid side mass transfer coefficient they employed Higbie's penetration theory. The contact time used in calculating this coefficient was determined from integration of the velocity profile for a period of the complex surface. The final form of the equation for calculating the liquid side coefficient was given as:

$$Sh_l = 0.4185\sqrt{\frac{\sin\theta}{l_{ratio}}}\ \mathrm{Re}_l^{1/3}\, Ga_l^{1/6}\, Sc_l^{1/2} \qquad (4.24)$$

l_{ratio} defined as the ratio of actual path length to path length for $\theta = 90^o$

In evaluating the interfacial area for mass transfer, Shetty and Cerro {1997} numerically integrated the free surface profiles as obtained from integration of film evolution equation. The interfacial area per unit packing width was calculated from the following equation:

$$A_W = 2\sum\sqrt{dy_{fs}^{\ 2} + dx^2} \tag{4.25}$$

Equation 4.25 was used in the evaluation of the solid surface area ($y = y_s$) and the free surface area ($y = y_{fs}$) per unit width. The effective area was defined as the ratio of the free surface to the solid surface area. The interfacial area per unit column volume was given as follows:

$$a_e = \frac{4\sum\sqrt{dy_{fs}^{\ 2} + dx^2}}{a^{\ 2}} \tag{4.26}$$

Where a is the solid surface period and x is the dimensional co-ordinate direction.

Crause {1998} used a modified wetted wall correlation to characterise the gas phase mass transfer rate in the mass transfer model for structured packed columns. In the modelling he assumed that total surface area is wetted and that liquid side resistance can de considered to be negligible in distillation applications. In the application of the model, he viewed liquid as flowing vertically through the packing. He modified the gas phase correlation by introducing a packing factor, F_p, and correlation given as follows:

$$Sh_g = 0.00283 F_p \,\mathrm{Re}_g \,\mathrm{Re}_l^{\ 0.08}\, Sc_g^{\ 0.5} \tag{4.27}$$

Evaluated an F_p factor of 1.03 for Mellapak 350Y.

Olujic et al. {1999} developed a corrugation geometry based model for performance of structured packed columns, commonly termed the Delft model. The model views the packing element as consisting of triangular flow channels. Furthermore from packing element to packing element, these triangular flow channels are viewed as describing a zigzag flow path. In calculating the gas phase mass transfer coefficient they assume that the

transfer coefficient can be represented by an average of laminar and turbulent flow contributions. This is given by the following equation:

$$k_g = \sqrt{k_{g,lam}{}^2 + k_{g,turb}{}^2} \tag{4.28}$$

and respective transfer coefficients are evaluated from:

$$Sh_{g,lam} = 0.664 Sc_g{}^{1/3} \sqrt{\mathrm{Re}_{g,r} \frac{d_{eq}}{l_{g,pe}}} \tag{4.29}$$

$$Sh_{g,turb} = \frac{\mathrm{Re}_{g,r}\, Sc_g \frac{f_{gl}\varphi}{8}}{1 + 12.7\sqrt{\frac{f_{gl}\varphi}{8}}\left(Sc_g{}^{2/3} - 1\right)} \left[1 + \left(\frac{d_{eq}}{l_{g,pe}}\right)^{2/3}\right] \tag{4.30}$$

Where, φ is the fraction of the cross-sectional area of the triangular flow channel occupied by liquid, $l_{g,pe}$ is the length of the gas flow channel in a packing element, f_{gl} is the gas-liquid friction factor. For the complete form of evaluating these parameters the reader is referred to the literature. The equivalent diameter was based on the triangular gas flow channel with a thin liquid film of constant thickness on the corrugation sides. The equation describing the equivalent diameter was given as follows:

$$d_{eq} = \frac{\frac{(Bh - 2\delta S)^2}{Bh}}{\left[\left(\frac{Bh - 2\delta B}{2h}\right)^2 + \left(\frac{Bh - 2\delta S}{B}\right)^2\right]^{0.5} + \frac{Bh + 2\delta S}{2h}} \tag{4.31}$$

In evaluating the liquid side resistance they used Higbie's penetration theory, which took on the same form as given by Rocha et al. {1996} with characteristic length in this case as that given by equation 4.31. They validated their mass transfer model with distillation work using Montz B1-250

and Ralu-pak 250YC structured packing. The model is based on complete wetting of the packing surface.

Erasmus {1999} used a wetted wall correlation to characterise the gas phase mass transfer rate in his mass transfer model. This correlation was fitted on wetted wall data for a column with a complex surface structure. The correlation is defined as follows:

$$Sh_g = 0.0081 \mathrm{Re}_{g,r}^{\ 0.94} Sc_g^{\ 0.5} \qquad (4.32)$$

In the model complete wetting of metal surface is assumed as well as negligible liquid phase resistance for distillation conditions. Fluid phase velocities are evaluated based on the triangular channel defined by the packing. In the model he assumed that the liquid and vapour phases were flowing in the triangular flow passages that are inclined at angle to the horizontal. The evaluated HETP values were corrected for the packing geometry. The equation for the corrected HETP values was given as follows:

$$HETP = HETP^{\#} \ \sin\theta \qquad (4.33)$$

Where $HETP^{\#}$ indicates the uncorrected HETP values.

4.3 Theory

In the distillation process species are transferred between the fluid phases. This transfer of mass between the phases can be described by Whitman's two-film theory. The theory pictures phase transfer as occurring by molecular transport only, in adjacent hypothetical films on either side of the fluid-fluid phase interface. It is also assumed that an insignificant mass transfer driving force exists in either fluid bulk phase. Through the film theory it is possible to relate overall transfer coefficients to individual fluid phases coefficients. The

form of the equation relating overall gas phase resistance to individual fluid phase resistances is given by, {Sherwood et al., 1975}:

$$\frac{1}{k_{og}} = \frac{1}{k_g} + \frac{m}{k_l} \tag{4.34}$$

A similar form of equation 4.34 can be derived for the overall liquid phase resistance, which is given as follows:

$$\frac{1}{k_{ol}} = \frac{1}{k_l} + \frac{1}{mk_g} \tag{4.35}$$

For a full derivation of equation 4.34 and that of the liquid side resistance reader referred to Bennett and Myers {1983}. The slope of the equilibrium line, m, can be written as {Nieuwoudt, 1994}:

$$m = K_i \left(\frac{\rho_v}{\rho_l} \right) \left(\frac{M_r^{liq}}{M_r^{vap}} \right) \tag{4.36}$$

Ordinarily under distillation conditions the equilibrium line is curved from the top to bottom of the column. This would therefore prevent the use of a single overall mass transfer coefficient i.e. equation 4.34 or 4.35 from being used. If it is assumed that over a theoretical stage the equilibrium line could be taken as a straight line this would then allow the use of overall mass transfer driving force. This approach, the use of straight equilibrium line over a theoretical stage, is the methodology that will be employed in this study in evaluating the mass transfer model.

In application of the countercurrent mass transfer theory as given by Nieuwoudt {1994}, a differential equation is obtained when a mass balance is performed over a control volume of a packed column and this is given as follows:

$$-u_{g,super} A dC_g = k_{og} \left(C_g^* - C_{gb}\right) a_e A dz \tag{4.37}$$

If k_{og} is considered to be independent of position and integrating over the packed height equation 4.37 can be shown to be:

$$\int_0^z dz = z = \frac{u_{g,super}}{k_{og}\, a_e} \int_{C_{gi}}^{C_{go}} \frac{dC_g}{\left(C_g^* - C_{gb}\right)} \tag{4.38}$$

$$z = H_{Tog} \times N_{Tog} \tag{4.39}$$

Where H_{Tog} is the overall height of transfer unit indicating inversely the relative ease with which a given column and packing can accomplish mass transfer

$$H_{Tog} = \frac{u_{g,super}}{k_{og}\, a_e} \tag{4.40}$$

and N_{Tog} is the number of transfer units indicating the difficulty of the separation.

$$N_{Tog} = \int_{C_{gi}}^{C_{go}} \frac{dC_g}{\left(C_g^* - C_{gb}\right)} \tag{4.41}$$

As mentioned earlier the use of a straight equilibrium line enables the use of overall mass transfer coefficients in describing mass transfer. The performance of a particular packing can then be expressed in terms of the HETP (height equivalent to a theoretical plate) value. The theoretical stage, where equilibrium and operating lines are straight can be illustrated by referring to figure 4.3.1.

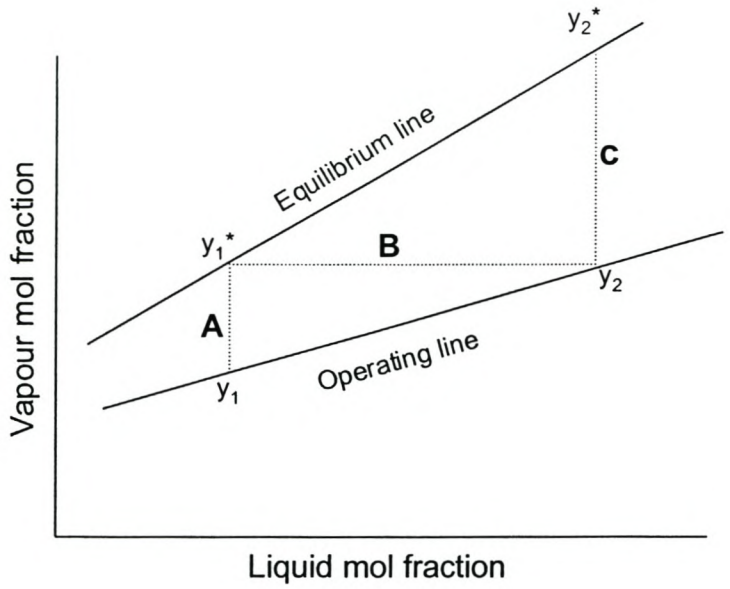

Figure 4.3.1 Theoretical stage

A theoretical stage causes composition to change from y_1 to y_2. The packed height, HETP, for this composition change can be evaluated from the required number of transfer units and the height of such a transfer unit.

Operating line equation given as follows:

$$d(Gy)=d(Lx) \tag{4.42}$$

If G and L are assumed constant over a theoretical stage,

$$\frac{dy}{dx}=\frac{L}{G}=\frac{A}{B} \tag{4.43}$$

Based on the assumption that the equilibrium line is straight over a theoretical stage, it can be shown that, Nieuwoudt {1994}:

$$\frac{\Delta y^*}{\Delta x}=\frac{C}{B} \tag{4.44}$$

The number of transfer units, equation 4.41, can be rewritten as follows in terms of mol fractions:

$$N_{Tog} = \int_{y_1}^{y_2} \frac{dy}{\left(y^* - y\right)} \tag{4.45}$$

Equation 4.45 can then be approximated by, Nieuwoudt {1994}:

$$N_{Tog} = \frac{\left(y_2 - y_1\right)}{\left(y^* - y\right)_{LM}} \tag{4.46}$$

where,

$$\left(y^* - y\right)_{LM} = \frac{\left(y_1^* - y_1\right) - \left(y_2^* - y_2\right)}{\ln \dfrac{\left(y_1^* - y_1\right)}{\left(y_2^* - y_2\right)}} \tag{4.47}$$

$$= \frac{\left(A - C\right)}{\ln\left(\dfrac{A}{C}\right)}$$

$$= \frac{A\left(\dfrac{G}{L}K_i - 1\right)}{\ln\left(\dfrac{G}{L}K_i\right)}$$

Substituting this expression into equation 4.46 yields:

$$N_{Tog} = \frac{\ln\left(\dfrac{G}{L}K_i\right)}{\left(\dfrac{G}{L}K_i - 1\right)} \tag{4.48}$$

Equation 4.48 is an indication of the number transfer units required per theoretical stage. In order to obtain the HETP (height equivalent to a theoretical stage) it is necessary to find the product of the height of a transfer unit and the number of transfer units:

$$HETP = H_{Tog} \frac{\ln\left(\frac{G}{L}K_i\right)}{\left(\frac{G}{L}K_i - 1\right)} \tag{4.49}$$

In this study two brands of the Flexipac 350Y structured packing are used in testing the mass transfer model. The structured packing is high capacity Flexipac 350Y (HC-350Y) and normal Flexipac 350Y. Both structured packing have the same nominal area and the same characteristic dimensions as given in table 4.1.

The difference in Flexipac HC-350Y and the normal 350Y is that for the former the fluid flow emerges and enters each packing element vertically. This is obvious from the design of the packing in that for HC-350Y the corrugated sheet metal is straightened for the bottom and top ends of each packing element (see figure 4.3.2). The straightened ends of the corrugated sheets in the packing elements are approximately 15mm in length. Note that the characteristics of both packing are the same.

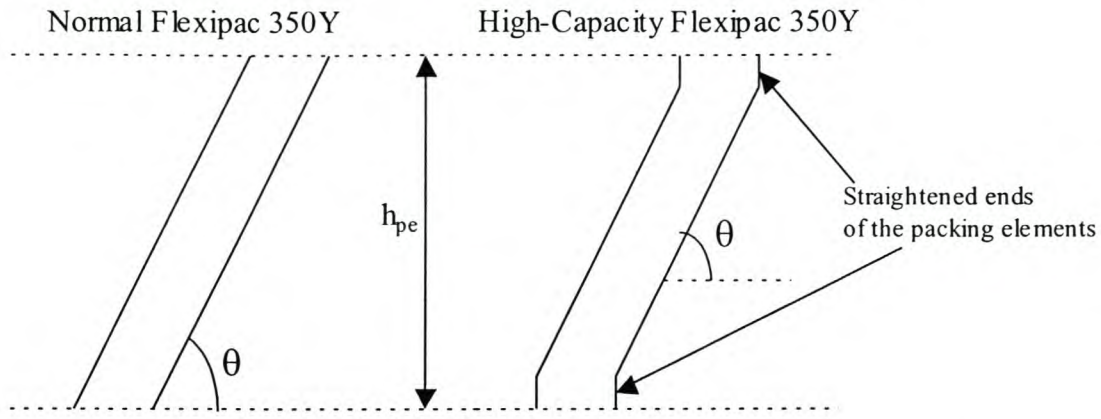

Figure 4.3.2 Comparison between Flexipac 350Y, normal and high-capacity packing.

Where h_{pe} in figure 4.3.2 indicates the height of a packing element. The height of each packing element is 265 mm. It is perceived that at increased loadings, flooding in this packing emanates from the ends of the packing elements. Consequently for the high capacity packing higher loadings may be achievable before flooding sets in, as there is no directional change in flow at the ends of the packing elements.

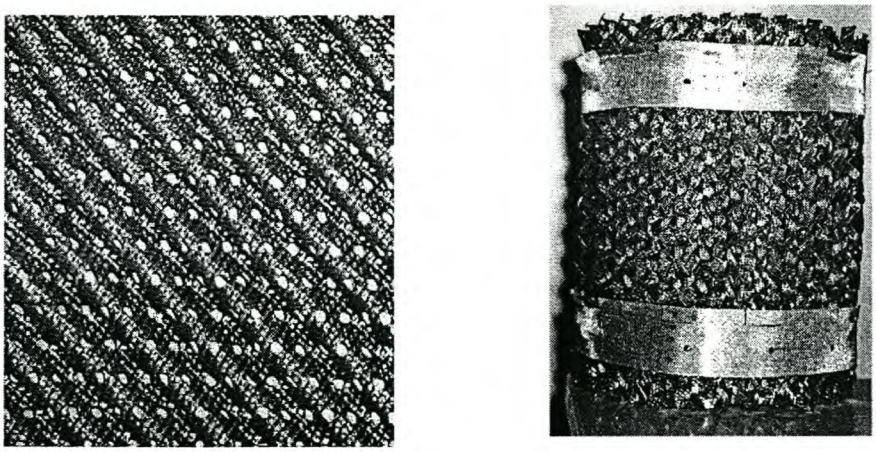

(a) (b)

Figure 4.3.3 Diagram of the packing surface (a) and the packing element (b) for Flexipac 350Y (normal)

Table 4.1 Characteristic dimensions of Flexipac packing, normal 350Y and HC-350Y

Dimension	Symbol	Value
Crimp height {mm}	h	8.5
Channel base {mm}	B	17.4
Channel side {mm}	S	12.1
Void fraction	ε	0.95
Corrugation angle {°}	θ	45
Wetted perimeter {m^{-1}}	p	350
Height of packing element {mm}	h_{pe}	265

The packing describes a triangular flow channel without a base for the gas-liquid flow. The dimensions of the flow passage are shown in figure 4.3.4. The equivalent diameter is based on the triangular flow channel with two wetted sides. It can be calculated as follows:

$$d_{eq}^{\#} = \frac{4}{\left(\frac{2S}{\frac{1}{2}Bh}\right)} \tag{4.50}$$

The liquid film is assumed to flow on the corrugation sides of the flow channel with a constant film thickness. The liquid film thickness is taken into consideration when calculating for the characteristic dimension of gas flow. The channel flow dimensions accounting for the liquid film thickness are calculated in terms of the original triangular channel dimensions. These channel flow dimensions are then used in evaluating the characteristic dimension for the gas flow. The modified form of equation 4.50 is then given as follows:

$$d_{eq} = \frac{\left(B - \frac{2S\delta}{h}\right)\left(h - \frac{S\delta}{h}\right)}{\left(S - \frac{B\delta}{2h}\right)} \tag{4.51}$$

This equation, 4.51, applies to both packing types as they define a flow passage of the same geometric configuration with the same characteristic dimensions. Equation 4.51 is used in evaluating the equivalent diameter for the gas flow in the mass transfer model. The characteristic dimension for liquid flow in the mass transfer model is taken as the liquid film thickness. The liquid film thickness is calculated implicitly from equation 4.56.

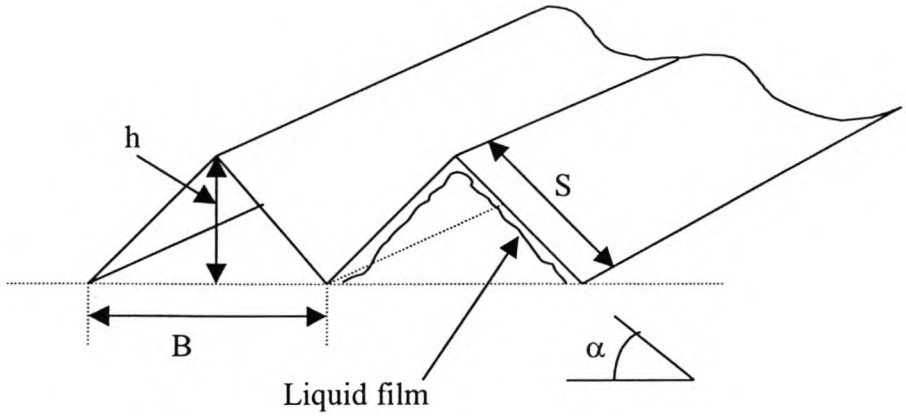

Figure 4.3.4 Dimensions of the flow passage

The liquid and vapour flow through the packing is viewed as flowing at angle θ to the horizontal (see figure 4.3.5). The liquid and vapour flow is counter current in nature. In the mass transfer model it is assumed that complete wetting of the packed surface occurs. A similar approach to that of Erasmus {1999} will be used in evaluating the phase velocities based on flow through a triangular channel. Triangular flow channels as shown in figure 4.3.4 define the flow passage in the packing. The packed column cross-section can be viewed as consisting of a number of these flow channels. To evaluate for the number of channels, the column cross-sectional area and the triangular flow channel area are required. The column cross-sectional area can be calculated as follows:

$$A_{column} = \frac{\pi d^2 \varepsilon}{4} \qquad (4.52)$$

Where ε accounts for the void fraction of the packed column.

The orientation of the triangular flow channels in the packed column is shown in figure 4.3.5. The area of the flow channel with the angle of inclination accounted for, is given as follows:

$$A_{triangular\ channel} = \frac{0.5\,B\,h}{\sin\theta} \tag{4.53}$$

The number of triangular flow channels in the column cross-section can be determined by dividing equation 4.53 into equation 4.52. The number of channels in the column cross-section can then be calculated as follows:

$$n = \frac{\pi\, d^2 \sin\theta\, \varepsilon}{2\,B\,h} \tag{4.54}$$

It can be assumed that the pressure drop over the column would result from the interfacial drag occurring at the vapour-liquid interface. Since in this particular case the pressure drop in these experiments is measured, the interfacial shear stress can then be evaluated from, Nieuwoudt {1994}:

$$\tau_i = \frac{\Delta P_{measured}}{\frac{\Delta h}{\sin\theta}} \frac{d_{eq}}{4} \tag{4.55}$$

The directional flow of fluid has to be accounted for in evaluating the interfacial shear stress. The reason being that the flow of gas and liquid is assumed to be flowing at angle θ to the horizontal (see figure 4.3.5). This explains the inclusion of the flow direction effect in equation 4.55.

Expressions for the evaluation of liquid film thickness and the interfacial velocity derived from a momentum balance of two-dimensional flow down an inclined plane. The liquid film thickness and interfacial velocity are calculated from the following equations, {Erasmus, 1999}:

$$\frac{\delta^3 g \sin\theta\left(\rho_l - \rho_g\right)}{3\mu_l} + \frac{\tau_i}{\mu_l}\left(\frac{\delta^2}{2} - \frac{4\delta^3}{3\left(d_{eq} - 2\delta\right)}\right) - u_{l,avg}\delta = 0 \qquad (4.56)$$

and

$$u_i = \frac{\delta^2 g \sin\theta\left(\rho_l - \rho_g\right)}{2\mu_l} + \frac{\tau_i}{\mu_l}\left(\delta - \frac{2\delta^2}{\left(d_{eq} - 2\delta\right)}\right) \qquad (4.57)$$

The film thickness is obtained implicitly from equation 4.56.

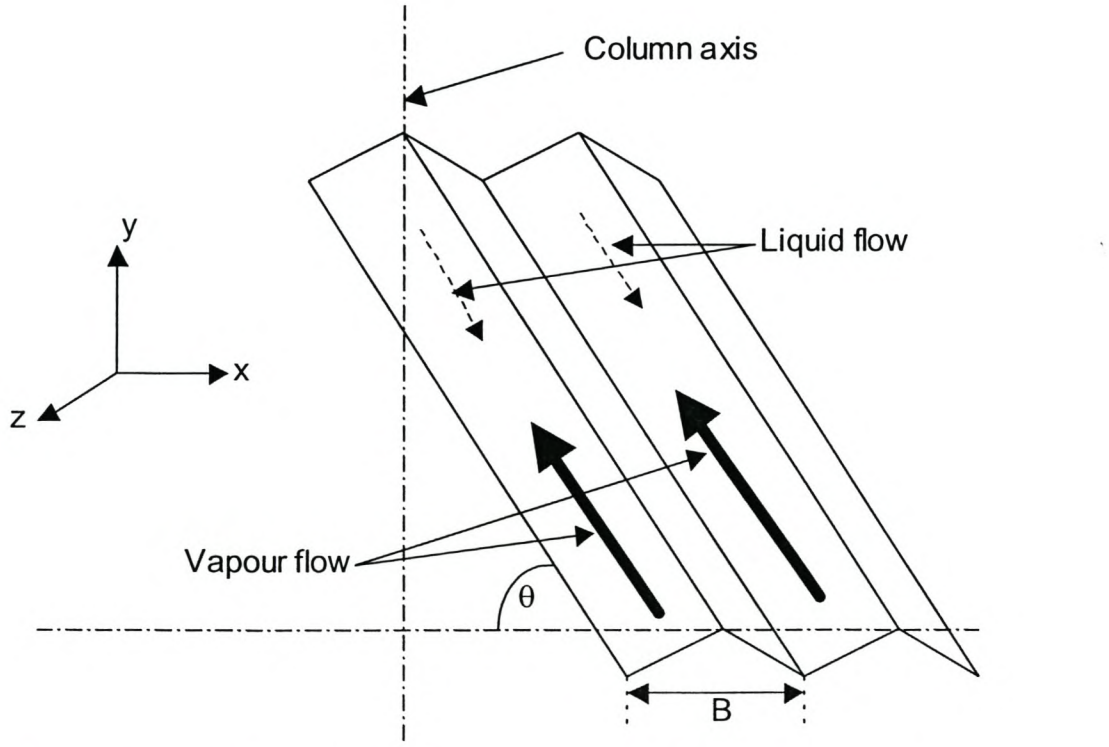

Figure 4.3.5 Liquid and vapour flow direction in the flow channels.

The liquid and vapour flow are viewed as flowing through triangular flow channels (see figure 4.3.5). The respective liquid and vapour velocities are then calculated from:

$$u_{l,avg} = \frac{Q_l}{n\delta\left(2S - \frac{2\delta}{\tan\alpha}\right)} \qquad (4.58)$$

and

$$u_{g,eff} = \frac{Q_g}{\frac{n}{2}\left(B - \frac{2S\delta}{h}\right)\left(h - \frac{S\delta}{h}\right)} \tag{4.59}$$

The angle α in equation 4.58 as defined in figure 4.3.4.

For the correlations that employ the relative velocity, this quantity is defined as:

$$u_{g,r} = u_{g,eff} + u_{l,i} \tag{4.60}$$

In evaluating the fluid velocities, volumetric flow rates for either phase are required. These can be determined from the hydraulics of the column. For this particular model the flow profile through the column was obtained from the simulation of the distillation runs with the software package PRO II. An example of the input and output files for the simulation runs are given in Appendix 5. Furthermore composition and temperature profiles can also be obtained from the simulation results. These can be then be used in evaluating the liquid film thickness and physical properties, and consequently the transfer rates and the height equivalent to a theoretical stage.

In this particular model the liquid phase transfer resistance is assumed to be negligible relative to gas phase resistance. The model assumes complete wetting of packed surface. The specific packed area is taken as the ratio of wetted surface area of the flow channel to the volume of the flow channel. The specific packed area is calculated as follows:

$$a_e = \frac{2\left(S - \frac{\delta}{\tan\alpha}\right)}{0.5\,B\,h} \tag{4.61}$$

This is then applied in evaluating the overall height of the transfer units from equation 4.40 and thus the HETP for each stage from equation 4.49. The

HETP evaluated in this form have to be corrected for packing geometry, as the liquid and vapour flow is viewed as flowing at an angle θ to the horizontal. Corrected as follows:

$$HETP = HETP_{uncorrected} \times \sin\theta \qquad (4.62)$$

The packed bed height is then evaluated from summing HETP values for all the stages required for a particular separation.

$$h_{pb} = \sum_{0}^{i} HETP_i \qquad (4.63)$$

4.4 Experimental

Experimental distillation work was carried out on the ethylbenzene/chlorobenzene binary system under total reflux conditions.

4.4.1 Distillation column description

The distillation column employed in the experimental work is set-up to operate at either vacuum or atmospheric pressure conditions. Furthermore the column is set-up such that the distillation runs can be operated under total reflux conditions. A simplified process flow diagram of the distillation column set-up is given in figure 4.4.1. The column consists of four glass sections with an internal diameter of 200mm. As mentioned earlier two brands of the Flexipac 350Y were used in the experiments, these being HC-350Y (high capacity) and normal 350Y. It should be noted that the characteristic dimensions of the packings are the same, as given in table 4.1, and each packing element has a height of 265mm. Each packed bed consisted of three packing elements and total packed height of the column is 3.18m. Chimney type liquid distributors, with a drip point density of 795m^{-1} were used in

redistributing liquid above each packed bed. The glass columns packed bed are insulated with ceramic wool and polyethylene foam.

The column was operated at either vacuum or atmospheric pressure conditions. For vacuum pressure experimental runs the column top pressure was controlled by a control valve on the vacuum line connected to a vacuum pump.

A thermosyphon reboiler without a baffle was used in the experimental work. The overhead vapour was condensed in a total condenser using cooling water. Two different sample products were drawn for most of the distillation runs whilst for the rest three different sample products drawn. In the case of two products, distillate product was drawn from a collection point below the condenser, whilst bottom product was drawn from the leg below the sump. In the instances were a third product was drawn, this intermediate product was drawn from the top of the first packing segment above the reboiler.

Controlled variables included:

- Top column pressure, and
- Reboiler duty.

Recorded variables included:

- Cooling water inlet and outlet temperatures of the condenser,
- Reboiler return temperature,
- Temperature below the packed column,
- Temperatures above the first three packed segments, and
- Pressure drop over the column.

Cooling water and condensate flowrates were also measured. A diagram of the flow process is given in figure 4.4.1.

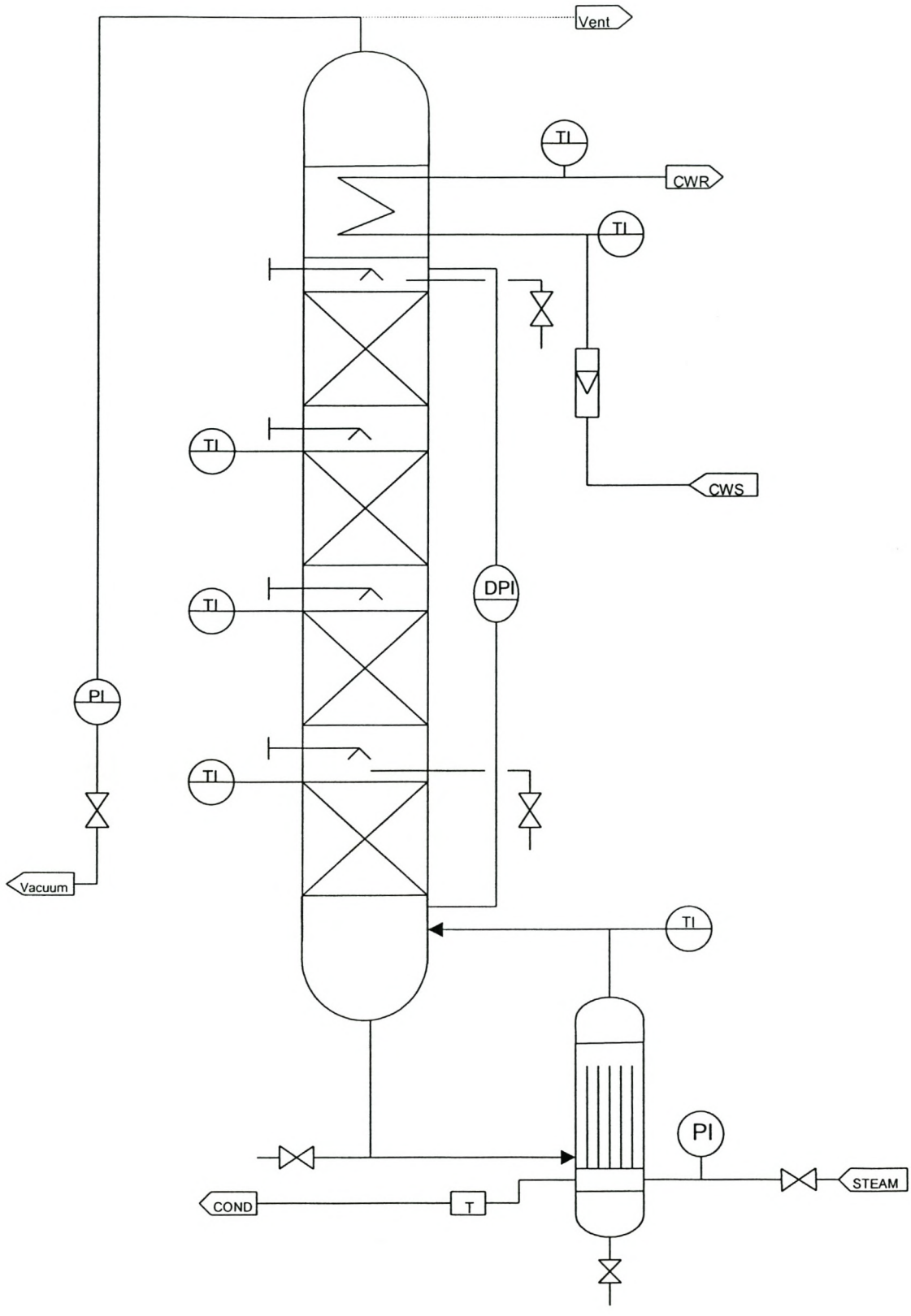

Figure 4.4.1 Process flow diagram of distillation column set-up

4.4.2 Experimental distillation runs

All experimental runs conducted under total reflux conditions. Altering the steam rate to the reboiler varied the column loading. The operating procedure was as follows:

The initial process involved filling the reboiler with the binary mixture. Upon starting up the column the reboiler duty is adjusted to the desired rate and the column is run until steady state is reached. Distillate and bottom product samples were drawn for all the distillation runs. Furthermore an intermediate sample was drawn for the runs, which included an intermediate line. The intermediate samples were taken in order to determine the composition change brought about by the sump, thus its fractional theoretical stage. Gas chromatography was used to determine the composition of all the samples.

4.5 Results

Total reflux runs were done for ethylbenzene/chlorobenzene mixture at three different pressure conditions. The column pressure was varied from 0.33-1atm, and this was done for both sets of packing used in this study. At each column pressure a number of experimental runs were performed by varying the column loading. Table 4.2 gives an indication of the entire range of physical properties at a particular pressure for the set of distillation runs. The complete set of experimental runs is given in Appendix 4. An input and output file from the simulation package Pro II is given in Appendix 5.

Table 4.2 Entire range of physical properties at individual pressure conditions along the column for the binary mixture investigated.

Physical property			
Pressure (atm)	0.33	0.66	1
Liquid density (kg/m^3)	993 – 870	962 – 847	934 - 830
Vapour density (kg/m^3)	1.09 - 1.07	2.06 - 1.97	3.24 - 3.16
Liquid viscosity (x10^{-4} Pa.s)	3.65 - 3.22	3.05 - 2.74	2.65 - 2.42
Vapour viscosity (x10^{-6} Pa.s)	8.99 - 8.45	9.48 - 8.90	9.89 - 9.34
Vapour diffusivity (x10^{-6} m^2/s)	14.4 - 13.5	8.15 - 7.79	5.13 - 5.05
Surface tension (mN/m)	24.4 - 22.2	21.8 - 19.8	19.7 - 18.0

Note: Physical properties calculated as indicated in Appendix 2.

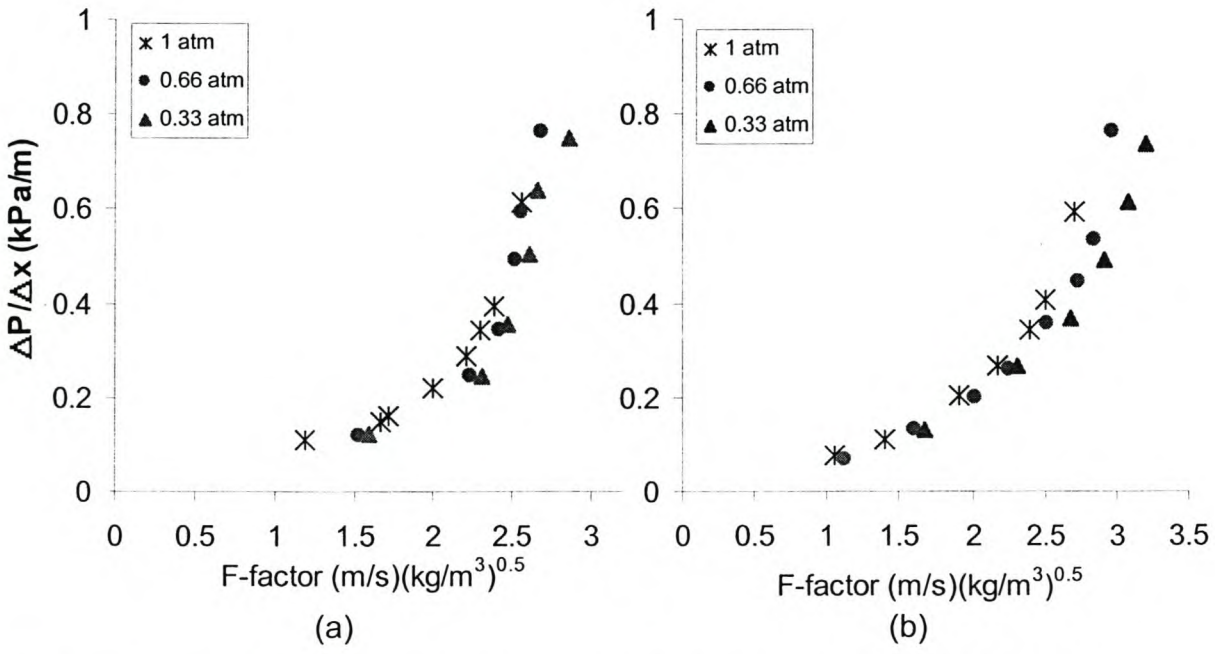

Figure 4.5.1 Plot of column pressure drop with F-factor for (a) Flexipac 350Y and (b) Flexipac HC-350Y

Figure 4.5.1 shows the pressure drop per unit length of packing for the experimental runs as function of the F-factor. It can be seen that for similar pressure drop values higher loading can be achieved for high-capacity Flexipac 350Y as compared to normal Flexipac 350Y.

able 4.3 Expe rimental HETP values

1 atm		0.66 atm		0.33 atm	
Run No.	HETP	Run No.	HETP	Run No.	HETP
Flexipac 350 Y – High Capacity					
1	0.295	1	0.287	1	0.257
3	0.259	2	0.254	2	0.236
4	0.246	3	0.243	3	0.233
5	0.238	4	0.237	4	0.231
6	0.228	5	0.231	5	0.224
2	0.227	6	0.228	6	0.217
7	0.216	7	0.221	N/A	N/A
N/A	N/A	8	0.214	N/A	N/A
Flexipac 350 Y – Normal					
1	0.250	1	0.247	1	0.249
2	0.243	2	0.234	2	0.238
7	0.239	3	0.228	3	0.230
3	0.236	4	0.218	4	0.225
4	0.229	5	0.213	5	0.221
5	0.228	N/A	N/A	6	0.214
8	0.223	N/A	N/A	N/A	N/A
6	0.218	N/A	N/A	N/A	N/A

he experiment tal values in table 4.3 are calculated from the physical packed eight and the number of stages obtained from the simulations. The physical acked height for all the experimental distillation runs was 3.18m. The verage packed heights at the different pressure conditions investigated are nown in table 4.4. These are the average values of the predicted packed eights by the respective correlations and mass transfer models. This is nown for both the Flexipac HC-350Y and Flexipac 350Y. The predicted acked heights for the individual distillation runs are given in Appendix 4. The verall average packed height for all the distillation runs is also included in ble 4.4.

Table 4.4 The average packed heights

Pressure (atm)	Corr 2.30a	Corr 2.34	Erasmus	Bravo	Delft
Flexipac 350Y – High Capacity					
0.33	2.99	3.14	2.89	4.14	4.42
0.66	2.76	3.15	2.73	3.88	4.31
1	2.53	3.07	2.55	3.65	4.20
Flexipac 350Y – normal					
0.33	3.04	3.14	2.91	4.22	4.41
0.66	2.82	3.15	2.84	4.04	4.52
1	2.64	3.20	2.66	3.81	4.38
Overall Ave.	2.80	3.14	2.76	3.96	4.37

The mass transfer models for the Bravo et al. {Fair et al., 2000}, Delft {Olujic et al., 1999} and Erasmus {Erasmus, 1999} methods are applied as proposed in the respective literature.

4.6 Discussion of results

For the particular system employed in the distillation experiments, it can be observed from table 4.2 that there is not a significant variation in physical properties along the length of the column. Consequently the following analysis will be based on a comparison between the HETP values calculated from the respective correlations and models and the experimental values. The experimental values (table 4.3) are evaluated from the physical packed height and the resulting number of stages from the simulations. Furthermore this should give an appropriate indication of how the respective models predict packed height as a function of column loadings.

Initially the model was tested with gas phase transfer correlations developed in chapter 2. Of the correlations developed in chapter 2 the two correlations which were able to predict packed height with the least overall error are

indicated in table 4.3, these being correlation 2.30a and 2.34. Figure 4.6.1-4.6.3 indicate the HETP values as predicted by the correlations as a function of F-factor.

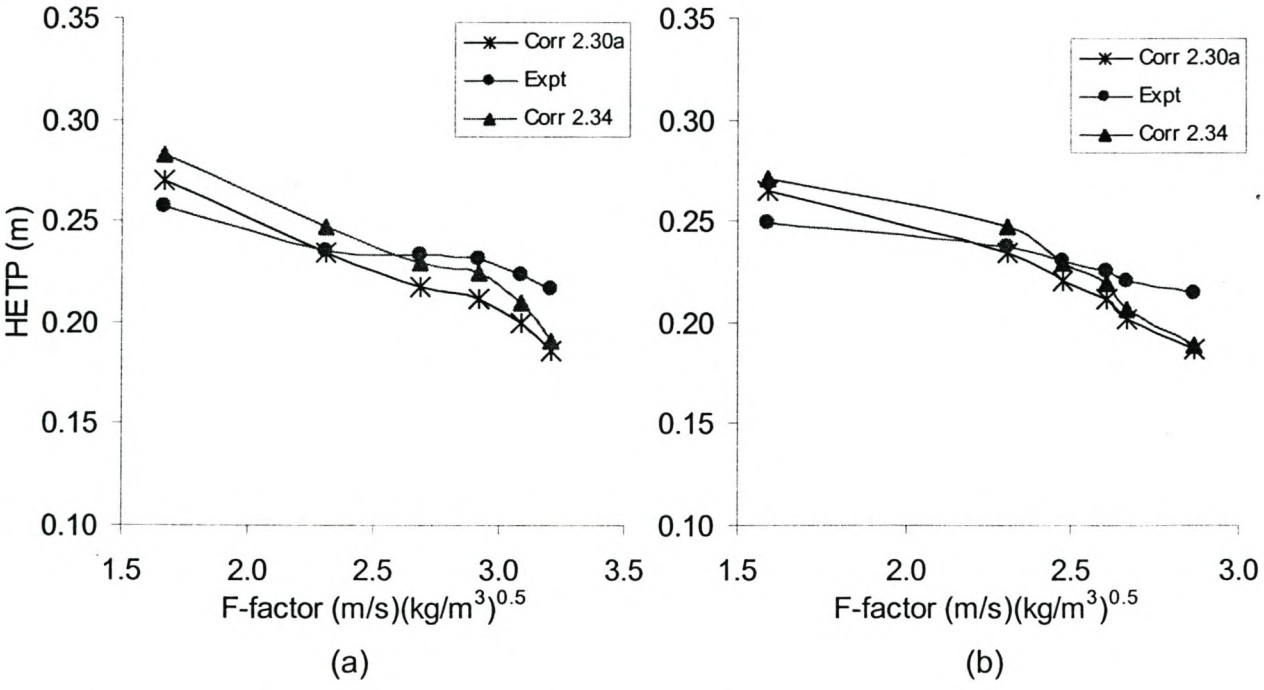

Figure 4.6.1 Plot of predicted and experimental HETP vs. F-factor at 0.33atm for correlations 2.30a and 2.34 for (a) HC-350Y and (b) normal 350Y

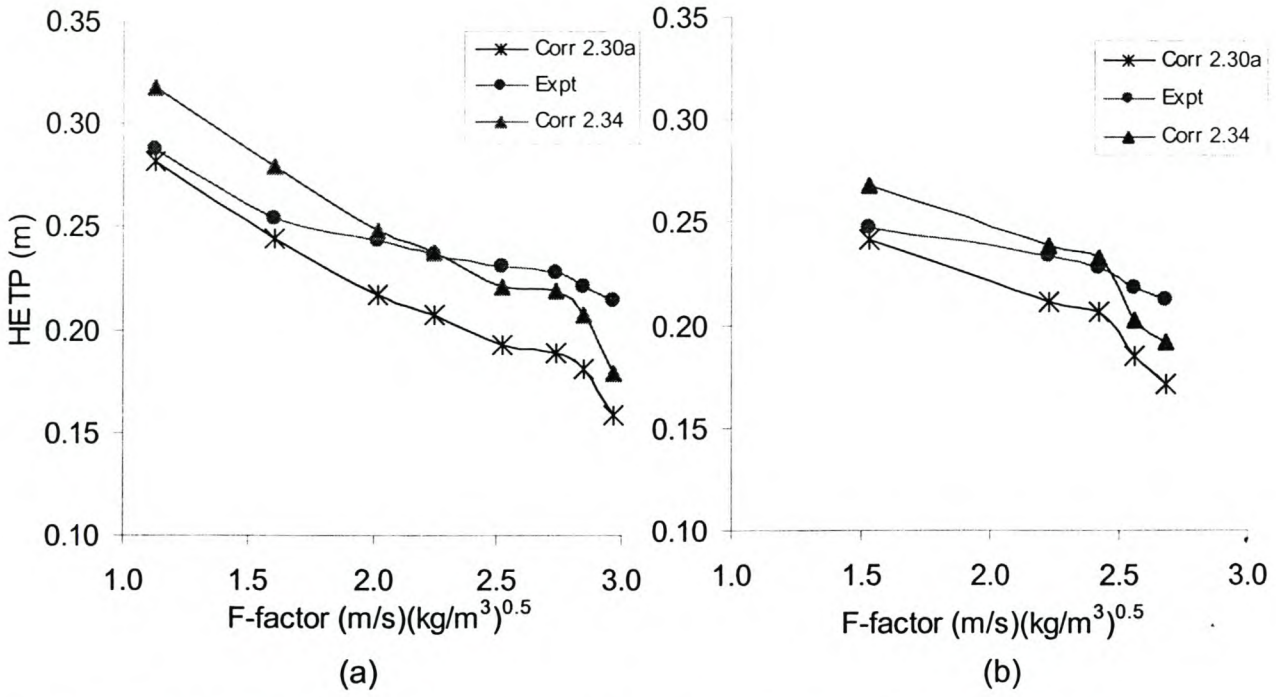

Figure 4.6.2 Plot of predicted and experimental HETP vs. F-factor at 0.66atm for correlations 2.30a and 2.34 for (a) HC-350Y and (b) normal 350Y

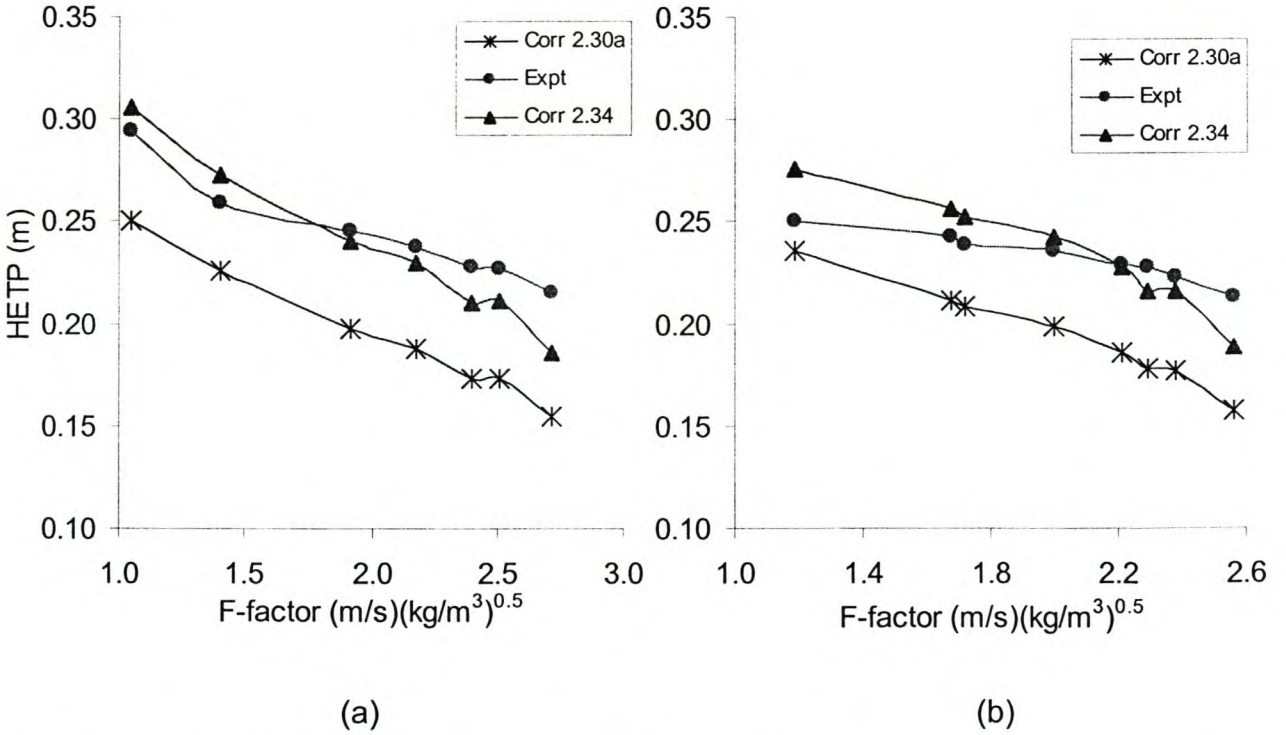

Figure 4.6.3 Plot of predicted and experimental HETP vs. F-factor at 1atm for correlations 2.30a and 2.34 for (a) HC-350Y and (b) normal 350Y

It can be observed that the correlations developed from a wetted wall column with a triangular flow channel are able to predict the trend of experimental HETP values (see figure 4.61-4.6.3). This is the case for all the pressure conditions investigated in this work. Granted, these correlations show a steeper increase in column performance with increased loading they do, however, follow the general trend of experimental values. The plots indicate that the correlations predict lower phase transfer resistance at increased column loading than is actually occurring in the column.

Based on the average packed height over a particular pressure the correlations seem to show an increase of predicted packed height with a decrease in pressure, see table 4.3. For correlation 2.30a, the average error in packed height decreases with decreasing pressure for both Flexipac HC-350Y and 350Y. In the case of correlation 2.34, for Flexipac HC-350Y, the average packed height at lower pressures is closer to the actual physical height. The error in the predicted packed heights is lower at atmospheric pressure. The predicted packed heights are higher at the lower pressures for Flexipac HC-350Y. Therefore, it follows that higher average values will be obtained at these pressures.

The two correlations, 2.30a and 2.34 are not too dissimilar. Differences being that correlation 2.34 uses absolute rather than relative velocity in the vapour Re number. The liquid effects on the mass transfer rates are included in the Fr_l number in both correlations. The Re_l term is also included in correlation 2.34. Though the exponent on the liquid Reynolds number in correlation 2.34 is negative, the increased exponent on Froude number counters its relative effect. The correlations predict substantially higher mass transfer rates than expected at extremely high column loadings. This indicates that the correlations are unable to extrapolate accurately the transfer rates at the higher vapour flows, as these flow rates are outside the range the correlations were developed from. It is possible that at the higher gas rates in the wetted wall experiments liquid got entrained in the gas phase. This could explain why the correlations over estimate the mass transfer coefficient at the higher column loadings. This increase in the transfer rates is not as significant for

correlation 2.34 as for correlation 2.30a. Since $k_g \propto u_g^a$, it can be expected that the correlation (2.34) with the lower exponent on the gas Re term will predict a smaller increase in the expected transfer rates.

On the whole correlation 2.34 is able to predict the physical height more accurately than correlation 2.30a. Further analysis in this section will refer to correlation 2.34 as the equation of choice for estimating the transfer rates.

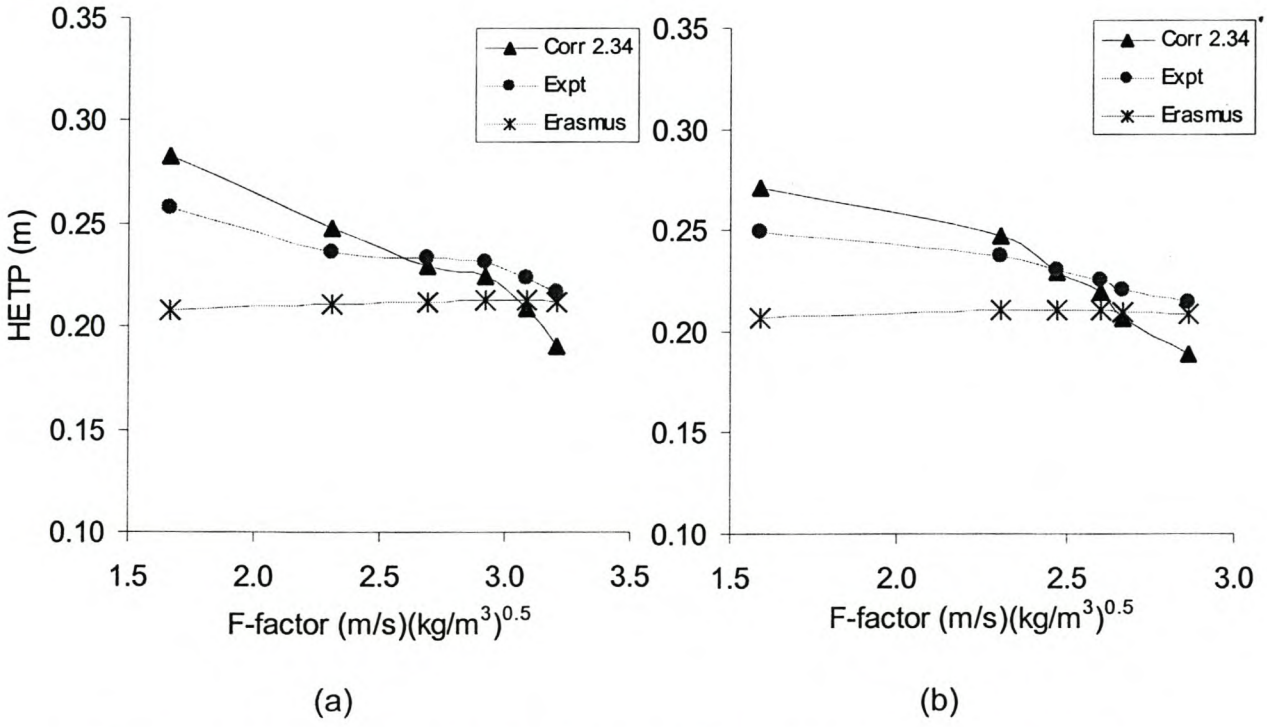

Figure 4.6 4 Plot of predicted and experimental HETP vs. F-factor at 0.33atm for correlations 2.34 and Erasmus {1999} for (a) HC-350Y and (b) normal 350Y

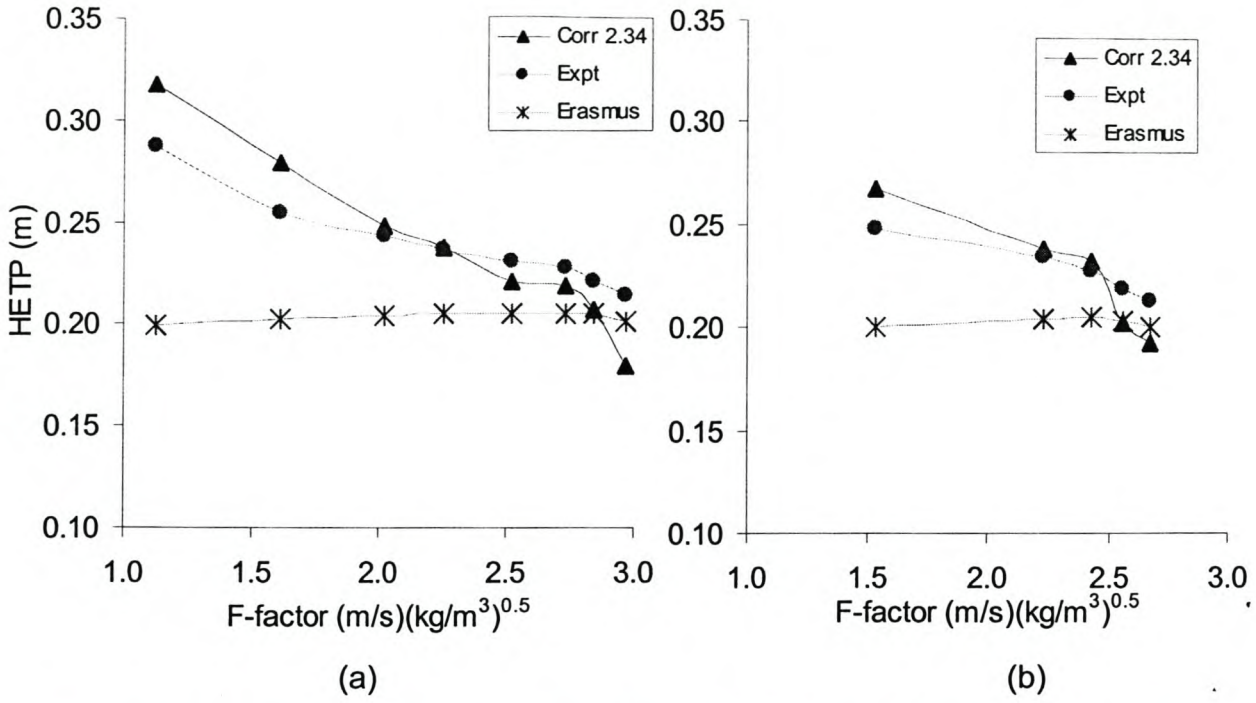

Figure 4.6.5 Plot of predicted and experimental HETP vs. F-factor at 0.66atm for correlations 2.34 and Erasmus {1999} for (a) HC-350Y and (b) normal 350Y

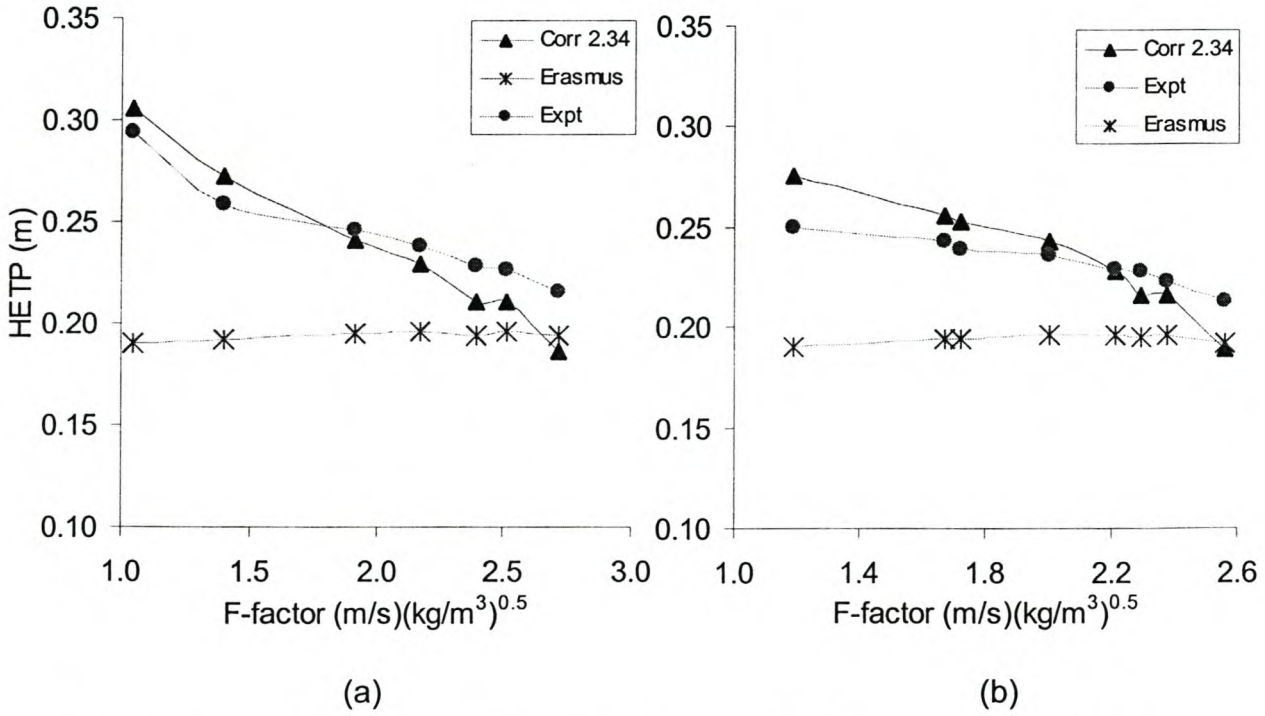

Figure 4.6 6 Plot of predicted and experimental HETP vs. F-factor at 1atm for correlations 2.34 and Erasmus {1999} for (a) HC-350Y and (b) normal 350Y

Figures 4.6.4 through to 4.6.6 show a comparison of predicted HETP values of this work to that of Erasmus {1999}. From the figures it can be observed that there is minimal variation of HETP with F-factor at any particular pressure as predicted by the model proposed by Erasmus {1999}. The average value of the predicted packed heights increases with decreasing pressure for the Erasmus model (see table 4.4). As observed in chapter 2 the correlations developed for a wetted wall column of circular cross-section tended to over-predict the transfer rates, thus under predicting packed height as seen in this section. The correlations were developed for liquid flow rates that are higher than those encountered in the structured packing. This could possibly explain why the Erasmus model over-predicts the separation efficiencies of the packing. Over the entire operating range, the model proposed by Erasmus {1999} predicts the expected packed height with an average error of 13.1%. For this work this error is about 6.0%. This indicates that the correlations developed with a geometric configuration similar to that described by the packing are capable of describing the transfer rates with such type of packing. It can be observed that the correlation developed for a wetted wall column of triangular section is able to predict the expected trend of packed height whereas that developed from a circular section is unable to. In order to cater for increased transfer rates at higher column loadings, as predicted by the correlations developed in this work, its imperative the correlations are extended to include higher gas flow rates.

A further comparison was done with methods proposed in the literature, namely the SRP model {Fair et al., 2000} referred to as Bravo et al. method and the Delft model {Olujic et al., 1999}. Figures 4.6.7 to 4.6.9 show the variation of predicted HETP values from these models as a function of F-factor.

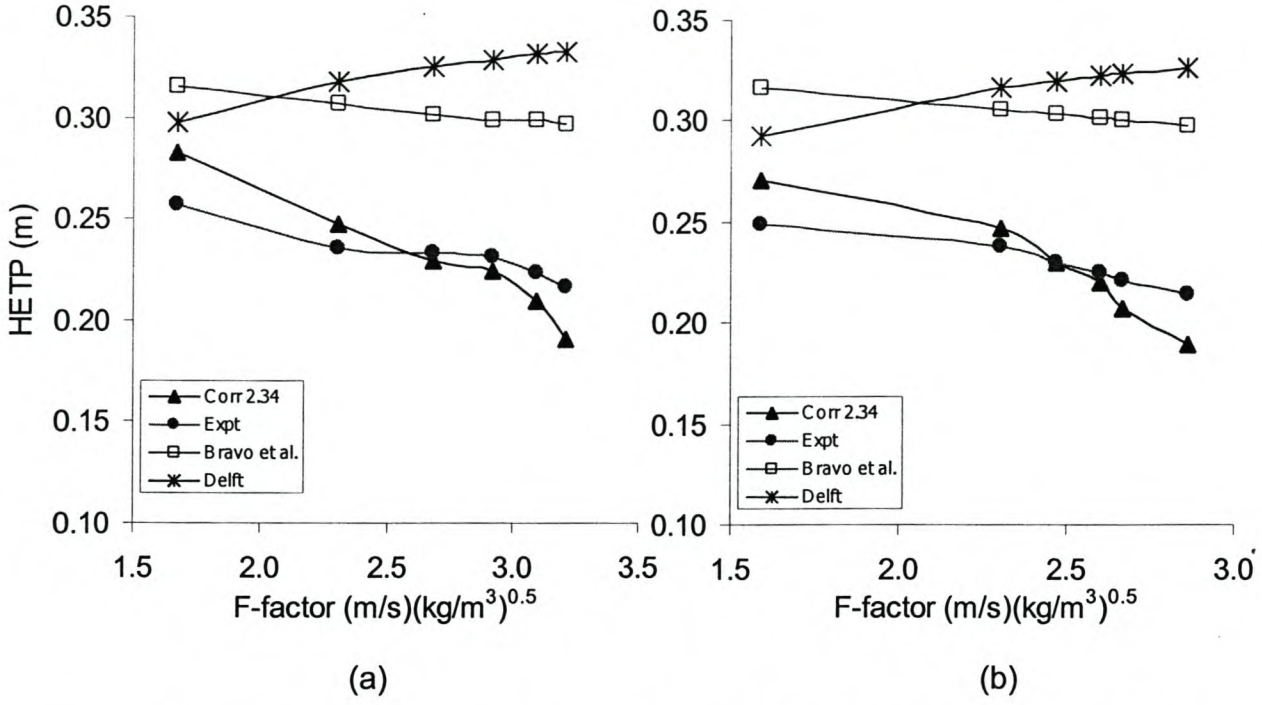

Figure 4.6.7 Plot of predicted and experimental HETP vs. F-factor at 0.33atm for this work, Bravo et al. and Delft methods for (a) HC-350Y and (b) normal 350Y

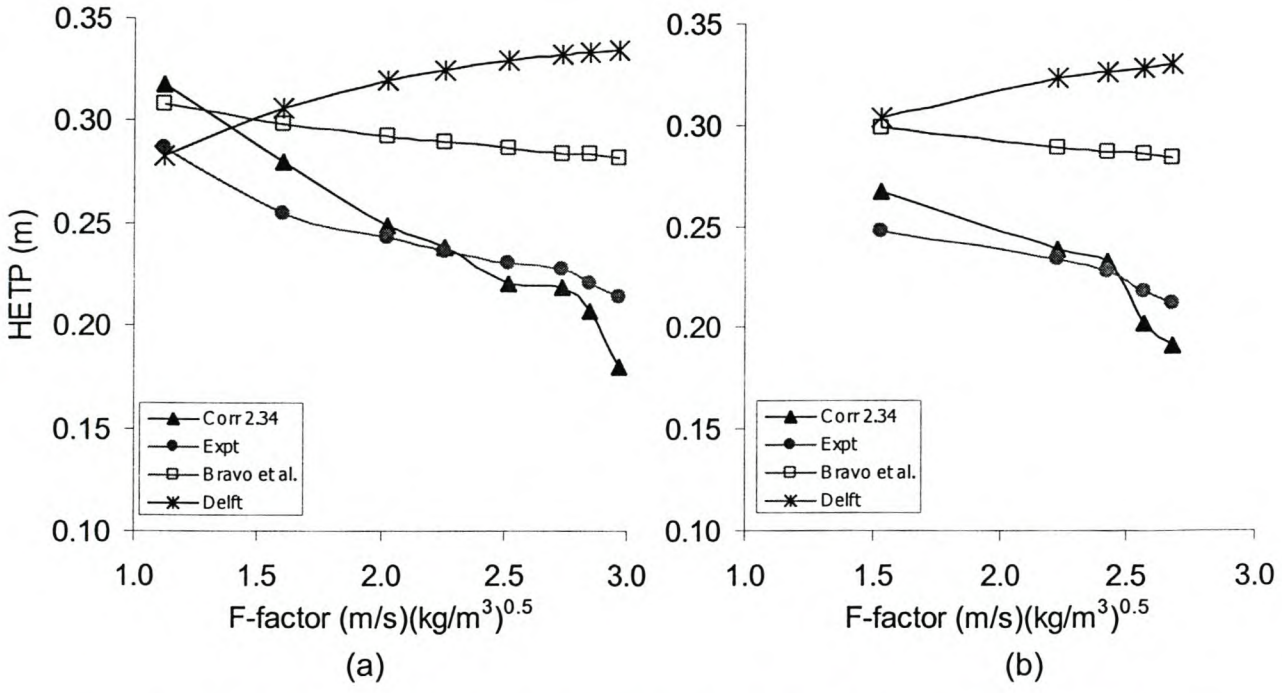

Figure 4.6.8 Plot of predicted and experimental HETP vs. F-factor at 0.66atm for this work, Bravo et al. and Delft methods for (a) HC-350Y and (b) normal 350Y

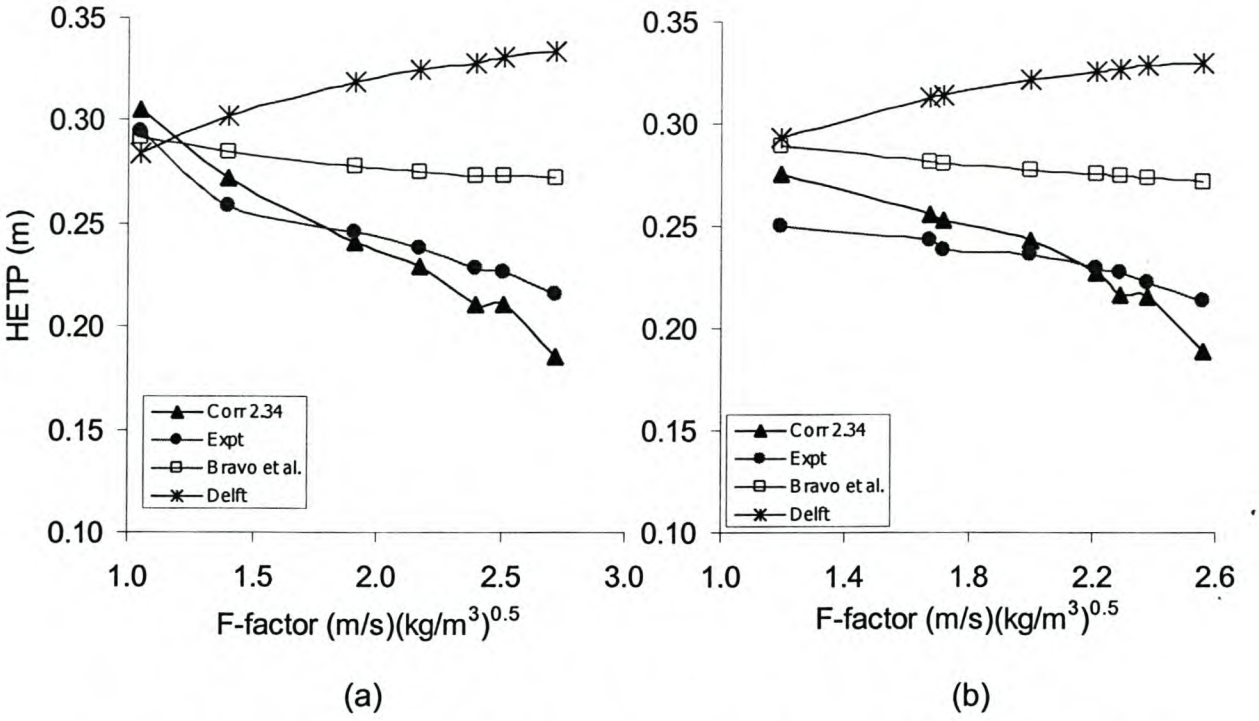

Figure 4.6.9 Plot of predicted and experimental HETP vs. F-factor at 1atm for this work, Bravo et al. and Delft methods for (a) HC-350Y and (b) normal 350Y

Neither method obtained from literature is able to accurately predict the packed height of the column. Both methods seem to improve in predicting the packed height with increasing pressure. The methods used in estimating the transfer rates in both models were not developed experimentally. In evaluating the transfer coefficients for the respective fluid phases, both models employ Higbie's penetration theory in calculating the liquid side coefficient. This, as explained in chapter 3, is not an appropriate way of describing liquid resistance for conventional distillation under turbulent conditions. In evaluating the gas phase transfer coefficient the Bravo et al. method uses a wetted wall analogy, which was fitted to experimental data. In the case of the Delft model it adapts expressions developed for heat transfer applications in estimating the gas phase transfer coefficient. Interestingly enough the Delft model predicts gas phase transfer coefficients of a similar magnitude to those found in this work, whereas the Bravo et al. method gives values that are about twice as high, see figure 4.6.10. A probable reason for the Delft model predicting similar values to that of an experimental method is

that its correlation caters for transfer enhancement due to entrance effects as well as the direct relationship it has with gas-liquid friction factor, {Fair et al., 2000}.

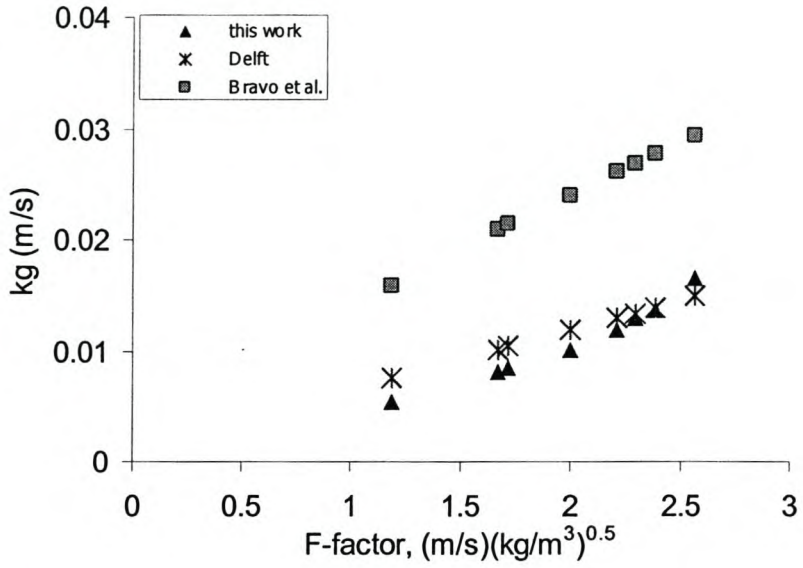

Figure 4.6.10 Comparison of predicted gas phase mass transfer coefficient for this work, Delft and Bravo et al. models, at 1atm for Flexipac 350Y.

On the whole both the Delft and Bravo et al. methods under-predict the expected overall mass transfer efficiency of this experimental work with the effect being less marked for the latter. The Bravo et al. method predicts a packed height about 24.5% higher than expected on average, whilst the Delft model predicts a height about 37.7% higher on average. Consequently this under-prediction of the transfer efficiency is bound to limit the applicability of these methods in conventional distillation applications.

4.7 Summary

- Of the correlations developed in chapter 2, correlation 2.34 best describes the performance of the column internals with the proposed model, predicting the packed height with an overall average of error of ± 6.0%.

The prediction of mass transfer efficiency of the structured packing improved with increasing pressure.

- The model as proposed by Erasmus {1999} over estimates the mass transfer efficiency, thus under-predicting the packed height with an overall average error of 13.1%.
- The Bravo et al. {Fair et al., 2000} and Delft {Olujic et al., 1999} models over-predicts for the packed height, predicting the height with an overall average error of 24.5% and 37.7%, respectively. The Delft model showed relatively good agreement of gas phase transfer coefficient with those determined by the experimental based correlation, 2.34, of this work.

For the structured packing investigated in this work it is proposed that the packing performance can be predicted by the mass transfer model as given in this chapter in the pressure range 0.33 - 1atm. The mass transfer coefficient required in the model can be estimated from correlation 2.34, given as follows:

$$Sh_g = 0.00728\, Re_g^{0.86}\, Re_l^{-0.106}\, Sc_g^{0.5}\, Fr_l^{0.35}$$

The above work shows that the use of correlations developed from wetted wall channels with triangular cross-section in the proposed mass transfer model are capable of predicting the expected trend of transfer rates found in the packing. To improve on the accuracy of predicting the transfer rate in packed columns, it would be advisable to extend the range of gas flow rates for which the correlations are developed from. The gas Reynolds number, for which the wetted wall correlations were fitted for, varied between 1800-4700. A much wider range of gas Reynolds number was covered in the distillation work, 3100 – 9300. The range of liquid Reynolds number investigated in the distillation work (21 – 90) was well within that of the wetted wall work (6 – 190).

In the mass transfer model that has been put forward in this work it has been assumed that liquid phase resistance is negligible and packing surface is completely wetted. The assumption of a completely wetted packed surface

warrants further investigation. The effective transfer area is influenced by the flow conditions in a column. It is perceived that to improve on the general applicability of the model, fundamental based models have to be developed to estimate both the effective transfer area and the liquid phase resistance. To illustrate the importance of these developments, the Delft model predicts gas phase coefficients of a similar magnitude to that of this work. But in evaluating their overall transfer rate, they add the liquid resistance as estimated from Higbie's theory, but this does not result in improved prediction of the expected transfer rates. Consequently this underlines the need for appropriate correlations in these areas.

Nomenclature

Symbol	Description	Unit
A	Area	$[m^2]$
a_e	Effective area	$[m^2/m^3]$
a_p	Geometric area	$[m^2/m^3]$
B	Structured packing corrugation channel base	[m]
C	Concentration	$[mol/m^3]$
D_{AB}	Diffusion coefficient of A in B	$[m^2/s]$
D_L	Liquid phase diffusion coefficient	$[m^2/s]$
d	Diameter	[m]
d_{eq}	Equivalent diameter	[m]
F-factor	Gas side factor ($=u_g\rho_g^{0.5}$)	$[(m/s)(kg/m^3)^{0.5}]$
F_p	Packing factor	
Fr	Froude number	
F_{SE}	Factor for surface enhancement	
g	Gravitational acceleration, 9.81	$[m/s^2]$
G	Vapour flow rate	[mol/s]
Ga	Galileo number	
h	Height	[m]
h_{pb}	Height of packed bed	[m]

HETP	Height equivalent to a theoretical stage	[m]
h_L	Liquid hold-up	
H_{TU}	Height of transfer unit	[m]
k	Mass transfer coefficient	[m/s]
K	Distribution coefficient	
l	Length	[m]
L	Liquid flow rate	[mol/s]
Ma	Marangoni number	
M_r	Molecular weight	[g/mol]
n	Number of flow channels	
N_{TU}	Number of transfer units	
p	Perimeter	[m]
P	Pressure	[Pa]
Re	Reynolds number	
S	Side length of corrugation	[m]
Sc	Schmidt number	
Sh	Sherwood number	
u	Velocity	[m/s]
We	Weber number	
x	Liquid mol fraction	
y	Vapour mol fraction	
z	Height	[m]

Greek symbols

Symbol	Description	Unit
α	Angle of packing as defined in fig 4.3.4	[°]
Δ	Difference	
δ	Liquid film thickness	[m]
ρ	Density	[kg/m^3]
μ	Viscosity	[Pa.s]
σ	Surface tension	[N/m]
γ	Contact angle	[°]

θ	Corrugation angle	[°]
ε	Void fraction	
φ	Fraction of flow channel occupied by liquid	
f	Friction factor	
τ	Interfacial shear force per unit area	[Pa]
τ	Time	[s]

Superscript

Symbol	Description
*	Property in equilibrium with bulk of the other phase

Subscript

Symbol	Description
b	bulk
eq	equivalent
eff	effective
fs	free surface
g	gas phase
i	interfacial
l	liquid phase
LM	logarithmic mean
o	overall
pe	packing element
r	relative
super	superficial

CHAPTER 5. Conclusions and Recommendations

- The two correlations which best described the gas phase mass transfer in a short triangular wetted wall channel with complex surface are given as follows:

$$Sh_g = 0.00219 Re_{g,r}\ Sc_g^{\ 0.5} Fr_l^{0.22} \qquad (2.30a)$$

$$Sh_g = 0.00728\, Re_g^{0.86}\, Re_l^{-0.106}\, Sc_g^{0.5}\, Fr_l^{0.35} \qquad (2.34)$$

- For the binary mixtures investigated enhancement of the gas phase mass transfer was observed. The enhancement of the gas phase mass transfer masks the liquid side resistance in the mixtures. The binary mixtures hexane/1-octanol and cyclohexane/n-tridecane did show some liquid side resistance.
- The enhancement of the gas phase mass transfer was independent of the difference in surface tension between the two binary components.
- The gas phase transfer mass transfer correlations fitted for the wetted wall work, were used to predict the separation efficiency of structured packing. The structured packing used in this work was high-capacity Flexipac 350Y and normal Flexipac 350Y. In the mass transfer model it was assumed that complete wetting of the packing surface occurs. The correlation that described the packing separation efficiency most accurately is correlation 2.34.
- In the application of the mass transfer model, correlation 2.34 was able to estimate the separation efficiency of both packings with an overall average error of ± 6.0% for the pressure range 0.33 – 1atm. The accuracy of the predicted separation efficiency by the mass transfer model improved with increasing pressure for both packings.

The gas phase mass transfer correlations developed from the wetted wall channel were fitted for a limited gas flow rate range. It would be advisable to extend the range of gas flow rates for which these correlations are fitted. This would improve the accuracy of the predicted transfer rates for gas flow rates outside the range the correlations are fitted for. A further recommendation would be to extend the wetted wall work to include liquids of higher surface tensions. For future work, the liquid film hydrodynamics should be based on the surface structure of the flow channel.

The appropriate quantification of the observed gas phase enhancement for binary systems is an area of study still requiring further investigation. More binary mixtures where the difference in surface tension between the solute and solvent is small should be investigated.

To extend the applicability of the mass transfer model more binary systems should be investigated as well as applying the model to pressures higher than atmospheric pressure. For future work, investigators should attempt to uncouple the effective mass transfer area and the mass transfer coefficient measurements.

REFERENCES

Banerjee, S., Rhodes, E., and Scott, D.S., (1967). "Mass transfer to falling wavy liquid films at low Reynolds numbers." **Chem. Eng. Sci. 22**: 43-48.

Barnet, W. I., and Kobe, K.A., (1941). "Heat and vapour transfer in a wetted-wall tower." **Ind. Eng. Chem. 33**(4): 436-442.

Bennett, C. O., and Myers, J. E., (1983). **Momentum, Heat and Mass Transfer,** Singapore, McGraw Hill, Chapter 31.

Bennett, D. L., and Kovak, K.W., (2000). "Optimise distillation columns." **Chem. Eng. Progr. 96**(5): 19-33.

Billet, R., and Schultes, M., (1993). "Predicting mass transfer in packed columns." **Chem. Eng. Tech. 16**: 1-9.

Billet, R., and Schultes, M., (1999). "Prediction of mass transfer columns with dumped and arranged packings." **Trans. Instn. Chem. Engrs. 77**(Part A): 498-504.

Bontozoglou, V., and Papaolymerou, G., (1997). "Laminar film flow down a wavy incline." **Int. J. Multiphase Flow 23**(1): 69-79.

Bravo, J. L., Rocha, J. R., and Fair, J. R., (1985). "Mass transfer in gauze packings." **Hydrocarbon processing 1**: 91-95.

Bravo, J. L. (1997). "Select structured packings or trays." **Chem. Eng. Progr. 93**(7): 36-41.

Brokaw, R. S. (1969). "Predicting transport properties of dilute gases." **I&EC Process Design and Development, 8**(2): 240-253.

Cairns, R. C., and Roper, G.H., (1954). "Heat and mass transfer at high humidities in a wetted wall column." **Chem. Eng. Sci. 3**: 97-109.

Chilton, T. H., and Colburn, E.I., (1934). "Mass Transfer (Absorption) Coefficients." **Ind. Eng. Chem. 26**(11): 1183-1187.

Coulson, J. M. and Richardson, J.F. (1997). **Chemical Engineering Volume 1**. 5th Edition, New York, Pergamon, Chapter 1.

Crause, C. J. (1998). **A fundamental mass transfer model for an extractive distillation application**. M. Eng thesis, University of Stellenbosch, South Africa.

Dassori, C. G., Deiber, A., and Cassano, A.E., (1982). "Slow two-phase flow through a sinusoidal channel." **Int. J. Multiphase Flow, 10**(2): 181-193.

de Nevers, N. (1991). **Fluid mechanics for chemical engineers**, 2nd Edition, New York, McGraw Hill, Chapter 13.

Dijkstra, H. A., and Drinkenburg, A. A. H., (1990). "Enlargement of wetted are and mass transfer due to surface tension gradients: The creeping film phenomenon." **Chem. Eng. Sci. 45**(4): 1079-1088.

Dudukovic, A., Milosvic, V., and Pjanovic, R., (1996). "Gas-solid and gas-liquid mass transfer coefficients." **A.I.Ch.E.J. 42**(1): 269-270.

Emmert, R. E., and Pigford, R. L., (1954). "Interfacial Resistance : A study of gas absorption in falling liquid films." **Chem. Eng. Progr. 50**(2): 87-93.

Erasmus, A. B. (1999). **Mass transfer in structured packing**. M.Sc. Eng thesis, University of Stellenbosch, South Africa.

Fair, J. R., and Bravo, J. L., (1987). "Prediction of mass transfer efficiencies and pressure drop for structured tower packings in vapour/liquid service." **I. Chem. E. Symposium Series 104**: A183-A201.

Fair, J. R., and Bravo, J.L., (1990). "Distillation columns containing structured packing." **Chem. Eng. Progr. 86**(1): 19-29.

Fair, J. R., Seibert, F.A., Behrens, M., Saraber, P. P., and Olujic, Z., (2000). "Structured packing performance-Experimental evaluation of two predictive models." **Ind. Eng. Chem. Res. 39**: 1788-1796.

Gilliland, E. R., and Sherwood, T.K., (1934). "Diffusion of vapours into air streams." **Ind. Eng. Chem. 26**(5): 516-523.

Gmehling, J., Onken, U., and Rarey, J.R., Ed. (1990). **Vapour-liquid equilibrium data collection**. Vol.1, Part 2f, Frankfurt, DECHEMA, 530-532.

Grant, C. D. (1988). Energy Management in Chemical Engineering in Gerhartz, W. (ed.), **Ullmann's Encyclopaedia of Industrial Chemistry**. VCH. **B3**: **12**-1 - **12**-16.

Gualito, J. J., Cerino, J. C., Cardenas, J. F., and Rocha, J. A., (1997). "Design method for distillation columns filled with metallic, ceramic, or plastic structured packing." **Ind. Eng. Chem. Res. 36**: 1747-1757.

Henstock, W. H., and Hanratty, T.J., (1979). "Gas absorption by a liquid layer flowing on the wall of a pipe." **A.I.Ch.E.J. 25**(1): 122-131.

Humphrey, J. L. (1995). "Separation Processes: Playing a critical role." **Chem. Eng. Progr. 87**(10): 31-41.

Imaishi, N., Suzuki, Y., Hozawa, M., and Fujinawa, K., (1982). "Interfacial turbulence in gas-liquid mass transfer." **Int. Chem. Eng. 22**(4): 659-665.

Incropera, F. P., De Witt. D.P., (1996). **Fundamentals of heat and mass transfer**. 4th Edition, New York, John Wiley & Sons, Chapter 6.

Jackson, M. L., and Ceaglske, N.H., (1950). "Distillation, vaporization and gas absorption in a wetted wall column." **Ind. Eng. Chem. 42**(6): 1188-1198.

Jasper, J. J., (1972). "The surface tension of pure liquid compounds." **J. Phys. Chem. Ref. Data, 1**(4): 841-1009.

Javdani, K., (1974). "Mass transfer in wavy liquid films." **Chem. Eng. Sci. 29**: 61-69.

Kafesjian, R., Plank, C.A., and Gerhard. E.R., (1961). "Liquid flow and gas phase mass transfer in wetted-wall towers." **A.I.Ch.E.J. 7**(3): 463-466.

Kang, F., and Chen, K., (1995). "Gravity-driven two layer flow down a slightly wavy periodic incline at low Reynolds numbers." **Int. J. Multiphase Flow, 21**(3): 501-513.

Lamourelle, A. P., and Sandall, O.C., (1972). "Gas absorption into a turbulent liquid." **Chem. Eng. Sci. 27**: 1035-1043.

Laso, M., Henriques de Brito, M., Bomio, P., and von Stockar, U., (1995). "Liquid-side mass transfer characteristics of a structured packing." **Chem. Eng. J. 58**: 251-258.

McCarter, R. J., and Stutzman, L.F., (1959). "Transfer resistance and fluid mechanics." **A.I.Ch.E.J. 5**(4): 502-505.

Nawrocki, P. A., Xu, Z. P., and Chuang., K.T., (1991). "Mass transfer in structured corrugated packing." **Can. J. Chem. Eng. 69**: 1991.

Negny, S., Meyer, M., and Prevost, M., (2001). "Study of a laminar falling film flowing over a wavy wall column: Part 1. Numerical investigation of flow pattern and the coupled heat and mass transfer." **Int. J. Heat Mass Transfer. 44**: 2137-2146.

Negny, S., Meyer, M., and Prevost, M., (2001). "Study of a laminar falling film flowing over a wavy wall column: Part 2. Experimental validation of hydrodynamic model." **Int. J. Heat Mass Transfer. 44**: 2147-2154.

Nelson, R. (1980). "Material properties in SI units, Part 4." **Chem. Eng. Progr. 76** (5): 83-85.

Nielsen, C. H. E., Kiil, S., Thomsen, W.H., and Dam-Johansen,K., (1998). "Mass transfer in wetted-wall columns: Correlations at high Reynolds numbers." **Chem. Eng. Sci. 53**(3): 495-503.

Nieuwoudt, I. (1994). **The fractionation of high molecular weight alkane mixtures with supercritical fluids**, PhD Dissertation, University of Stellenbosch, South Africa, Chapter 4.

Nooijen, J. L., Kusters, K.A., and Pek, J.J.B., (1997). "The performance of packing in high pressure distillation applications." **I. Chem. E. Symposium Series**: 885-897.

Olujic, Z., Kamerbeek, A.B., and de Graauw, J., (1999). "A corrugation geometry based model for the efficiency of structured distillation packing." **Chem. Eng. Process. 38**: 683-695.

Peramanu, S. and Sharma, A., (1998). "Nonlinear instabilities of falling films on a heated vertical plane with gas absorption." **Can. J. Chem. Eng. 76**(4): 211-223.

Portalski, S., and Clegg, A.J., (1971). "Interfacial area increase in rippled film flow on wetted wall columns." **Chem. Eng. Sci. 26**: 773-784.

Porter, K. E. (1995). "Why research is needed in distillation." **Trans. Instn. Chem. Engrs. 73**(A): 357-362.

Porter, K. E. (2001). "Review: Developments in distillation and separation technology." **A.I.Ch.E.J. 47**(5): 1060-1066.

Pozrikidis, C. (1988). "The flow of a liquid film along a periodic wall." **J. Fluid Mech. 188**: 275-300.

Reid, R. C., Prausntiz, J. M., and Poling, B. E., (1987.). **The properties of gases and liquids.** 4th Edition, New York, McGraw Hill.

Reker, R. J., Plank, C.A., and Gerhard, E.R., (1966). "Liquid surface area effects in a wetted-wall column." **A.I.Ch.E.J. 12**(5): 1008-1010.

Rocha, J. A., Bravo, J.L., and Fair, J.R., (1993). "Distillation columns containing structured packings: A comprehensive model for their performance. 1. Hydraulic Models." **Ind. Eng. Chem. Res. 32**: 641-651.

Rocha, J. A., Bravo, J.L., and Fair, J.R., (1996). "Distillation columns containing structured packings: A comprehensive model for their performance. 2. Mass transfer model." **Ind. Eng. Chem. Res. 35**: 1660-1667.

Sadatomi, M., Sato, Y., and Saruwatari, S., (1982). "Two-phase flow in vertical noncircular channels." **Int. J. Multiphase Flow, 8**(6): 641-655.

Seader, J. D., and Henley, E.J., (1998). **Separation Process Principles**. 1st Edition, New York, John Wiley & Sons, Chapter 6.

Semkov, K. R., and Kolev, N., (1991). "On the evaluation of the interfacial turbulence in gas-liquid mass transfer. Part 1. A method for estimating the interfacial turbulence effect." **Chem. Eng. Process. 29**: 77-82.

Sherwood, T. K., Pigford, R.L., and Wilke, C.R., (1975). **Mass Transfer**. 1st Edition, New York, McGraw Hill, Chapter 5.

Shetty, S., and Cerro, R.L., (1993). "Flow of a thin film over a periodic surface." **Int. J. Multiphase Flow, 19**(6): 1013-1027.

Shetty, S., and Cerro, R.L., (1997). "Fundamental liquid flow correlations for the computation of design parameters for ordered packings." **Ind. Eng. Chem. Res. 36**(3): 771-783.

Shi, M. G., and Mersmann, A., (1985). "Effective interfacial area in packed columns." **Ger. Chem. Eng. 8**: 87-96.

Spedding, L., and Jones, M.T., (1988). "Heat and mass transfer in wetted-wall columns: 1." **Chem. Eng. J. 37**: 165-176.

Spiegel, L., and Meier, W., (1987). "Correlations of the performance characteristics of the various Mellapak types." **I. Chem. E. Symposium Series No. 104**: A203-A215.

Stephan, K., and Hildwein, H., (1987). **Recommended data of selected compounds and binary mixtures,**. Part 1+2, Frankfurt/Main, DECHEMA, 463-493.

Sternling, C. V., and Scriven, L.E., (1959). "Interfacial turbulence: Hydrodynamic instability and the Marangoni effect." **A.I.Ch.E.J. 5**(4): 514-523.

Striba, C., and Hurt, D.M., (1955). "Turbulence in falling liquid films." **A.I.Ch.E.J. 1**(2): 178-184.

Strigle, R. F. (1994). **Packed Tower Design and Applications: Random and Structured packings**. 2nd Edition, Houston, Gulf, Chapter 2.

Strumillo, C., and Porter, K. E., (1965). "The evaporation of carbon tetrachloride in a wetted-wall column." **A.I.Ch.E.J. 11**(6): 1139-1142.

Treybal, R. E. (1980). **Mass Transfer Operations**, 3rd Edition, Tokyo, McGraw-Hill, Chapter 9.

Trifonov, Y. Y. (1998). "Viscous liquid film flows over a periodic surface." **Int. J. Multiphase Flow, 24**: 1139-1161.

Triplett, K. A., Ghiaasiaan, S.M., Abdel-Khalik, S.I., Sadowski, D.L., (1999). "Gas-liquid two phase flow in microchannels Part1: two-phase flow patterns." **Int. J. Multiphase Flow, 25**: 377-394.

Vazquez, G., Antorrena, G., Navaza, J.M., and Santos, V., (1994). "Effective interfacial area in the presence of induced turbulence." **Int. Chem. Eng. 34**(2): 247-254.

Vetere, A. (1991). "On the calculation of the second virial coefficients of pure compounds and mixtures." **Chem. Eng. Sci. 46**(7): 1787-1794.

Vivian, J. E., and Peaceman, D.W., (1956). "Liquid side resistance in gas absorption." **A.I.Ch.E.J. 2**(4): 437-443.

Wang, C. Y. (1981). "Liquid film flowing slowly down a wavy incline." **A.I.Ch.E.J. 27**(2): 207 -212.

Wankat, P. C., and Knaebel, K.S., (1997). Mass Transfer in Perry, R.H. and Green, D. W. (ed.), **Perry's chemical engineers' handbook**. 7th Edition, New York, McGraw Hill, 5-42 - 5-79.

Wasden, F. K., and Dukler, A.E., (1990). "A numerical study of mass transfer in free falling wavy films." **A.I.Ch.E.J. 36**(9): 1379- 1390.

Weiland, R. H., and Ahlgren, K.R., and Evans, M., (1993). "Mass-Transfer characteristics of some structured packings." **Ind. Eng. Chem. Res. 32**: 1411-1418.

Winterfeld, P. H., Scriven, L.E., and Davis, H.T., (1978). "An approximate theory of interfacial tensions of multicomponent systems: Applications to binary liquid-vapour tensions,." **A.I.Ch.E.J. 24**(6): 1010-1014.

Wolk, G., Dreyer, M., and Rath, J.H., (2000). "Flow patterns in small diameter vertical non-circular channels." **Int. J. Multiphase Flow, 26**: 1037-1061.

Yaws, C. L. (1977). **Physical properties**. New York, McGraw Hill, Chapter 20.

Yoshimura, P. N., Nosoko, T., and Nagata, T., (1996). "Enhancement of mass transfer into a falling laminar liquid film by two-dimensional surface waves - some experimental observations and modelling." **Chem. Eng. Sci. 51**(8): 1231-1240.

Zhao, L., and Cerro, R.L., (1992). "Experimental characterisation of viscous film flows over complex surfaces." **Int. J. Multiphase Flow, 18**(4): 495-516.

Zhao, T. S. and Bi, Q.C., (2001). "Co-current air-water flow patterns in vertical triangular microhannels." **Int. J. Multiphase Flow, 27**: 765-782.

Zlokarnik, M. (1991). **Dimensional analysis and scale-up in chemical engineering.** 1st Edition, Berlin, Springer-Verlag, Chapter 1.

APPENDIX 1. Liquid Film hydrodynamics and the wetted wall channel equivalent diameter.

A1.1 Film thickness and interfacial velocity

To characterise liquid film flow over a complex surface is complicated somewhat as the flow structure of the liquid film may vary significantly. It is known that with increasing liquid rate the liquid interface is disturbed considerably due to the presence of waves, Negny et al. {2001}. In this case complex surface liquid film hydrodynamics are approximated with that of a smooth surface. The liquid film hydrodynamics are developed from the case of a liquid film down an inclined channel with countercurrent gas flow, {Erasmus, 1999}. The interfacial velocity and liquid film thickness can then be calculated by applying the momentum equation in two dimensions {Incropera et al., 1996}.

$$\frac{\partial\{(\rho u)u\}}{\partial x}+\frac{\partial\{(\rho v)u\}}{\partial x}=\frac{\partial\sigma_{xx}}{\partial x}-\frac{\partial P}{\partial x}+\frac{\partial\tau_{yx}}{\partial y}+X \qquad \text{(A1.1)}$$

If it can be assumed that:

- No velocity component perpendicular to the liquid surface, $(u>>v)$
- Incompressible flow (constant ρ)
- Newtonian fluid, $\tau_{yx}=\mu\frac{\partial u}{\partial y}$
- The change of velocity along the surface is negligible, $\frac{\partial u}{\partial y}>>\frac{\partial u}{\partial x}$
- The deviatoric stress component σ_{xx}, is very small
- The change in pressure is a consequence of the gravity of the vapour phase and friction:

$$\frac{\partial P}{\partial x} = \rho_v \, g \, sin\theta + \frac{4\tau}{d_{eq} - 2\delta}$$

- Body force on a liquid element is due to gravitational force, $X = \rho_l \, g$ sir

Then through the application of these assumptions and the continuity equa as well as the expansion of the derivatives, equation A1.1 can be writte {Erasmus, 1999}:

$$\mu \frac{\partial^2 u}{\partial y^2} = (\rho_v - \rho_l) g \sin\theta + \frac{4\tau}{d_{eq} - 2\delta} \qquad \text{(A1.2)}$$

With the following boundary conditions:

No slip at the packing surface:

$$u(y)\big|_{y=0} = 0 \qquad \text{(A1.3)}$$

The interfacial shear stress is denoted by:

$$\mu_l = \frac{\partial u}{\partial y}\Big|_{y=\delta} = \tau_w \qquad \text{(A1.4)}$$

Solving for these boundary conditions yields the following equation for velocity profile as function of y-coordinate.

$$u(y) = \frac{1}{2}\left[(\rho_v - \rho_l)\, g \, \sin\theta + \frac{4\tau}{d_{eq} - 2\delta}\right] y^2 + \ldots$$
$$\ldots + \left[\tau\left(1 - \frac{4\delta}{d_{eq} - 2\delta}\right) + (\rho_l - \rho_v) g \, \delta \sin\theta\right] y \qquad \text{(A1.5)}$$

The average velocity can be evaluated from:

$$u_{avg} = \frac{\int_0^{\delta} u\, dy}{\int_0^{\delta} dy} \qquad \text{(A1.6)}$$

which therefore yields:

$$\frac{\delta^3 g \sin\theta(\rho_l - \rho_g)}{3\mu_l} + \frac{\tau_i}{\mu_l}\left(\frac{\delta^2}{2} - \frac{4\delta^3}{3(d_{eq} - 2\delta)}\right) - u_{l,avg}\delta = 0 \qquad \text{(A1.7)}$$

The interfacial velocity can be calculated from:

$$u_i = \frac{\delta^2 g \sin\theta(\rho_l - \rho_g)}{2\mu_l} + \frac{\tau_i}{\mu_l}\left(\delta - \frac{2\delta^2}{(d_{eq} - 2\delta)}\right) \qquad \text{(A1.8)}$$

A1.2 Interfacial friction

In order to evaluate liquid film thickness and interfacial velocity as given by equations A1.8 and A1.9, the interfacial shear stress has to known. The interfacial shear stress is defined as follows:

$$\tau_i = \frac{1}{2} f_i \rho_v u^2 \qquad \text{(A1.9)}$$

In the distillation experiments the pressure drop is measured, therefore the interfacial shear stress can be evaluated from equation 4.55. It then follows that equation A1.9 applies only to the wetted wall channel work.

It is not known how the interfacial shear stress will vary for a circular channel as compared to that of a non-circular channel for turbulent flow conditions. It is thought that the friction factor curve of a triangular channel only differs slightly from that of a circular tube, {Olujic et al., 1999}. If this were assumed

to be valid it would allow one to use the correlations of friction factor for pipe flow to estimate the friction factor in a triangular channel. The friction factors for the triangular channel were calculated explicitly from the Colebrook and White equation {Olujic et al., 1999}. The equation is given as follows:

$$f_i = \left\{ -2\log\left[\frac{\left(\varepsilon / d_{eq}\right)}{3.7} - \frac{5.02}{\mathrm{Re}_{g,r}} \log\left(\frac{\left(\varepsilon / d_{eq}\right)}{3.7} + \frac{14.5}{\mathrm{Re}_{g,r}} \right) \right] \right\}^{-2} \qquad \text{(A1.10)}$$

The appropriate velocity to use in the Reynolds term is the air velocity relative to the liquid film. The equivalent diameter as applies to the triangular flow channel was used in the equation A1.10.

A1.3 The equivalent diameter for the wetted wall channel.

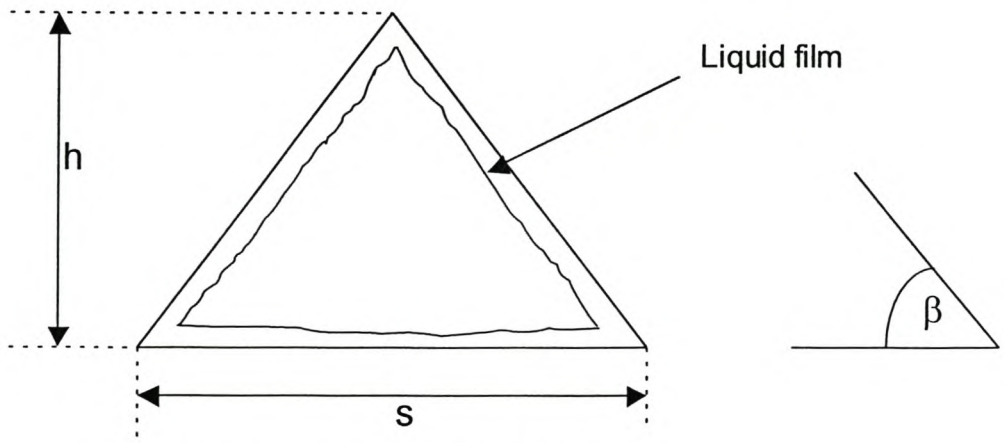

Cross-section of the wetted wall channel

Figure A1.1 Flow channel geometry

The cross-section geometry of the wetted wall channel is an equilateral triangular section. The cross-section of the flow geometry is shown in figure A1.1. The channel sides of the flow channel are all the same length. It is assumed that the liquid flow on all the channel sides is of constant film thickness. The flow channel side with the film thickness accounted for is calculated as follows:

$$s_f = s - 2\left[\frac{\delta}{sin\beta} + \frac{\delta}{tan\beta}\right] \qquad \text{(A1.11)}$$

The equivalent diameter for gas flow can be defined as follows:

$$d_{eq} = 4\frac{Area\ for\ gas\ flow}{Wetted\ perimeter}$$

The equivalent diameter for gas flow in the wetted wall channel can be calculated as follows:

$$d_{eq} = 4\frac{0.5\, s_f\, h_f}{3 s_f} = \frac{2}{3} h_f \qquad \text{(A1.12)}$$

where h_f is the height of the gas flow channel and is evaluated as follows:

$$h_f = \frac{1}{2}\, s_f\, sin\,\beta \qquad \text{(A1.13)}$$

It should be noted that the characteristic dimension for liquid flow in the wetted wall channel is taken as the liquid film thickness.

APPENDIX 2. Physical property correlations

A2.1 Pure component properties

Liquid density: The Rackett equation was used to correlate density values for all the components. The Rackett constants were obtained from Reid et al. {1987}. For 2-methoxyethanol, 2-methyl-2-propanol the densities were calculated with the modified Rackett equation, Yaws {1977}. For 1-octanol, the Rackett constant obtained from the SIMSCI databank.

Liquid viscosity: The liquid viscosity correlations for all the components obtained from Reid et al. {1987} apart from 2-methoxyethanol and 2-methyl-2-propanol. The Riedel viscosity correlation was used for these components and the correlation coefficients were obtained from the SIMSCI databank.

Surface tension: The pure component surface tension correlations were obtained from the extensive databank complied by Jasper {1972}.

Gas/vapour density: The density of air was calculated using the ideal gas law. The densities of the pure components were calculated from the virial equation with the virial coefficients being evaluated from the method proposed by Vetere {1991}.

Gas/vapour viscosity: The viscosity of air calculated from the correlation given by Nelson {1980}. The viscosity of ethylbenzene and chlorobenzene calculated with the method proposed by Brokaw {1969}.

Vapour pressure: The vapour pressure correlations for all the components obtained from the databank in Reid and Praustniz {1987}, excluding 2-methoxyethanol. The vapour pressure correlation for this component obtained from the SIMSCI databank.

A2.2 Mixture properties

Liquid mixture density: In evaluating the liquid mixture densities, Cheuh and Prausnitz {Reid and Prausnitz, 1987} mixing rules were used in estimating the mixture critical properties. Then the modified Rackett equation as given in Reid and Prausnitz {1987} was used in calculating the liquid mixture density.

Liquid mixture viscosity: The viscosity of all the liquid mixtures were calculated from the method of Grunberg and Nissan, {Reid and Prausnitz, 1987}.

Liquid mixture surface tension: The correlation as given by Winterfeld et al. {1978} was used to calculate the surface tension of all the liquid mixtures.

Liquid phase diffusivity: The liquid phase diffusivity at infinite dilution for all the binary mixtures was evaluated from the method of Tyn and Calus as described in Reid and Praustniz {1987}. The Vignes correlation {Reid and Praustniz, 1987} was used to correct the diffusivity values for the liquid concentration.

Liquid mixture vapour pressure: The vapour phase composition and vapour pressure for the liquid mixtures were evaluated from the NRTL equation, {Reid and Praustniz, 1987}. For the hexane/1-octanol mixture the binary interaction parameters were obtained from the extensive DECHEMA databank. In the case of n-tridecane/cyclohexane and n-decane/cyclohexane the interaction parameters were obtained from PRO II. These parameters are estimated with the UNIFAC group contribution method.

Gas/vapour phase diffusivity: All gas and vapour diffusivities were calculated using the method of Fuller et al. as described in Reid et al. {1987}.

Vapour phase density: The vapour phase density for the vapour mixture calculated by the virial equation. The interaction parameters and second virial coefficient were evaluated from the method proposed by Vetere {1991}.

Vapour phase viscosity: The vapour phase viscosity for ethylbenzene/chlorobenzene mixture was calculated with the method proposed by Brokaw {1969}.

APPENDIX 3. Wetted wall channel experimental results

Table A3-1 Experimental results for pure components

Run no.	Air rate g/s	Liquid rate ml/s	Evap rate ml/min	T_{avg} (T1-T4) °C	T5 °C	T6 °C	Pt kPa	P1 kPa	Sh_g	Sc_g	Re_g	Re_l	Fr_l
Methanol													
1	0.732	1.71	4.6	44.6	37.8	24.7	100.5	2.67	9.1	0.97	2507	51	21.10
2	0.677	2.25	4.9	44.2	37.9	25	100.5	2.67	10.0	0.97	2552	67	16.53
3	0.678	2.70	5.1	44.2	38.1	25.1	100.5	2.67	10.4	0.97	2535	80	32.95
4	0.677	3.14	5.3	44.4	38.4	25.2	100.5	2.67	10.6	0.97	2540	93	38.31
5	0.678	3.31	5.3	44.4	38.5	25.4	100.5	2.67	10.8	0.97	2543	98	40.40
6	0.677	3.65	5.6	44.3	38.6	25.1	100.5	2.67	11.4	0.97	2550	108	44.52
7	0.677	4.03	6.0	44.5	39.0	25.3	100.5	2.67	12.2	0.97	2553	120	49.31
8	0.765	1.71	5.0	44.7	37.6	27.4	100.3	3.07	9.7	0.97	2809	51	22.16
9	0.764	2.25	5.4	44.5	37.8	27.7	100.3	3.07	10.7	0.97	2827	67	29.09
10	0.764	2.70	5.6	44.3	37.9	27.5	100.3	3.07	11.3	0.97	2841	80	34.54
11	0.764	3.14	5.7	44.5	37.9	27.3	100.3	3.07	11.5	0.97	2847	93	40.08
12	0.765	3.31	6.1	44.4	38.4	27.4	100.3	3.07	12.4	0.97	2851	98	42.25
13	0.765	3.65	6.4	44.4	38.2	27.3	100.3	3.07	13.0	0.97	2857	108	46.60
14	0.764	4.03	6.6	44.5	38.4	27.3	100.3	3.07	13.4	0.97	2863	120	51.53
15	0.848	1.71	5.6	44.6	36.9	27.4	100.4	3.47	11.0	0.97	3125	51	23.30
16	0.848	2.25	5.7	44.2	37.1	27	100.4	3.47	11.6	0.97	3148	66	30.25
17	0.848	2.70	6.1	44.4	37.2	27	100.4	3.47	12.3	0.97	3155	80	36.31
18	0.849	3.14	6.3	44.3	37.1	26.9	100.4	3.47	12.8	0.97	3166	93	42.07
19	0.848	3.31	6.6	44.3	37.7	27.4	100.4	3.47	13.5	0.97	3170	98	44.31
20	0.849	3.65	6.9	44.7	37.7	27.2	100.4	3.47	13.8	0.97	3169	108	49.02
21	0.848	4.03	7.2	44.8	38.0	27.4	100.4	3.47	14.4	0.97	3175	120	54.21
22	0.930	1.71	6.4	44.3	36.5	27	100.3	4.00	12.8	0.97	3435	51	24.54
23	0.930	2.25	7.1	44.1	35.7	23	100.6	4.00	14.7	0.97	3466	66	31.87

Table A3-1 Continued - Methanol

Run No.	Air Rate g/s	Liquid rate ml/s	Evap rate ml/min	T_{avg} (T1-T4) °C	T5 °C	T6 °C	Pt kPa	P1 kPa	Sh_g	Sc_g	Re_g	Re_l	Fr_l
24	0.928	2.70	8.5	44.0	35.9	23.5	100.6	4.00	17.8	0.97	3479	80	38.14
25	0.929	3.14	8.0	44.2	36.0	23.6	100.6	4.00	16.6	0.97	3487	93	44.23
26	0.928	3.31	8.1	44.1	36.1	24.1	100.6	4.00	17.0	0.97	3492	98	46.57
27	0.929	3.65	8.4	44.3	36.0	23.8	100.6	4.00	17.5	0.97	3495	108	51.40
28	0.929	4.03	8.5	44.3	36.2	24.2	100.6	4.00	17.7	0.97	3503	120	56.78
29	1.013	1.44	8.0	44.3	32.5	24.9	100.3	4.53	16.1	0.97	3725	42	21.92
30	1.012	1.71	8.4	44.3	32.5	24.2	100.3	4.53	17.2	0.97	3737	51	25.93
31	1.012	2.25	9.0	44.3	32.7	24.4	100.3	4.53	18.4	0.97	3754	66	33.69
32	1.013	2.70	9.3	44.2	34.9	27.4	100.5	4.53	19.4	0.97	3775	80	40.24
33	1.013	3.14	9.7	44.3	34.3	26.9	100.5	4.53	20.2	0.97	3784	93	46.65
34	1.012	3.65	9.9	44.2	35.1	27.1	100.5	4.53	20.9	0.97	3798	108	54.06
35	1.099	1.71	8.6	44.1	32.9	27.5	100.5	5.07	17.7	0.97	4074	50	27.57
36	1.099	2.25	9.5	44.3	32.8	27.6	100.5	5.07	19.5	0.97	4088	66	35.81
37	1.100	2.70	9.7	44.1	33.7	27.7	100.5	5.07	20.2	0.97	4106	80	42.71
38	1.101	2.95	10.0	44.2	33.7	27.6	100.4	5.07	20.8	0.97	4107	87	46.54
39	1.099	3.14	10.3	44.6	33.8	27.8	100.5	5.07	21.0	0.97	4106	93	49.62
40	1.098	3.65	10.5	44.3	33.8	27.5	100.5	5.07	21.9	0.97	4126	108	57.38
41	1.181	1.44	8.7	44.4	32.6	27.4	100.4	5.73	17.4	0.97	4345	42	25.25
42	1.181	1.97	9.2	44.4	32.4	27.4	100.4	5.73	18.6	0.97	4368	58	33.43
43.	1.180	2.43	10.0	44.1	32.4	27.4	100.4	5.73	20.8	0.97	4393	71	40.71
44	1.181	2.70	10.6	44.2	33.0	27.3	100.4	5.73	22.0	0.97	4398	80	45.20
45	1.180	3.14	11.0	44.1	32.8	27	100.4	5.73	23.1	0.97	4414	93	52.21

Table A3-1 Continued - Ethanol

Run no.	Air Rate g/s	Liquid rate ml/s	Evap rate ml/min	Tavg (T1-T4) °C	T5 °C	T6 °C	Pt kPa	P1 kPa	Sh_g	Sc_g	Re_g	Re_l	Fr_l
Ethanol													
1	0.718	1.30	3.8	50.4	41.0	23.0	100.3	2.67	10.5	1.28	2426	24	10.67
2	0.717	1.74	3.8	50.6	42.1	23.2	100.3	2.67	10.6	1.28	2436	32	14.22
3	0.717	2.16	4.0	50.5	43.0	23.3	100.3	2.67	11.2	1.28	2450	40	17.52
4	0.717	2.50	4.3	50.6	43.4	23.4	100.3	2.67	11.9	1.28	2457	46	20.34
5	0.718	2.67	4.3	50.4	43.0	23.6	100.3	2.67	12.1	1.28	2463	49	21.63
6	0.717	2.83	4.4	50.6	43.9	23.4	100.3	2.67	12.2	1.28	2464	52	22.94
7	0.717	3.31	4.5	50.6	44.3	23.5	100.3	2.67	12.7	1.28	2473	62	26.84
8	0.808	1.30	4.2	50.1	41.0	23.2	100.3	3.07	12.0	1.28	2729	24	11.57
9	0.807	1.74	4.4	50.0	41.5	23.2	100.3	3.07	12.7	1.28	2747	32	14.96
10	0.807	2.16	4.5	50.4	42.6	23.1	100.3	3.07	12.8	1.28	2754	40	18.56
11	0.807	2.50	4.7	50.4	42.9	23.1	100.3	3.07	13.4	1.28	2763	46	21.49
12	0.807	2.67	4.9	50.4	43.2	23.4	100.3	3.07	13.9	1.28	2766	49	23.26
13	0.807	2.83	5.0	50.5	43.5	23.4	100.3	3.07	14.1	1.28	2770	52	24.07
14	0.808	3.31	5.1	50.5	43.8	23.4	100.3	3.07	14.4	1.28	2780	61	28.34
15	0.897	1.30	4.5	50.1	41.5	23.8	100.3	3.47	12.6	1.28	3029	24	12.08
16	0.897	1.74	4.9	50.2	42.4	24.4	100.3	3.47	13.8	1.28	3044	32	16.01
17	0.896	2.16	5.1	50.4	41.8	24.6	100.3	3.47	14.2	1.28	3054	40	19.77
18	0.896	2.50	5.6	50.3	42.9	24.7	100.3	3.47	15.8	1.28	3066	46	22.85
19	0.896	2.67	5.8	50.5	43.3	25.4	100.3	3.47	16.3	1.28	3067	49	24.40
20	0.897	2.83	6.0	50.5	43.4	25.3	100.3	3.47	17.0	1.28	3072	52	25.79
21	0.897	3.31	6.2	50.5	43.9	25.7	100.3	3.47	17.7	1.28	3083	61	30.11
22	0.985	1.30	5.2	50.2	41.4	25.8	100.3	4.00	14.7	1.28	3322	24	12.95
23	0.985	1.74	5.8	50.1	41.8	25.8	100.3	4.00	16.6	1.28	3342	32	17.07

Table A3-1 Continued - Ethanol

Run No.	Air Rate g/s	Liquid rate ml/s	Evap rate ml/min	T_{avg} (T1-T4) °C	T5 °C	T6 °C	Pt kPa	P1 kPa	Sh_g	Sc_g	Re_g	Re_l	Fr_l
24	0.985	2.16	6.1	50.7	42.2	25.8	100.3	4.00	17.0	1.28	3345	40	21.18
25	0.985	2.50	6.3	50.3	42.3	25.7	100.3	4.00	18.0	1.28	3363	46	24.37
26	0.985	2.67	6.5	50.4	42.4	26.0	100.3	4.00	18.4	1.28	3366	49	25.99
27	0.984	2.83	6.6	50.5	42.4	26.0	100.3	4.00	18.8	1.28	3369	52	27.49
28	0.984	3.31	7.0	50.5	42.7	25.8	100.3	4.00	20.0	1.28	3382	61	32.06
29	1.070	1.30	5.6	50.0	40.8	24.6	100.1	4.53	16.0	1.28	3612	24	13.83
30	1.070	1.74	6.2	50.1	41.3	24.8	100.1	4.53	17.7	1.28	3627	32	18.27
31	1.069	2.16	6.6	50.2	41.9	25.3	100.1	4.53	18.7	1.28	3641	40	22.47
32	1.069	2.50	6.9	50.5	42.1	25.6	100.1	4.53	19.3	1.28	3646	46	26.09
33	1.070	2.67	6.9	50.4	42.4	26.4	100.1	4.53	19.4	1.28	3652	49	27.70
34	1.070	2.83	7.2	50.7	42.6	26.0	100.1	4.53	20.1	1.28	3651	52	29.38
35	1.070	3.31	7.4	50.6	42.9	26.1	100.1	4.53	20.9	1.28	3666	61	34.21
36	1.164	1.30	5.9	50.2	41.7	28.0	100.0	5.07	16.5	1.28	3915	24	14.68
37	1.163	1.74	6.6	50.0	41.8	28.1	100.0	5.07	18.9	1.28	3938	32	19.65
38	1.161	2.16	6.9	50.3	42.2	28.3	100.0	5.07	19.6	1.28	3949	40	24.18
39	1.162	2.50	7.5	50.2	42.2	28.4	100.0	5.07	21.3	1.28	3962	46	27.90
40	1.165	2.67	7.6	50.5	42.4	28.3	100.0	5.07	21.3	1.28	3962	49	29.79
41	1.165	2.83	7.9	51.0	42.3	28.4	100.0	5.07	21.5	1.28	3955	53	31.71
42	1.164	3.03	8.3	50.6	42.4	28.3	100.0	5.07	23.3	1.28	3970	56	33.68
43	1.252	1.30	6.2	49.8	41.5	28.1	100.0	5.73	17.9	1.28	4209	24	16.02
44	1.250	1.74	6.8	49.8	41.7	28.2	100.0	5.73	19.4	1.28	4230	32	21.02
45	1.250	2.16	7.5	50.3	41.4	27.7	100.0	5.73	21.2	1.28	4236	40	25.91
46	1.250	2.30	8.1	50.2	41.0	27.6	100.0	5.73	23.2	1.28	4243	42	27.51
47	1.249	2.50	8.7	50.6	40.8	27.3	100.0	5.73	24.3	1.28	4241	46	30.03

Table A3-1 Continued – Hexane

Run no.	Air rate g/s	Liquid rate ml/s	Evap rate Ml/min	Tavg (T1-T4) °C	T5 °C	T6 °C	Pt kPa	P1 kPa	Sh_g	Sc_g	Re_g	Re_l	Fr_l
Hexane													
1	0.758	1.97	10.8	31.5	24.4	26.1	99.7	2.67	26.7	2.04	2668	75	49.95
2	0.762	2.25	10.3	29.4	24.5	23.1	99.6	2.67	28.6	2.04	2704	84	55.93
3	0.762	2.70	10.9	29.5	24.9	23.4	99.6	2.67	30.1	2.04	2711	101	67.02
4	0.762	3.29	10.8	29.4	24.9	23.2	99.6	2.67	30.2	2.04	2721	123	81.23
5	0.762	3.81	11.0	29.4	25.0	23.3	99.6	2.67	30.8	2.04	2728	142	94.31
6	0.762	4.35	11.2	29.4	25.4	23.3	99.6	2.67	31.4	2.04	2736	162	108.57
7	0.762	4.93	11.4	29.5	25.7	23.6	99.6	2.67	31.9	2.04	2740	184	122.74
8	0.858	1.97	11.0	29.2	24.9	23.6	99.7	3.07	30.6	2.04	3035	73	56.48
9	0.858	2.48	11.2	29.3	24.5	23.6	99.7	3.07	31.1	2.04	3044	93	69.71
10	0.859	2.70	11.2	29.0	24.5	25.4	99.7	3.07	31.6	2.04	3055	100	75.36
11	0.857	2.93	11.7	29.5	24.6	23.8	99.7	3.07	32.1	2.04	3048	110	83.45
12	0.856	3.62	11.8	29.8	25.3	25.0	99.7	3.07	32.1	2.04	3055	135	101.38
13	0.856	4.04	12.3	29.8	25.5	25.0	99.7	3.07	33.6	2.04	3060	152	113.44
14	0.857	4.62	12.7	29.7	25.7	25.0	99.7	3.07	35.2	2.04	3070	173	129.90
15	0.955	1.97	11.7	29.3	23.8	22.8	99.9	3.47	32.3	2.04	3372	73	64.25
16	0.955	2.48	12.2	29.3	23.9	23.0	99.9	3.47	33.8	2.04	3383	92	78.92
17	0.954	2.70	12.2	29.5	24.6	24.6	99.9	3.47	33.5	2.04	3382	101	85.89
18	0.955	2.93	12.7	29.3	24.1	23.4	99.9	3.47	35.3	2.04	3391	109	93.06
19	0.954	3.62	13.3	29.4	24.4	23.6	99.9	3.47	37.2	2.04	3400	135	114.56
20	0.954	4.04	13.4	29.5	24.5	23.8	99.9	3.47	37.3	2.04	3405	151	128.09
21	0.954	4.35	13.8	29.5	24.8	24.2	99.9	3.47	38.4	2.04	3408	162	137.88
22	1.049	1.97	12.8	29.5	25.0	25.2	99.9	4.00	35.0	2.04	3694	73	74.55
23	1.048	2.48	13.2	29.6	24.4	25.3	99.9	4.00	35.9	2.04	3706	93	89.94

Table A3-1 Continued - Hexane

Run no.	Air rate g/s	Liquid rate ml/s	Evap rate ml/min	T_{avg} (T1-T4) °C	T5 °C	T6 °C	Pt kPa	P1 kPa	Sh_g	Sc_g	Re_g	Re_l	Fr_l
24	1.047	2.70	13.8	30.0	25.4	26.6	99.9	4.00	36.9	2.04	3699	101	99.68
25	1.048	2.93	13.8	29.6	24.5	25.3	99.9	4.00	37.9	2.04	3714	109	105.60
26	1.047	3.62	14.8	30.0	25.2	26.2	99.9	4.00	40.1	2.04	3717	136	130.08
27	1.047	4.04	15.2	30.0	25.3	26.5	99.9	4.00	41.1	2.04	3723	152	145.36
28	1.052	4.35	15.5	30.0	25.3	26.5	99.9	4.00	42.1	2.04	3746	163	157.35
29	1.140	1.67	14.0	29.9	25.4	26.7	99.9	4.53	37.3	2.04	3998	62	70.24
30	1.140	1.97	14.0	30.0	25.3	27.3	99.9	4.53	37.2	2.04	4002	74	83.39
31	1.140	2.25	14.0	29.9	24.8	26.8	99.9	4.53	37.4	2.04	4013	84	92.88
32	1.140	2.70	15.5	30.0	25.3	26.9	99.9	4.53	41.6	2.04	4021	101	110.28
33	1.140	3.29	16.2	29.9	25.3	27.1	99.9	4.53	43.8	2.04	4034	123	133.41
34	1.141	3.62	14.7	29.5	24.3	26.5	99.9	4.53	40.4	2.04	4050	135	146.12
35	1.248	1.97	14.0	29.1	23.6	25.5	100.2	4.93	38.9	2.04	4388	73	93.56
36	1.248	2.25	14.8	29.0	23.2	24.6	100.2	4.93	41.7	2.04	4398	84	105.51
37	1.248	2.48	15.3	29.0	23.2	24.7	100.2	4.93	43.3	2.04	4404	92	115.84
38	1.247	2.70	16.2	29.1	23.3	25.2	100.2	4.93	45.6	2.04	4405	100	125.12
39	1.336	1.97	16.7	29.9	25.9	27.9	100.1	5.33	44.6	2.04	4679	74	106.09
40	1.338	2.25	16.4	29.4	24.1	26.9	100.1	5.33	45.1	2.04	4702	84	119.28
n-propanol													
1	0.678	1.26	5.3	68.4	56.1	27.8	100.1	2.67	12.8	1.55	2188	19	9.33
2	0.677	1.64	5.6	68.8	57.2	28.2	100.1	2.67	13.4	1.55	2195	25	12.08
3	0.678	2.00	5.8	68.6	58.3	28.7	100.1	2.67	14.0	1.55	2207	31	14.65
4	0.677	2.24	5.8	68.8	59.1	30.0	100.1	2.67	13.9	1.55	2212	35	15.97
5	0.678	2.45	6.0	68.5	59.0	29.0	100.1	2.67	14.7	1.55	2220	38	17.41
6	0.677	2.91	6.1	68.8	60.0	29.4	100.1	2.67	14.7	1.55	2226	45	20.71

Table A3-1 Continued n-propanol

Run no.	Air rate g/s	Liquid rate ml/s	Evap rate ml/min	T_{avg} (T1-T4) °C	T5 °C	T6 °C	Pt kPa	P1 kPa	Sh_g	Sc_g	Re_g	Re_l	Fr_l
7	0.677	3.27	6.6	68.9	60.5	29.5	100.1	2.67	15.9	1.55	2231	51	23.31
8	0.765	1.26	5.8	67.9	53.4	24.8	100.3	3.07	14.5	1.54	2470	19	9.99
9	0.764	1.64	5.9	68.3	55.4	25.0	100.3	3.07	14.5	1.55	2477	25	12.92
10	0.764	2.00	6.0	68.5	57.0	25.7	100.3	3.07	14.6	1.55	2487	31	15.23
11	0.764	2.24	6.3	68.3	58.3	26.3	100.3	3.07	15.6	1.55	2495	34	17.24
12	0.765	2.45	6.4	68.1	58.3	25.8	100.3	3.07	16.2	1.55	2504	38	18.51
13	0.765	2.91	6.6	68.2	59.3	26.1	100.3	3.07	16.6	1.55	2514	45	21.92
14	0.764	3.27	6.7	68.3	59.9	26.3	100.3	3.07	16.8	1.55	2520	50	24.65
15	0.848	1.26	6.4	68.5	54.8	26.4	100.3	3.47	15.4	1.55	2730	19	10.93
16	0.848	1.64	6.5	68.5	56.4	26.6	100.3	3.47	15.6	1.55	2743	25	14.03
17	0.848	2.00	6.7	68.7	57.8	26.9	100.3	3.47	16.2	1.55	2755	31	16.44
18	0.849	2.24	6.9	68.4	58.6	27.0	100.3	3.47	16.9	1.55	2767	34	18.26
19	0.848	2.45	6.9	68.6	58.5	26.9	100.3	3.47	16.8	1.55	2768	38	20.05
20	0.849	2.91	7.2	68.4	59.7	27.0	100.3	3.47	17.7	1.55	2783	45	23.61
21	0.848	3.27	7.6	68.6	60.3	27.0	100.3	3.47	18.6	1.55	2789	51	26.55
22	0.930	1.26	6.9	68.4	54.7	30.3	99.9	4.00	16.6	1.55	2989	19	11.81
23	0.930	1.64	8.0	68.4	55.8	30.6	99.9	4.00	19.5	1.55	3005	25	14.56
24	0.928	2.00	8.5	69.1	56.5	31.0	99.9	4.00	20.0	1.55	3006	31	17.81
25	0.929	2.24	8.5	68.6	57.4	31.2	99.9	4.00	20.7	1.55	3022	35	19.72
26	0.928	2.45	8.6	69.0	57.2	31.0	99.9	4.00	20.6	1.55	3022	38	21.68
27	0.929	2.91	8.7	68.8	58.0	31.2	99.9	4.00	21.1	1.55	3039	45	25.02
28	0.929	3.27	9.3	68.8	58.8	31.3	99.9	4.00	22.5	1.55	3046	51	28.60
29	1.013	1.26	7.9	68.4	54.1	31.1	100.0	4.53	19.1	1.55	3251	19	12.81
30	1.012	1.64	8.3	68.7	55.3	31.2	100.0	4.53	19.9	1.55	3264	25	15.79

Table A3-1 Continued n-propanol

Run no.	Air rate g/s	Liquid rate ml/s	Evap rate ml/min	T_{avg} (T1-T4) °C	T5 °C	T6 °C	Pt kPa	P1 kPa	Sh_g	Sc_g	Re_g	Re_l	Fr_l
31	1.012	2.00	8.8	68.6	56.0	31.2	100.0	4.53	21.4	1.55	3279	31	19.05
32	1.013	2.24	8.9	68.3	57.1	29.9	99.9	4.53	22.0	1.55	3291	34	21.13
33	1.013	2.45	9.0	68.1	57.3	29.6	99.9	4.53	22.6	1.55	3301	38	23.00
34	1.012	2.91	9.1	68.6	58.0	28.9	99.9	4.53	22.2	1.55	3304	45	27.35
35	1.012	3.27	9.4	68.7	58.4	31.8	100.0	4.53	22.8	1.55	3314	51	30.70
36	1.099	1.26	8.1	68.2	54.5	33.4	99.7	5.07	19.8	1.55	3526	19	13.96
37	1.099	1.64	8.7	68.3	56.0	33.4	99.7	5.07	21.1	1.55	3544	25	16.92
38	1.100	2.00	9.6	68.1	56.7	33.8	99.7	5.07	23.8	1.55	3561	31	20.52
39	1.101	2.24	9.8	68.2	56.9	30.4	99.9	5.07	24.2	1.55	3572	34	22.92
40	1.099	2.45	9.9	68.2	57.0	33.6	99.7	5.07	24.7	1.55	3575	38	24.99
41	1.098	2.91	10.2	68.6	58.1	34.0	99.7	5.07	24.7	1.55	3581	45	29.63
42	1.099	3.27	10.3	68.5	58.8	34.6	99.7	5.07	25.4	1.55	3592	50	33.59
43	1.181	1.26	9.1	68.2	53.8	34.3	99.7	5.73	22.1	1.55	3782	19	15.15
44	1.181	1.64	9.7	68.3	55.0	34.6	99.7	5.73	23.7	1.55	3801	25	18.46
45	1.180	2.00	10.5	68.6	55.9	34.8	99.7	5.73	25.5	1.55	3810	31	22.33
46	1.181	2.24	10.9	68.2	56.7	34.6	99.7	5.73	27.0	1.55	3826	34	24.73
47	1.180	2.45	11.0	68.6	56.7	34.8	99.7	5.73	26.7	1.55	3825	38	27.15
48	1.180	2.91	11.3	68.4	57.6	34.8	99.7	5.73	28.0	1.55	3845	45	31.81
2-Methoxyethanol													
1	0.646	1.21	4.5	88.0	70.3	24.4	100.9	2.67	10.9	1.67	1958	39	20.51
2	0.647	1.61	4.6	87.8	72.3	25.0	100.9	2.67	11.4	1.67	1968	52	26.97
3	0.646	1.96	4.8	87.9	73.5	25.2	100.9	2.67	11.9	1.67	1973	63	32.57
4	0.646	2.32	5.0	88.0	75.5	25.6	100.9	2.67	12.3	1.67	1978	75	38.50
5	0.646	2.72	5.1	88.2	76.6	25.8	100.9	2.67	12.4	1.67	1983	89	43.97

Table A3-1 Continued 2-methoxyethanol

Run no.	Air r rate g/s	Liquid rate ml/s	Evap rate ml/min	T_{avg} (T1-T4) °C	T5 °C	T6 °C	Pt kPa	P1 kPa	Sh_g	Sc_g	Re_g	Re_l	Fr_l
6	0.646	3.13	5.2	88.2	77.5	25.8	100.9	2.67	12.8	1.67	1989	102	50.89
7	0.726	1.21	5.3	88.4	70.5	25.8	100.8	3.07	12.7	1.67	2194	40	21.95
8	0.725	1.61	5.1	88.5	71.8	25.8	100.8	3.07	12.1	1.67	2201	53	29.76
9	0.726	1.96	5.5	88.4	73.2	25.9	100.8	3.07	13.2	1.67	2209	64	35.72
10	0.726	2.32	5.6	88.0	73.6	26.2	100.7	3.07	13.9	1.67	2221	75	40.57
11	0.725	2.72	5.7	88.3	74.4	26.2	100.7	3.07	13.9	1.67	2223	89	47.60
12	0.726	3.13	5.8	87.9	74.7	26.3	100.7	3.07	14.6	1.67	2235	102	53.51
13	0.808	1.21	5.6	88.2	69.0	22.1	100.9	3.47	13.5	1.67	2439	39	24.62
14	0.807	1.61	5.9	88.2	70.2	22.3	100.9	3.47	14.2	1.67	2449	53	32.33
15	0.808	1.96	6.1	88.1	71.0	22.2	100.9	3.47	15.1	1.67	2460	64	37.49
16	0.808	2.32	6.1	87.8	72.0	22.5	100.9	3.47	15.3	1.67	2471	75	43.97
17	0.807	2.72	6.4	88.4	72.5	22.7	100.9	3.47	15.6	1.67	2469	89	51.77
18	0.806	3.13	6.8	88.7	73.8	22.8	100.9	3.47	16.2	1.67	2470	103	59.69
19	0.886	1.21	6.1	87.5	66.5	22.0	100.5	4.00	15.3	1.67	2678	39	26.62
20	0.886	1.61	6.4	88.5	69.5	22.8	100.9	4.00	15.2	1.67	2684	53	35.19
21	0.886	1.96	6.7	88.6	70.3	22.6	100.9	4.00	16.0	1.67	2690	64	41.28
22	0.887	2.32	6.8	88.1	71.4	22.7	100.9	4.00	16.6	1.67	2705	76	48.21
23	0.887	2.72	7.6	88.4	72.7	22.7	100.9	4.00	18.7	1.67	2708	89	56.98
24	0.887	3.13	8.0	88.3	74.2	22.9	100.9	4.00	19.7	1.67	2717	102	64.41
25.	0.957	0.83	6.9	88.4	68.0	25.4	100.0	4.53	16.3	1.67	2869	27	20.89
26	0.957	1.21	7.3	88.4	70.2	25.8	100.0	4.53	17.3	1.67	2883	40	28.72
27	0.957	1.61	7.7	88.3	70.5	25.8	100.0	4.53	18.4	1.67	2895	53	38.32
28	0.967	1.96	7.7	87.7	70.3	22.7	100.9	4.53	19.3	1.67	2939	63	44.40
29	0.967	2.32	8.0	87.7	71.6	22.7	100.9	4.53	20.0	1.67	2947	75	52.13

Table A3-1 Continued 2-methyoxyethanol

Run no.	Air rate g/s	Liquid rate ml/s	Evap rate ml/min	T_{avg} (T1-T4) °C	T5 °C	T6 °C	Pt kPa	P1 kPa	Sh_g	Sc_g	Re_g	Re_l	Fr_l
30	0.966	2.72	8.3	88.0	72.1	22.9	100.9	4.53	20.7	1.67	2950	88	60.96
31	1.046	0.83	6.7	86.8	66.8	25.8	100.1	5.07	17.1	1.67	3146	26	22.67
32	1.044	1.21	6.8	87.7	68.0	26.0	100.1	5.07	16.7	1.67	3146	39	32.32
33	1.043	1.61	7.3	87.8	70.0	26.2	100.1	5.07	17.9	1.67	3155	52	42.18
34	1.044	1.96	7.8	87.4	71.5	26.4	100.0	5.07	19.6	1.67	3170	63	49.36
35	1.043	2.32	8.3	87.6	72.9	26.4	100.0	5.07	20.8	1.67	3175	75	56.89
36	1.042	2.72	8.6	87.9	73.5	26.4	100.0	5.07	21.4	1.67	3179	88	66.97
37	1.120	0.83	6.9	87.4	66.9	26.0	99.9	5.73	17.0	1.67	3358	27	25.56
38	1.120	1.21	7.3	87.4	67.5	26.0	99.9	5.73	18.1	1.67	3374	39	35.08
39	1.119	1.61	8.0	87.5	69.3	26.2	99.9	5.73	19.8	1.67	3385	52	45.68
40	1.120	1.96	8.3	87.4	71.1	26.2	99.9	5.73	20.8	1.67	3397	63	52.32
41	1.122	2.32	9.2	88.2	70.8	23.4	100.3	5.73	22.3	1.67	3408	76	62.69
2-methyl-2-propanol													
1	0.710	0.59	4.3	54.6	40.9	20.9	100.5	2.67	9.8	1.76	2360	6	2.95
2	0.709	0.89	4.4	54.8	41.3	21.0	100.5	2.67	9.8	1.76	2373	9	4.56
3	0.709	1.16	4.6	55.0	43.1	21.4	100.5	2.67	10.2	1.76	2386	11	5.71
4	0.708	1.49	5.0	55.0	44.6	21.8	100.5	2.67	11.2	1.76	2398	15	7.28
5	0.709	1.87	5.5	54.9	45.5	21.9	100.5	2.67	12.5	1.76	2412	18	9.03
6	0.708	2.29	5.7	55.0	46.4	22.1	100.5	2.67	12.8	1.76	2424	23	11.05
7	0.798	0.59	4.9	54.5	41.2	22.4	100.5	3.07	11.1	1.76	2651	6	3.21
8	0.798	0.89	5.3	54.7	41.1	22.6	100.5	3.07	11.9	1.76	2665	9	4.95
9	0.797	1.16	5.4	55.1	41.8	22.7	100.5	3.07	12.0	1.76	2673	11	6.52
10	0.797	1.49	5.7	55.0	43.9	23.0	100.5	3.07	12.7	1.76	2693	15	7.88
11	0.797	1.87	6.6	54.8	44.9	23.2	100.5	3.07	15.2	1.76	2710	18	9.74

Table A3-1 Continued 2-methyl-2-propanol

Run no.	Air rate g/s	Liquid rate ml/s	Evap rate ml/min	T_{avg} (T1-T4) °C	T5 °C	T6 °C	Pt kPa	P1 kPa	Sh_g	Sc_g	Re_g	Re_l	Fr_l
12	0.798	2.29	6.5	54.7	45.8	23.4	100.5	3.07	15.0	1.76	2726	22	11.83
13	0.887	0.59	5.3	54.0	40.3	23.5	100.4	3.47	12.5	1.76	2946	6	3.58
14	0.887	0.89	5.7	54.1	40.4	23.6	100.4	3.47	13.3	1.76	2966	8	5.28
15	0.886	1.16	6.0	54.6	42.1	23.7	100.4	3.47	13.7	1.76	2971	11	7.00
16	0.885	1.49	6.2	54.4	43.0	24.9	100.3	3.47	14.3	1.76	2989	14	8.43
17	0.884	1.87	6.5	54.7	44.2	25.0	100.3	3.47	15.0	1.76	3000	18	10.55
18	0.884	2.29	6.8	54.8	45.1	25.0	100.3	3.47	15.6	1.76	3015	22	12.85
19	0.974	0.59	5.8	53.9	39.9	25.2	100.3	4.00	13.7	1.76	3231	6	3.93
20	0.974	0.89	6.2	53.9	40.7	25.2	100.3	4.00	14.7	1.76	3256	8	5.60
21	0.973	1.16	6.8	54.3	41.9	25.3	100.3	4.00	15.9	1.76	3262	11	7.58
22	0.972	1.49	6.9	54.7	43.0	25.4	100.3	4.00	15.7	1.76	3274	15	9.29
23	0.972	1.87	7.4	54.8	43.8	25.3	100.3	4.00	16.8	1.76	3289	18	11.54
24	0.973	2.29	7.8	54.2	44.5	25.3	100.3	4.00	18.5	1.76	3318	22	13.74
25	1.061	0.59	6.5	53.9	40.0	25.2	100.3	4.53	15.4	1.76	3517	6	4.19
26	1.060	0.89	6.9	54.2	39.6	25.3	100.3	4.53	16.1	1.76	3531	9	6.41
27	1.059	1.16	7.5	54.5	41.0	25.4	100.3	4.53	17.1	1.76	3543	11	8.35
28	1.060	1.49	7.6	54.4	42.2	25.3	100.3	4.53	17.7	1.76	3567	14	10.02
29	1.059	1.87	7.8	54.5	43.2	25.3	100.3	4.53	18.1	1.76	3583	18	12.43
30	1.059	2.29	8.4	54.7	43.1	25.3	100.3	4.53	19.4	1.76	3597	22	15.17
31	1.153	0.59	7.2	54.1	40.2	25.2	100.3	5.07	16.7	1.76	3812	6	4.68
32	1.152	0.89	7.2	54.5	39.5	25.1	100.3	5.07	16.4	1.76	3827	9	7.15
33	1.152	1.16	8.0	54.4	40.7	25.0	100.3	5.07	18.4	1.76	3850	11	8.77
34	1.153	1.49	8.6	54.2	41.6	25.0	100.3	5.07	20.2	1.76	3874	14	10.97
35	1.151	1.87	9.0	54.7	42.7	25.0	100.3	5.07	20.5	1.76	3882	18	13.76

Table A3-1 Continued 2-methyl-2-prpopanol

Run no.	Air rate g/s	Liquid rate ml/s	Evap rate ml/min	T_{avg} (T1-T4) °C	T5 °C	T6 °C	Pt kPa	P1 kPa	Sh_g	Sc_g	Re_g	Re_l	Fr_l
36	1.151	2.29	9.1	54.8	43.6	25.0	100.3	5.07	20.8	1.76	3898	22	16.71
37	1.240	0.59	7.3	54.2	39.1	23.5	100.5	5.73	16.9	1.76	4091	6	5.40
38	1.241	0.89	7.8	54.0	39.5	23.5	100.5	5.73	18.4	1.76	4124	8	7.77
39	1.241	1.16	8.4	54.1	40.2	23.4	100.5	5.73	19.8	1.76	4145	11	9.50
40	1.241	1.49	9.2	54.2	41.0	23.4	100.5	5.73	21.6	1.76	4163	14	12.00
41	1.239	1.87	9.9	54.7	42.0	23.4	100.5	5.73	22.7	1.76	4170	18	15.02

Table A3-2 Experimental results for binary mixtures

Run no.	Air rate	Liquid rate	Evap rate	Tavg (T1-T4)	T5	T6	Pt	P1
	g/s	ml/s	ml/min	°C	°C	°C	kPa	kPa
n-tridecane(1)/cyclohexane(2) {mass fraction = 0.25 of component 2}								
1	0.739	1.03	2.45	45.3	36.1	19.0	101.3	2.67
2	0.738	1.40	2.56	45.4	37.7	19.0	101.3	2.67
3	0.735	1.83	2.65	45.1	38.7	17.5	100.7	2.67
4	0.734	2.23	2.88	45.5	39.8	18.0	100.7	2.67
5	0.734	2.72	3.06	45.4	40.4	18.3	100.7	2.67
6	0.830	1.03	2.79	45.3	34.3	17.2	101.1	3.07
7	0.831	1.40	2.88	44.9	36.7	17.5	101.1	3.07
8	0.830	1.83	2.94	45.3	38.2	17.7	101.1	3.07
9	0.829	2.23	3.00	45.5	39.1	18.0	101.1	3.07
10	0.830	2.72	3.18	45.4	40.1	18.3	101.1	3.07
11	0.922	1.03	2.88	45.1	35.3	18.6	101.1	3.60
12	0.922	1.40	3.06	45.2	37.2	18.5	101.1	3.60
13	0.922	1.83	3.25	45.1	38.4	18.5	101.1	3.60
14	0.922	2.23	3.44	45.2	39.0	18.3	101.1	3.60
15	0.922	2.72	3.56	45.2	39.8	18.2	101.1	3.60
16	1.016	1.03	3.00	45.1	34.4	15.3	101.2	4.00
17	1.015	1.40	3.43	45.1	36.8	16.0	101.2	4.00
18	1.015	1.83	3.57	45.3	38.4	16.3	101.2	4.00
19	1.015	2.23	3.71	45.2	39.2	16.6	101.2	4.00
20	1.015	2.72	3.86	45.2	39.7	17.0	101.2	4.00
21	1.109	1.03	3.46	44.9	35.3	17.3	101.2	4.40
22	1.108	1.40	4.00	45.0	37.0	17.7	101.2	4.40
23	1.108	1.83	4.08	45.2	38.1	18.2	101.2	4.40

Table A3-2 Continued n-tridecane/cyclohexane

Run no.	Air rate	Liquid rate	Evap rate	Tavg (T1-T4)	T5	T6	Pt	P1
	g/s	ml/s	ml/min	°C	°C	°C	kPa	kPa
24	1.107	2.23	4.33	45.3	38.8	18.3	101.2	4.40
25	1.107	2.72	4.45	45.3	39.7	18.4	101.2	4.40
26	1.211	1.03	3.83	45.1	35.4	18.6	101.3	5.07
27	1.211	1.40	4.17	45.1	37.1	18.6	101.3	5.07
28	1.211	1.83	4.45	45.3	38.3	18.7	101.3	5.07
29	1.211	2.23	4.73	45.2	38.5	18.9	101.3	5.07
30	1.211	2.72	4.80	45.3	39.1	19.0	101.3	5.07
n-tridecane(1)/cyclohexane(2) {mass fraction = 0.53 of component 2}								
1	0.739	1.05	3.43	44.9	33.0	13.6	101.3	2.67
2	0.739	1.43	3.57	44.8	35.8	14.2	101.1	2.67
3	0.740	1.88	3.79	44.8	36.3	14.3	101.3	2.67
4	0.738	2.34	3.93	45.1	38.1	14.4	101.1	2.67
5	0.739	2.82	4.00	45.0	38.2	14.6	101.3	2.67
6	0.832	1.05	3.75	44.7	33.4	14.6	101.2	3.07
7	0.832	1.43	4.00	44.7	35.9	14.3	101.3	3.07
8	0.830	1.88	4.25	45.1	37.4	15.4	101.1	3.07
9	0.832	2.34	4.42	45.0	37.9	14.5	101.3	3.07
10	0.831	2.82	4.55	45.4	38.8	15.2	101.3	3.07
11	0.923	1.05	4.08	44.6	34.4	15.5	101.0	3.60
12	0.921	1.43	4.36	45.1	36.0	15.6	101.0	3.60
13	0.922	1.88	4.55	45.2	37.4	14.5	101.1	3.60
14	0.913	2.34	4.73	45.0	36.7	12.7	100.0	3.60
15	0.912	2.82	4.80	45.2	37.4	13.0	100.0	3.60
16	1.017	1.05	4.45	45.1	32.7	13.1	101.3	4.00

Table A3-2 Continued – n-tridecane/cyclohexane

Run no.	Air rate	Liquid rate	Evap rate	Tavg (T1-T4)	T5	T6	Pt	P1
	g/s	ml/s	ml/min	°C	°C	°C	kPa	kPa
17	1.016	1.43	4.82	45.3	35.1	13.4	101.3	4.00
18	1.016	1.88	5.10	45.4	36.8	13.8	101.3	4.00
19	1.017	2.34	5.30	45.1	37.6	13.8	101.3	4.00
20	1.017	2.82	5.44	45.2	38.3	13.8	101.3	4.00
21	1.110	1.05	4.90	44.8	33.5	13.8	101.3	4.40
22	1.110	1.43	5.20	45.0	35.0	13.8	101.3	4.40
23	1.110	1.88	5.56	45.0	36.3	13.8	101.3	4.40
24	1.110	2.34	5.78	45.0	37.3	14.0	101.3	4.40
25	1.110	2.82	5.88	45.0	38.1	14.0	101.3	4.40
26	1.214	1.05	5.00	44.7	33.0	14.0	101.3	5.07
27	1.213	1.43	5.60	44.9	34.7	14.2	101.3	5.07
28	1.212	1.88	6.00	45.1	36.2	14.2	101.3	5.07
29	1.213	2.34	6.13	45.0	37.0	14.1	101.3	5.07
30	1.211	2.82	6.25	45.4	37.9	14.2	101.3	5.07
n-tridecane(1)/cyclohexane(2) {mass fraction = 0.74 of component 2}								
1	0.738	1.20	6.67	44.8	33.3	14.3	101.0	2.67
2	0.738	1.66	6.75	44.7	35.1	14.6	101.0	2.67
3	0.737	2.12	7.00	45.0	36.1	14.7	101.0	2.67
4	0.738	2.62	7.43	44.9	36.8	14.7	101.0	2.67
5	0.738	3.05	7.57	44.8	37.5	14.8	101.0	2.67
6	0.830	1.20	7.71	45.0	33.7	15.8	101.1	3.07
7	0.830	1.66	8.00	44.9	34.9	16.0	101.1	3.07
8	0.830	2.12	8.33	44.9	35.8	16.1	101.1	3.07
9	0.830	2.62	8.67	44.9	36.5	16.2	101.1	3.07

Table A3-2 Continued n-tridecane/cyclohexane

Run no.	Air rate	Liquid rate	Evap rate	Tavg (T1-T4)	T5	T6	Pt	P1
	g/s	ml/s	ml/min	°C	°C	°C	kPa	kPa
10	0.830	3.05	9.00	44.9	37.3	16.2	101.1	3.07
11	0.923	1.20	8.33	44.8	33.8	16.3	101.1	3.60
12	0.923	1.66	8.67	44.9	34.7	16.6	101.1	3.60
13	0.922	2.12	8.92	45.0	35.5	16.7	101.1	3.60
14	0.923	2.62	9.20	44.9	36.2	16.8	101.1	3.60
15	0.923	3.05	9.50	44.8	36.8	16.7	101.1	3.60
16	1.015	1.20	8.83	45.0	33.4	16.6	101.1	4.00
17	1.015	1.66	9.40	44.9	34.7	16.6	101.1	4.00
18	1.015	2.12	9.64	44.9	35.3	16.6	101.1	4.00
19	1.015	2.62	9.82	44.8	35.8	16.6	101.1	4.00
20	1.015	3.05	10.20	44.8	36.7	16.6	101.1	4.00
21	1.107	1.20	9.64	44.9	33.6	16.5	101.1	4.40
22	1.107	1.66	10.20	44.8	34.0	16.4	101.1	4.40
23	1.107	2.12	10.40	44.9	34.7	16.5	101.1	4.40
24	1.108	2.62	10.55	44.8	35.2	16.2	101.1	4.40
25	1.107	3.05	10.80	45.0	36.1	16.2	101.1	4.40
26	1.210	1.20	9.60	44.9	33.3	15.1	101.1	5.07
27	1.209	1.66	10.26	45.1	34.4	15.4	101.1	5.07
28	1.209	2.12	10.60	45.0	35.1	15.7	101.1	5.07
29	1.209	2.62	11.00	45.0	36.0	15.8	101.1	5.07

Table A3-2 Continued 1-Octanol/n-hexane

Run no.	Air rate	Liquid rate	Evap rate	Tavg (T1-T4)	T5	T6	Pt	P1
	g/s	ml/s	ml/min	°C	°C	°C	kPa	kPa
1-Octanol(1)/n-hexane(2) {mass fraction = 0.25 of component 2}								
1	0.757	0.85	2.88	36.2	27.9	17.7	100.8	2.67
2	0.758	1.04	3.00	35.9	28.4	16.3	100.9	2.67
3	0.757	1.43	3.20	36.2	29.7	16.7	100.8	2.67
4	0.757	1.82	3.66	36.2	30.7	17.1	100.8	2.67
5	0.757	2.20	3.77	36.1	31.4	17.5	100.8	2.67
6	0.852	0.85	3.00	36.2	28.5	18.0	100.8	3.07
7	0.851	1.04	3.43	36.2	29.2	17.6	100.8	3.07
8	0.851	1.43	3.57	36.3	30.4	17.8	100.8	3.07
9	0.852	1.82	4.00	36.2	30.8	17.9	100.8	3.07
10	0.852	2.20	4.08	36.2	31.4	18.0	100.8	3.07
11	0.948	0.85	3.13	36.0	25.7	13.5	100.9	3.60
12	0.947	1.04	3.50	36.4	28.8	14.3	100.9	3.60
13	0.946	1.43	3.64	36.5	29.4	14.9	100.9	3.60
14	0.947	1.82	3.79	36.2	30.3	15.1	100.9	3.60
15	0.947	2.20	4.14	36.3	31.1	15.6	100.9	3.60
16	1.038	0.85	3.50	35.9	27.2	17.4	100.5	4.00
17	1.037	1.04	3.85	36.2	28.9	17.4	100.5	4.00
18	1.038	1.43	4.08	36.0	29.3	17.3	100.5	4.00
19	1.038	1.82	4.17	36.1	30.4	17.2	100.5	4.00
20	1.037	2.20	4.33	36.1	31.0	17.3	100.5	4.00
21	1.130	0.85	3.62	35.8	27.2	17.5	100.2	4.40
22	1.130	1.04	4.00	35.9	28.1	17.7	100.2	4.40
23	1.129	1.43	4.15	36.0	30.1	17.8	100.2	4.40

Table A3-2 Continued, 1-Octanol/n-hexane

Run no.	Air rate	Liquid rate	Evap rate	Tavg (T1-T4)	T5	T6	Pt	P1
	g/s	ml/s	ml/min	°C	°C	°C	kPa	kPa
24	1.129	1.82	4.33	36.2	30.7	17.8	100.2	4.40
25	1.130	2.20	4.58	35.9	31.0	17.9	100.2	4.40
26	1.232	0.85	3.92	35.9	27.1	17.0	100.0	5.07
27	1.232	1.04	4.17	35.8	27.7	17.0	100.0	5.07
28	1.231	1.43	4.42	36.1	28.9	16.7	100.0	5.07
29	1.231	1.82	4.73	36.0	30.3	16.9	100.0	5.07
30	1.231	2.20	4.91	36.1	30.6	17.0	100.0	5.07
1-Octanol(1)/n-hexane(2) {mass fraction = 0.50 of component 2}								
1	0.749	1.18	6.13	35.7	28.9	15.2	99.6	2.67
2	0.748	1.64	6.88	36.1	29.9	15.4	99.6	2.67
3	0.748	2.08	7.43	36.0	30.6	15.4	99.6	2.67
4	0.748	2.51	7.86	36.0	30.9	15.6	99.6	2.67
5	0.748	2.98	8.31	36.1	31.2	15.6	99.6	2.67
6	0.842	1.18	7.29	35.9	28.9	15.4	99.5	3.07
7	0.841	1.64	7.86	36.0	29.8	15.5	99.5	3.07
8	0.841	2.08	8.46	36.2	30.5	15.6	99.5	3.07
9	0.841	2.51	8.83	36.1	30.8	15.6	99.5	3.07
10	0.841	2.98	9.17	36.1	31.2	15.6	99.5	3.07
11	0.935	1.18	8.50	36.2	29.1	15.7	99.6	3.60
12	0.935	1.64	8.83	36.1	29.5	15.7	99.6	3.60
13	0.935	2.08	9.33	36.1	30.2	15.7	99.6	3.60
14	0.935	2.51	9.80	36.1	30.5	15.7	99.6	3.60
15	0.935	2.98	10.17	36.1	30.8	15.7	99.6	3.60
16	1.035	1.18	8.33	36.0	28.8	14.5	100.2	4.00

Table A3-2 Continued 1-Octanol/n-hexane

Run no.	Air rate g/s	Liquid rate ml/s	Evap rate ml/min	Tavg (T1-T4) °C	T5 °C	T6 °C	Pt kPa	P1 kPa
17	1.035	1.64	9.17	36.1	29.1	14.7	100.2	4.00
18	1.035	2.08	9.82	36.1	29.7	14.9	100.2	4.00
19	1.035	2.51	10.00	36.1	29.1	15.0	100.2	4.00
20	1.035	2.98	10.20	36.0	30.6	15.1	100.2	4.00
21	1.143	1.18	9.00	35.8	28.3	15.2	101.3	4.40
22	1.142	1.64	10.00	35.9	29.2	15.3	101.3	4.40
23	1.142	2.08	10.60	36.0	29.6	15.2	101.3	4.40
24	1.142	2.51	11.00	35.9	29.9	15.2	101.3	4.40
25	1.141	2.98	11.11	36.2	30.3	15.4	101.3	4.40
26	1.233	1.18	9.40	36.0	28.0	15.4	100.1	5.07
27	1.234	1.64	10.40	35.9	29.0	15.4	100.1	5.07
28	1.234	2.08	10.80	35.8	29.0	15.4	100.1	5.07
29	1.233	2.51	11.20	36.1	29.2	15.5	100.1	5.07
1-Octanol(1)/n-hexane(2) {mass fraction = 0.75 of component 2}								
1	0.763	1.85	10.80	35.2	28.4	13.3	101.3	2.67
2	0.763	2.24	11.20	35.2	29.1	13.5	101.3	2.67
3	0.763	2.78	11.60	35.3	29.7	13.6	101.3	2.67
4	0.763	3.27	11.78	35.5	29.9	13.7	101.3	2.67
5	0.762	3.76	12.21	35.6	30.2	13.8	101.3	2.67
6	0.858	1.85	11.60	35.4	28.6	13.8	101.3	3.07
7	0.858	2.24	12.00	35.4	28.8	13.8	101.3	3.07
8	0.859	2.78	12.89	35.2	29.3	13.8	101.3	3.07
9	0.858	3.27	13.56	35.3	29.5	13.8	101.3	3.07
10	0.858	3.76	14.00	35.4	29.7	14.0	101.3	3.07

Table A3-2 Continued 1-Octanol/n-hexane

Run no.	Air rate	Liquid rate	Evap rate	Tavg (T1-T4)	T5	T6	Pt	P1
	g/s	ml/s	ml/min	°C	°C	°C	kPa	kPa
11	0.954	1.85	12.89	35.2	28.0	14.2	101.3	3.60
12	0.954	2.24	13.78	35.3	28.1	14.2	101.3	3.60
13	0.955	2.78	14.25	35.0	28.4	14.2	101.3	3.60
14	0.954	3.27	14.89	35.1	28.6	14.3	101.3	3.60
15	0.954	3.76	15.75	35.4	28.8	14.4	101.3	3.60
16	1.049	1.85	14.22	35.3	27.4	14.4	101.3	4.00
17	1.049	2.24	15.11	35.5	27.8	14.6	101.3	4.00
18	1.049	2.52	15.75	35.3	27.9	14.6	101.3	4.00
19	1.048	2.78	16.25	35.7	27.9	14.7	101.3	4.00
20	1.049	3.27	16.75	35.4	28.0	14.7	101.3	4.00
21	1.146	1.85	14.44	35.0	26.8	14.7	101.3	4.40
22	1.144	2.24	15.50	35.4	27.3	14.7	101.3	4.40
23	1.144	2.52	16.50	35.6	27.4	14.7	101.3	4.40
24	1.142	2.78	17.75	36.0	27.3	14.6	101.3	4.40
n-decane(1)/cyclohexane(2) {mass fraction = 0.25 of component 2}								
1	0.740	1.60	3.64	44.8	37.4	16.6	101.3	2.67
2	0.740	2.11	3.69	45.0	38.5	17.0	101.3	2.67
3	0.740	2.63	3.77	45.1	39.0	16.2	101.3	2.67
4	0.740	3.08	3.92	45.1	39.9	17.4	101.3	2.67
5	0.739	3.59	4.08	45.4	40.6	18.1	101.3	2.67
6	0.832	1.60	4.00	45.2	37.9	18.6	101.3	3.07
7	0.832	2.11	4.15	45.2	38.7	18.2	101.3	3.07
8	0.832	2.63	4.36	45.1	39.4	18.3	101.3	3.07
9	0.831	3.08	4.55	45.4	40.1	18.7	101.3	3.07

Table A3-2 n-decane/cyclohexane

Run no.	Air rate	Liquid rate	Evap rate	Tavg (T1-T4)	T5	T6	Pt	P1
	g/s	ml/s	ml/min	°C	°C	°C	kPa	kPa
10	0.832	3.59	4.64	45.2	40.5	18.7	101.3	3.07
11	0.918	1.60	4.25	44.9	37.3	17.1	100.5	3.60
12	0.925	2.11	4.27	45.0	38.7	19.4	101.3	3.60
13	0.917	2.63	4.45	45.1	39.1	16.6	100.5	3.60
14	0.916	3.08	4.82	45.4	39.8	17.5	100.5	3.60
15	0.918	3.59	5.00	44.9	40.4	17.8	100.5	3.60
16	1.008	1.60	5.00	45.1	37.8	18.8	100.5	4.00
17	1.009	2.11	5.10	44.9	38.6	18.2	100.5	4.00
18	1.007	2.63	5.30	45.4	39.5	19.0	100.5	4.00
19	1.008	3.08	5.50	45.1	39.8	18.5	100.5	4.00
20	1.007	3.59	5.78	45.4	40.3	18.9	100.5	4.00
21	1.100	1.60	5.63	45.0	37.7	19.5	100.5	4.40
22	1.100	2.11	5.88	45.0	38.4	19.3	100.5	4.40
23	1.100	2.63	6.23	45.1	39.1	19.0	100.5	4.40
24	1.099	3.08	6.50	45.3	39.5	19.8	100.5	4.40
25	1.099	3.31	6.67	45.3	39.8	20.0	100.5	4.40
26	1.200	1.60	5.89	44.9	38.0	21.8	100.3	5.07
27	1.198	2.11	6.38	45.3	38.6	21.4	100.3	5.07
28	1.199	2.37	6.67	45.2	39.0	22.1	100.3	5.07
29	1.199	2.63	6.93	45.1	39.2	22.4	100.3	5.07
n-decane(1)/cyclohexane(2) {mass fraction = 0.50 of component 2}								
1	0.740	1.49	4.60	44.9	36.9	17.4	101.3	2.67
2	0.740	2.00	4.75	45.0	38.0	17.7	101.3	2.67
3	0.740	2.20	4.80	44.8	38.2	17.1	101.3	2.67

Table A3-2 Continued n-decane/cyclohexane

Run no.	Air rate	Liquid rate	Evap rate	Tavg (T1-T4)	T5	T6	Pt	P1
	g/s	ml/s	ml/min	°C	°C	°C	kPa	kPa
4	0.740	2.49	4.90	45.0	38.5	16.9	101.3	2.67
5	0.740	2.94	5.00	44.9	39.2	17.2	101.3	2.67
6	0.739	3.44	5.11	45.3	39.9	17.5	101.3	2.67
7	0.833	1.49	5.10	44.9	36.9	17.8	101.3	3.07
8	0.832	2.00	5.33	45.0	37.8	17.8	101.3	3.07
9	0.832	2.20	5.40	45.0	38.2	17.8	101.3	3.07
10	0.832	2.49	5.50	45.0	38.5	17.6	101.3	3.07
11	0.832	2.94	5.78	45.0	39.1	17.8	101.3	3.07
12	0.833	3.44	6.00	44.9	39.5	17.6	101.3	3.07
13	0.925	1.49	5.67	44.9	36.7	17.8	101.3	3.60
14	0.925	2.00	5.89	44.8	37.7	17.8	101.3	3.60
15	0.925	2.20	6.00	45.0	38.0	17.8	101.3	3.60
16	0.925	2.49	6.13	44.9	38.3	17.7	101.3	3.60
17	0.925	2.94	6.38	45.0	38.9	17.8	101.3	3.60
18	0.925	3.44	6.63	45.1	39.4	17.8	101.3	3.60
19	1.009	1.49	5.75	44.7	36.1	15.0	100.4	4.00
20	1.009	2.00	6.00	44.8	37.0	14.9	100.4	4.00
21	1.008	2.20	6.25	45.1	37.4	15.1	100.4	4.00
22	1.008	2.49	6.50	45.1	37.8	15.2	100.4	4.00
23	1.008	2.94	6.71	45.0	38.5	15.2	100.4	4.00
24	1.008	3.44	7.00	45.1	38.9	15.4	100.4	4.00
25	1.101	1.49	6.57	44.6	35.7	15.4	100.4	4.40
26	1.100	2.00	6.86	44.8	36.6	15.4	100.4	4.40
27	1.099	2.20	7.14	45.2	37.0	15.4	100.4	4.40

Table A3-2 Continued n-decane/cyclohexane

Run no.	Air rate	Liquid rate	Evap rate	Tavg (T1-T4)	T5	T6	Pt	P1
	g/s	ml/s	ml/min	°C	°C	°C	kPa	kPa
28	1.100	2.49	7.29	44.8	37.4	15.5	100.4	4.40
29	1.100	2.94	8.00	44.9	37.8	15.5	100.4	4.40
n-decane(1)/cyclohexane(2) {mass fraction = 0.75 of component 2}								
1	0.731	1.45	7.00	44.7	34.9	15.1	100.0	2.67
2	0.731	1.92	7.29	44.8	35.8	15.3	100.0	2.67
3	0.731	2.16	7.33	44.8	36.2	15.6	100.0	2.67
4	0.731	2.43	7.50	44.7	36.6	15.4	100.0	2.67
5	0.731	2.87	7.83	44.7	37.1	15.6	100.0	2.67
6	0.730	3.39	8.17	44.9	37.9	15.5	100.0	2.67
7	0.821	1.45	8.17	44.7	34.8	15.6	99.9	3.07
8	0.821	1.92	8.50	44.6	35.6	15.7	99.9	3.07
9	0.822	2.16	8.67	44.5	35.9	15.9	99.9	3.07
10	0.821	2.43	8.76	44.7	36.2	15.8	99.9	3.07
11	0.820	2.87	9.29	44.9	36.8	15.8	99.9	3.07
12	0.821	3.39	9.87	44.6	37.3	15.8	99.9	3.07
13	0.912	1.45	8.67	44.5	34.8	15.8	99.8	3.60
14	0.912	1.92	8.83	44.7	35.4	15.9	99.8	3.60
15	0.912	2.16	9.09	44.8	35.9	16.0	99.8	3.60
16	0.912	2.43	9.27	44.5	36.2	16.0	99.8	3.60
17	0.911	2.87	9.82	44.9	36.8	16.1	99.8	3.60
18	0.912	3.39	10.00	44.4	37.4	16.0	99.8	3.60
19	1.011	1.45	9.27	44.3	34.2	14.4	100.5	4.00
20	1.010	1.92	9.64	44.4	34.6	14.6	100.5	4.00
21	1.010	2.16	9.80	44.7	35.6	15.6	100.5	4.00

Table A3-2 Continued n-decane/cyclohexane

Run no.	Air rate	Liquid rate	Evap rate	Tavg (T1-T4)	T5	T6	Pt	P1
	G/s	ml/s	ml/min	°C	°C	°C	kPa	kPa
22	1.010	2.43	10.00	44.4	35.2	15.0	100.5	4.00
23	1.009	2.87	10.40	44.9	36.0	15.4	100.5	4.00
24	1.009	3.20	10.65	44.7	36.9	15.8	100.5	4.00
25	1.101	1.45	10.00	44.8	34.2	15.9	100.5	4.40
26	1.109	1.92	10.20	44.4	35.0	17.0	101.1	4.40
27	1.109	2.16	10.80	44.5	35.5	17.4	101.1	4.40
28	1.109	2.43	11.02	44.5	35.9	17.8	101.1	4.40
29	1.109	2.57	11.20	44.4	36.1	17.8	101.1	4.40

APPENDIX 4. Experimental results: Distillation data

Table A4-1 Experimental distillation data for Flexipac 350Y (High Capacity)

Run	Conc first comp [mass fr.]		Flowrate kg/hr	Temperatures [°C]					P_{top}	dP_{seg}	Q_{reb}	Q_{cond}
no	Distillate	Bottoms	Reflux	Reboiler	Sump	Sec 1	Sec 2	Sec 3	[mmHg]	[mmH_2O]	[kW]	[kW]
chlorobenzene/ethylbenzene (1atm)												
1	0.7789	0.4839	213.0	135.5	135.1	135.0	134.5	134.3	758	6	22.2	16.7
3	0.7874	0.4520	285.1	135.8	135.4	135.0	134.6	134.2	758	9	27.8	24.0
4	0.7799	0.4237	389.6	136.0	135.6	135.3	134.9	134.2	756	17	37.8	33.3
5	0.7742	0.4053	441.1	136.2	135.9	135.4	134.9	134.4	756	22	43.2	37.4
6	0.7674	0.3816	488.0	136.4	136.0	135.7	135.0	134.3	756	28	46.8	42.3
2	0.7812	0.3955	512.0	136.5	136.0	135.8	134.5	134.4	757	33	49.3	43.9
7	0.7931	0.3913	554.1	136.7	136.3	135.8	134.9	134.2	754	48	51.8	49.3
chlorobenzene/ethylbenzene (0.66atm)												
1	0.8075	0.4832	180.5	116.4	115.8	115.2	114.8	114.2	444	6	18.6	15.2
2	0.8238	0.4621	258.2	116.5	116.0	115.4	114.6	114.2	444	11	25.6	22.7
3	0.8196	0.4379	325.3	116.7	116.2	115.5	115.0	114.2	444	16	32.4	28.5
4	0.8179	0.4246	363.3	117.0	116.3	115.5	114.9	114.3	445	21	35.9	32.2
5	0.8122	0.4065	406.9	117.8	117.2	116.2	115.6	114.7	446	29	39.6	36.8
6	0.8033	0.3901	443.8	118.1	117.5	116.6	115.8	115.1	450	36	43.3	40.0
7	0.8011	0.3741	459.9	117.8	117.3	116.4	115.6	114.7	444	44	45.1	41.3
8	0.7964	0.3560	481.1	118.2	118.0	116.6	115.7	115.0	444	62	47.1	43.2
chlorobenzene/ethylbenzene (0.33atm)												
1	0.8507	0.4642	197.9	95.0	94.6	93.7	93.2	92.2	225	11	20.6	17.7
2	0.8539	0.4308	274.2	96.3	95.8	94.6	94.0	93.1	223	22	27.8	25.2
3	0.8460	0.4128	319.7	97.0	96.3	95.0	94.2	93.1	223	30	31.8	30.0
4	0.8365	0.3953	349.1	97.8	97.3	95.7	94.8	93.6	224	40	35.4	32.1
5	0.8397	0.3857	369.3	97.9	97.3	95.8	94.6	93.4	222	50	37.7	33.8
6	0.8371	0.3671	383.8	98.8	98.2	96.4	95.4	94.2	221	60	38.5	35.7

Table A4-2 Experimental distillation data for Flexipac 350Y (normal)

Run	Conc first comp [mass fr.]			Flowrate kg/hr	Temperatures [°C]					P_{top}	dP_{seg}	Q_{reb}	Q_{cond}
no	Distillate	Intermed.	Bottoms	Reflux	Reboiler	Sump	Sec 1	Sec 2	Sec 3	[mmHg]	[mmH_2O]	[kW]	[kW]
chlorobenzene/ethylbenzene (1atm)													
1	0.8053	N/A	0.4641	242.5	135.8	135.3	134.9	134.3	134.0	760	8	24.9	19.3
2	0.7969	N/A	0.4416	341.2	136.0	135.5	135.0	134.4	134.2	759	12	34.0	28.1
7	0.7845	0.5289	0.4201	349.9	135.9	135.4	135.0	134.5	134.0	755	13	34.1	29.7
3	0.7891	N/A	0.4209	407.8	136.2	135.7	135.3	134.6	134.2	759	18	40.0	34.4
4	0.7854	N/A	0.4051	450.9	136.5	135.8	135.4	134.6	134.2	759	24	44.1	38.1
5	0.7809	N/A	0.397	467.9	136.6	135.8	135.5	134.6	134.2	759	28	45.3	39.8
8	0.7796	0.5082	0.3885	484.9	136.6	135.8	135.4	134.8	134.2	755	32	46.3	42.2
6	0.7817	N/A	0.3732	523.4	136.8	136.0	135.6	134.6	134.2	758	50	50.6	44.9
chlorobenzene/ethylbenzene (0.66atm)													
1	0.8248	N/A	0.4536	248.2	116.9	116.3	115.7	115.2	114.5	452	10	25.1	21.4
2	0.8121	N/A	0.4137	364.2	118.0	117.4	116.6	115.6	115.0	458	20	35.8	32.5
3	0.8096	0.5352	0.3979	388.9	117.0	116.3	115.4	114.7	113.8	439	28	37.9	34.7
4	0.8061	0.5126	0.4874	402.7	116.9	116.4	115.2	114.5	113.8	434	40	40.1	35.6
5	0.8027	0.5101	0.3717	410.6	117.0	116.2	115.4	114.5	113.8	434	48	41.1	36.0
6	0.8076	0.508	0.3668	429.9	117.2	117.0	115.7	114.8	114.2	434	62	42.6	38.2
chlorobenzene/ethylbenzene (0.33atm)													
1	0.8485	0.5865	0.4467	186.6	94.8	94.4	93.1	92.6	91.9	220	10	19.9	16.2
2	0.8394	0.5598	0.4138	274.8	96.0	95.7	94.3	93.0	92.6	226	20	27.9	25.3
3	0.8409	0.5497	0.3995	291.7	96.3	95.7	94.2	93.3	92.6	219	29	30.3	26.2
4	0.835	0.5362	0.382	308.9	97.0	96.6	94.8	94.0	93.1	220	41	31.5	28.1
5	0.8303	0.5228	0.368	317.7	97.2	96.6	95.0	94.0	93.1	220	52	32.7	28.8
6	0.8321	0.5062	0.3576	343.5	98.2	97.6	96.0	94.8	93.6	222	61	34.8	31.7

Table A4-3 Calculated packed heights for Flexipac 350Y (High Capacity)

Run no.	Packed Height (m) as evaluated from different correlations				
	2.30	2.34	Erasmus	Bravo et al.	Delft
chlorobenzene/ethylbenzene (1atm)					
1	2.76	3.30	2.06	3.15	3.06
3	2.78	3.35	2.37	3.50	3.72
4	2.56	3.12	2.52	3.59	4.12
5	2.51	3.07	2.62	3.68	4.33
6	2.41	2.93	2.71	3.80	4.56
2	2.43	2.96	2.76	3.84	4.65
7	2.28	2.74	2.86	4.01	4.92
Chlorobenzene/ethylbenzene (0.66atm)					
1	3.12	3.52	2.21	3.41	3.13
2	3.05	3.50	2.54	3.73	3.83
3	2.84	3.25	2.67	3.83	4.18
4	2.79	3.20	2.76	3.89	4.37
5	2.66	3.05	2.82	3.95	4.54
6	2.64	3.05	2.87	3.97	4.64
7	2.61	2.99	2.96	4.08	4.80
8	2.35	2.66	2.99	4.18	4.96
Chlorobenzene/ethylbenzene (0.33atm)					
1	3.33	3.50	2.57	3.90	3.68
2	3.17	3.34	2.85	4.13	4.28
3	2.97	3.13	2.90	4.12	4.44
4	2.91	3.09	2.93	4.11	4.52
5	2.84	2.97	3.03	4.24	4.71
6	2.73	2.80	3.11	4.35	4.88

Table A4-4 Calculated packed heights for Flexipac 350Y (normal)

Run no.	Packed Height (m) as evaluated from different correlations				
	2.30	2.34	Erasmus	Bravo et al.	Delft
chlorobenzene/ethylbenzene (1atm)					
1	3.00	3.51	2.42	3.68	3.73
2	2.76	3.35	2.55	3.69	4.10
7	2.77	3.37	2.59	3.74	4.18
3	2.67	3.27	2.65	3.74	4.33
4	2.58	3.16	2.72	3.82	4.51
5	2.49	3.03	2.72	3.83	4.56
8	2.53	3.08	2.80	3.91	4.69
6	2.34	2.82	2.87	4.05	4.91
Chlorobenzene/ethylbenzene (0.66atm)					
1	3.10	3.44	2.57	3.83	3.90
2	2.87	3.24	2.78	3.92	4.40
3	2.88	3.25	2.87	4.01	4.57
5	2.69	2.94	2.96	4.16	4.79
6	2.56	2.87	2.99	4.25	4.94
Chlorobenzene/ethylbenzene (0.33atm)					
1	3.39	3.46	2.64	4.04	3.74
2	3.13	3.31	2.82	4.08	4.24
3	3.05	3.18	2.91	4.19	4.42
4	3.00	3.11	2.98	4.26	4.56
5	2.90	2.98	3.02	4.32	4.65
6	2.78	2.81	3.10	4.42	4.84

APPENDIX 5. Examples of Input and Output files for the distillation simulations

Pro II input file for run # 3 for Flexipac 350Y at atmospheric pressure.

```
TITLE
DIMENSION SI, STDTEMP=273.15, STDPRES=101.325
SEQUENCE SIMSCI
CALCULATION RVPBASIS=APIN, TVP=310.93
COMPONENT DATA
LIBID 1,EBENZENE/2,CLBZ
VP (L,C,KPA) CORRELATION=21,LN, DATA=1,250,0,13.9612,-3252.81, &
211.972
VP (L,C,KPA) CORRELATION=21,LN, DATA=2,359.25,-45.55,13.9096,-3203.5, &
213.024
THERMODYNAMIC DATA
METHOD SYSTEM=NRTL, SET=NRTL01, DEFAULT
STREAM DATA
PROPERTY STREAM=S1, PRESSURE=102.3, PHASE=L, RATE (WT)=100, &
COMPOSITION (WT)=1,0.5791/2,0.4209, NORMALIZE, SET=DEFAULT
PROPERTY STREAM=S3, PRESSURE=102.3, PHASE=L, RATE (WT)=100, &
COMPOSITION (M)=1,0.5791/2,0.4209
UNIT OPERATIONS
COLUMN UID=T1
PARAMETER TRAY=16,IO=200
FEED S1,15
PRODUCT  OVHD (WT)=S2,1E-5, BTMS(WT)=S3,100, SUPERSEDE=OFF
CONDENSER TYPE=BUBB, PRESSURE=100.99, TEST=407.35
DUTY 1,1/2,16
PSPEC PTOP=101.13, DPCOLUMN=0.8522
PRINT COMPOSITION=WT, PROPTABLE=PART, KVALUE, SUMMARY=WT, &
DIAGRAM
ESTIMATE MODEL=CONVENTIONAL, RRATIO=1000, CTEMP=407.35, &
TTEMP=407.35, BTEMP=409.35, RTEMP=409.35
TEMPERATURE 1,407.35/2,407.35/15,409.35/16,409.35
SPEC STREAM=S2, RATE (WT,KG/H),TOTAL,WET, VALUE=1E-5, RTOLER=0.1
```

SPEC REFLUX (WT,KG/H), VALUE=407.82
VARY DUTY=1,2
PLOT PROFILE
REBOILER TYPE=THERMOSIPHON, BAFFLE=NO, LFRA(M)=0.95
METHOD SET=NRTL01
END

Pro II output file for run # 3 for Flexipac 350Y at atmospheric pressure.

COLUMN SUMMARY

			-------- NET FLOW RATES ----------				HEATER
TRAY	TEMP	PRESSURE	LIQUID	VAPOR	FEED	PRODUCT	DUTIES
	DEG K	KPA		KG/HR			M*KJ/HR
1C	405.6	100.99	407.8			0.0L	-0.134
2	405.7	101.13	407.5	407.8			
3	405.8	101.2	407.1	407.5			
4	405.9	101.27	406.7	407.1			
5	406.1	101.34	406.2	406.7			
6	406.2	101.41	405.7	406.2			
7	406.3	101.49	405.2	405.7			
8	406.5	101.56	404.7	405.2			
9	406.6	101.63	404.1	404.7			
10	406.8	101.7	403.6	404.1			
11	406.9	101.77	403	403.6			
12	407.1	101.84	402.4	403			
13	407.2	101.91	401.8	402.4			
14	407.4	101.98	401.3	401.8			
15S	407.5	101.98	8011	0.1	100.0M	100.0L	
16R	407.6	101.98	7609.7	401.2			0.134

TRAY WEIGHT COMPOSITIONS

COMPONENT	TRAY 1 X	TRAY 1 Y	TRAY 2 X	TRAY 2 Y
1 EBENZENE	0.21013	0.19261	0.22898	0.21013
2 CLBZ	0.78987	0.80739	0.77102	0.78987
RATE, KG/HR	407.827	0.000	407.503	407.827

COMPONENT	TRAY 3 X	TRAY 3 Y	TRAY 4 X	TRAY 4 Y
1 EBENZENE	0.24921	0.22898	0.27084	0.24921
2 CLBZ	0.75079	0.77102	0.72916	0.75079
RATE, KG/HR	407.100	407.503	406.671	407.100

COMPONENT	TRAY 5 X	TRAY 5 Y	TRAY 6 X	TRAY 6 Y
1 EBENZENE	0.29386	0.27084	0.31825	0.29386
2 CLBZ	0.70614	0.72916	0.68175	0.70614
RATE, KG/HR	406.214	406.671	405.731	406.214

COMPONENT	TRAY 7 X	TRAY 7 Y	TRAY 8 X	TRAY 8 Y
1 EBENZENE	0.34396	0.31825	0.37091	0.34396
2 CLBZ	0.65604	0.68175	0.62909	0.65604
RATE, KG/HR	405.225	405.731	404.696	405.225

COMPONENT	TRAY 9 X	TRAY 9 Y	TRAY 10 X	TRAY 10 Y
1 EBENZENE	0.39897	0.37091	0.42802	0.39897
2 CLBZ	0.60103	0.62909	0.57198	0.60103
RATE, KG/HR	404.148	404.696	403.584	404.148

COMPONENT	TRAY 11 X	TRAY 11 Y	TRAY 12 X	TRAY 12 Y
1 EBENZENE	0.45785	0.42802	0.48827	0.45785
2 CLBZ	0.54215	0.57198	0.51173	0.54215
RATE, KG/HR	403.009	403.584	402.426	403.009

COMPONENT	TRAY 13 X	TRAY 13 Y	TRAY 14 X	TRAY 14 Y
1 EBENZENE	0.51904	0.48827	0.54992	0.51904
2 CLBZ	0.48096	0.51173	0.45008	0.48096
RATE, KG/HR	401.841	402.426	401.299	401.841

COMPONENT	TRAY 15 X	TRAY 15 Y	TRAY 16 X	TRAY 16 Y
1 EBENZENE	0.57910	0.54836	0.58064	0.54992
2 CLBZ	0.42090	0.45164	0.41936	0.45008
RATE, KG/HR	8010.954	7.021E-02	7609.726	401.229

STREAM ID	F	D	B
NAME			
PHASE	LIQUID	LIQUID	LIQUID
FLUID WEIGHT FRACTIONS			
1 EBENZENE	0.5791	0.2101	0.5791
2 CLBZ	0.4209	0.7899	0.4209
TOTAL RATE, KG/HR	100	1.00E-05	100
TEMPERATURE, K	407.6612	405.5836	407.5456
PRESSURE, KPA	102.3	100.9917	101.9822
ENTHALPY, M*KJ/HR	0.0227	2.02E-09	0.0227
MOLECULAR WEIGHT	108.768	111.1532	108.768
WEIGHT FRAC VAPOR	0.0000	0.0000	0.0000
WEIGHT FRAC LIQUID	1.0000	1.0000	1.0000

APPENDIX 6. Dimensional Analysis

Dimensional analysis is used in the modelling of the gas phase mass transfer coefficient because it allows for the reduction of the independent variables. The reduction of the number of independent variables is achieved through the formation of dimensionless groups. The dimensionless groups are formed from the variables deemed to have an influence on the dependent variable (mass transfer coefficient). The variables thought to influence the mass transfer coefficient include physical and geometric properties. In the examples below it is illustrated how the different dimensionless groups can be derived from the properties. It should be noted that dimensional analysis does not give any information about the form of the functions derived from the analysis.

Example 1:

The properties thought to have an influence the target variable are listed below:

$$k_g = f(D_{AB}, \rho_g, \mu_g, u_g, d_{eq}, \rho_l, \mu_l, u_l, \delta, \sigma, g)$$

The list of properties is based on the present understanding of the mass transfer process. The dimensionless parameters can then be derived from the complete set of the properties including the target variable:

$$f(k_g, D_{AB}, \rho_g, \mu_g, u_g, d_{eq}, \rho_l, \mu_l, u_l, \delta, \sigma, g) = 0$$

In the development of the dimensionless groups a similar approach to that illustrated by Coulson and Richardson {1997} will be used in this case. The dimensionless groups are obtained by applying the Buckingham Pi theorem. The initial stage involves selecting a set of repeating variables. These are selected from the entire set of properties, with the condition that no

dimensionless group can be formed from this set. A set of repeating variables that satisfy the given condition are:

$$u_g = LT^{-1} \qquad d_{eq} = L \qquad \rho_g = ML^{-3}$$

Furthermore, the fundamental dimensions have to be explicitly obtained from the set of repeating variables. The fundamental dimensions in this case are taken as mass (M), length (L) and time (T). The fundamental dimensions can be determined as follows:

$$L = d_{eq} \qquad M = \rho_g d_{eq}^{3} \qquad T = d_{eq} u_g^{-1}$$

The dimensionless groups are obtained by making each of the remaining variables dimensionless with the variables from the recurring set. The number of dimensionless groups that can be obtained is equal to the number of properties minus the number of fundamental dimensions.

The dimensionless groups are formed as follows:

The fundamental units of k_g are LT^{-1}; therefore to make a dimensionless group, Π_1, it follows that:

$$\Pi_1 = k_g L^{-1}T = k_g (d_{eq})^{-1} (d_{eq} u_g^{-1}) = k_g u_g^{-1}$$

The above method of determining the dimensionless groups applies to all the remaining variables. The dimensionless groups are obtained as follows:

$$\Pi_2 = D_{AB} L^{-2} T = D_{AB} (d_{eq})^{-2} (d_{eq} u_g^{-1}) = D_{AB} d_{eq}^{-1} u_g^{-1}$$

$$\Pi_3 = \mu_g M^{-1} L T = \mu_g (\rho_g d_{eq}^{3})^{-1} (d_{eq}) (d_{eq} u_g^{-1}) = \mu_g d_{eq}^{-1} \rho_g^{-1} u_g^{-1}$$

$$\Pi_4 = \rho_l M^{-1} L^{3} = \rho_l (\rho_g d_{eq}^{3})^{-1} (d_{eq})^{3} = \rho_l \rho_g^{-1}$$

$$\Pi_5 = \mu_l M^{-1} L T = \mu_l (\rho_g d_{eq}^{3})^{-1} (d_{eq}) (d_{eq} u_g^{-1}) = \mu_l d_{eq}^{-1} \rho_g^{-1} u_g^{-1}$$

$$\Pi_6 = u_l L^{-1} T = u_l (d_{eq})^{-1} (d_{eq} u_g^{-1}) = u_l u_g^{-1}$$

$$\Pi_7 = \delta L^{-1} = \delta (d_{eq})^{-1} = \delta d_{eq}^{-1}$$

$$\Pi_8 = \sigma M^{-1} T^2 = \sigma (\rho_g d_{eq}^3)^{-1} (d_{eq} u_g^{-1})^2 = \sigma \rho_g^{-1} d_{eq}^{-1} u_g^{-2}$$

$$\Pi_9 = g L^{-1} T^2 = g (d_{eq})^{-1} (d_{eq} u_g^{-1})^2 = g d_{eq} u_g^{-2}$$

Some of the dimensionless groups obtained are not in the form normally encountered in literature. It would be appropriate to rearrange such groups and represent them in more suitable forms. This can be achieved by the recombining some of the dimensionless groups with the other groups.

$$Sh_g = \Pi_1 \Pi_2^{-1} = k_g u_g^{-1} (D_{AB} d_{eq}^{-1} u_g^{-1})^{-1} = \frac{k_g d_{eq}}{D_{AB}}$$

$$Sc_g = \Pi_2^{-1} \Pi_3 = (D_{AB} d_{eq}^{-1} u_g^{-1})^{-1} (\mu_g d_{eq}^{-1} \rho_g^{-1} u_g^{-1}) = \frac{\mu_g}{\rho_g D_{AB}}$$

$$Re_g = \Pi_3^{-1} = (\mu_g d_{eq}^{-1} \rho_g^{-1} u_g^{-1})^{-1} = \frac{\rho_g d_{eq} u_g}{\mu_g}$$

$$Re_l = \Pi_5^{-1} \Pi_4 \Pi_6 \Pi_7 = (\mu_l d_{eq}^{-1} \rho_g^{-1} u_g^{-1})^{-1} (\rho_l \rho_g^{-1}) (u_l u_g^{-1}) (\delta d_{eq}^{-1}) = \frac{\rho_l \delta u_l}{\mu_l}$$

$$We_l = \Pi_8^{-1} \Pi_4 \Pi_6^2 \Pi_7 = (\sigma \rho_g^{-1} d_{eq}^{-1} u_g^{-2})^{-1} (\rho_l \rho_g^{-1}) (u_l u_g^{-1})^2 (\delta d_{eq}^{-1}) = \frac{\rho_l u_l^2 \delta}{\sigma}$$

$$Fr_l = \Pi_8^{-1} \Pi_6^2 \Pi_7^{-1} = (g d_{eq} u_g^{-2})^{-1} (\delta d_{eq}^{-1})^{-1} (u_l u_g^{-1})^2 = \frac{u_l^2}{g\delta}$$

It then follows that:

$$f\left(\frac{k_g d_{eq}}{D_{AB}}, \frac{\mu_g}{\rho_g D_{AB}}, \frac{\rho_g d_{eq} u_g}{\mu_g}, \frac{\rho_l \delta u_l}{\mu_l}, \frac{\rho_l u_l^2 \delta}{\sigma}, \frac{u_l^2}{g\delta}, \frac{\rho_l}{\rho_g}, \frac{u_l}{u_g}, \frac{\delta}{d_{eq}}\right) = 0$$

If the last three terms in the dimensionless groups can be assumed to have a negligible effect on the mass transfer coefficient. The remaining relevant groups are related by the general functional equation given as follows:

$$0 = f\left(Sh_g, Sc_g, Re_g, Re_l, We_l, Fr_l\right)$$

These terms can then be used to correlate the mass transfer data with the functional form of the target group (Sherwood number). The mass transfer coefficient would be described as:

$$Sh_g = f\left(Sc_g, Re_g, Re_l, We_l, Fr_l\right)$$

In correlating the mass transfer rate different correlations were used. The dimensionless terms in a correlation are determined by the influencing properties and the selected repeating variables. A further example is given of how a different combination of dimensionless terms can be obtained. The same methodology of deriving the dimensionless groups as in example 1 is used.

Example 2:

The properties thought to have an influence on the target variable are given as:

$$k_g = f\left(D_{AB}, \rho_g, \mu_g, u_g, d_{eq}, \rho_l, \mu_l, u_l, \delta, \sigma, g\right)$$

A set of repeating variables can be selected from the list of properties. This set of repeating variables is different from that in example 1.

$g = LT^{-2}$ $\sigma = M T^{-2}$ $\mu_l = M L^{-1}T^{-1}$

The fundamental dimensions have to be obtained explicitly from the repeating set of variables:

$L = \sigma^2 \mu_l^{-2} g^{-1}$ $M = \sigma^3 \mu_l^{-2} g^{-2}$ $T = \sigma \mu_l^{-1} g^{-1}$

The dimensionless groups are obtained as follows:

$\Pi_1 = k_g L^{-1}T = k_g (\sigma^2 \mu_l^{-2} g^{-1})^{-1} (\sigma \mu_l^{-1} g^{-1}) = k_g \mu_l \sigma^{-1}$

$\Pi_2 = D_{AB} L^{-2} T = D_{AB} (\sigma^2 \mu_l^{-2} g^{-1})^{-2} (\sigma \mu_l^{-1} g^{-1}) = D_{AB} \mu_l^3 \sigma^{-3} g$

$\Pi_3 = \rho_g M^{-1} L^3 = \rho_g (\sigma^3 \mu_l^{-2} g^{-2})^{-1} (\sigma^2 \mu_l^{-2} g^{-1})^3 = \rho_g \mu_l^{-4} \sigma^3 g^{-1}$

$\Pi_4 = \mu_g M^{-1} L T = \mu_g (\sigma^3 \mu_l^{-2} g^{-2})^{-1} (\sigma^2 \mu_l^{-2} g^{-1}) (\sigma \mu_l^{-1} g^{-1})$

$= \mu_g \mu_l^{-1}$

$\Pi_5 = u_g L^{-1} T = u_g (\sigma^2 \mu_l^{-2} g^{-1})^{-1} (\sigma \mu_l^{-1} g^{-1}) = u_g \sigma^{-1} \mu_l$

$\Pi_6 = d_{eq} L^{-1} = d_{eq} (\sigma^2 \mu_l^{-2} g^{-1})^{-1} = d_{eq} \sigma^{-2} \mu_l^2 g$

$\Pi_7 = \rho_l M^{-1} L^3 = \rho_l (\sigma^3 \mu_l^{-2} g^{-2})^{-1} (\sigma^2 \mu_l^{-2} g^{-1})^3 = \rho_l \sigma^3 g^{-1} \mu_l^{-4}$

$\Pi_8 = u_l L^{-1} T = u_l (\sigma^2 \mu_l^{-2} g^{-1})^{-1} (\sigma \mu_l^{-1} g^{-1}) = u_l \sigma^{-1} \mu_l$

$\Pi_9 = \delta L^{-1} = \delta (\sigma^2 \mu_l^{-2} g^{-1})^{-1} = \delta \sigma^{-2} \mu_l^2 g$

Recombining some of the dimensionless into suitable forms:

$Sh_g = \Pi_1 \Pi_2^{-1} \Pi_6 = k_g \mu_l \sigma^{-1} (D_{AB} \mu_l^3 \sigma^{-3} g)^{-1} (d_{eq} \sigma^{-2} \mu_l^2 g) = \dfrac{k_g d_{eq}}{D_{AB}}$

$Sc_g = \Pi_2^{-1} \Pi_3^{-1} \Pi_4 = (D_{AB} \mu_l^3 \sigma^{-3} g)^{-1} (\rho_g \mu_l^{-4} \sigma^3 g^{-1})^{-1} (\mu_g \mu_l^{-1}) = \dfrac{\mu_g}{\rho_g D_{AB}}$

$Re_g = \Pi_3 \Pi_6 \Pi_5 \Pi_4^{-1} = (\rho_g \mu_l^{-4} \sigma^3 g^{-1}) (d_{eq} \sigma^{-2} \mu_l^2 g) (u_g \sigma^{-1} \mu_l) (\mu_g \mu_l^{-1})^{-1}$

$= \dfrac{\rho_g d_{eq} u_g}{\mu_g}$

$\Pi_5^* = \Pi_5 \Pi_8^{-1} = (u_g \sigma^{-1} \mu_l) (u_l \sigma^{-1} \mu_l)^{-1} = \dfrac{u_g}{u_l}$

$\Pi_6^* = \Pi_6 \Pi_9^{-1} = (d_{eq} \sigma^{-2} \mu_l^2 g) (\delta \sigma^{-2} \mu_l^2 g)^{-1} = \dfrac{d_{eq}}{\delta}$

$Re_l = \Pi_7 \Pi_9 \Pi_8 = (\rho_l \sigma^3 g^{-1} \mu_l^{-4}) (\delta \sigma^{-2} \mu_l^2 g) (u_l \sigma^{-1} \mu_l) = \dfrac{\rho_l \delta u_l}{\mu_l}$

$Ca_l = \Pi_8^{-1} = (u_l \sigma^{-1} \mu_l)^{-1} = \dfrac{\sigma}{\mu_l u_l}$

$$Fr_l = \Pi_9^{-1}\Pi_8^2 = (\delta\,\sigma^{-2}\,\mu_l^2\,g)^{-1}\,(u_l\,\sigma^{-1}\,\mu_l)^2 = \frac{u_l^2}{g\delta}$$

It then follows that:

$$f\left(\frac{k_g d_{eq}}{D_{AB}}, \frac{\mu_g}{\rho_g D_{AB}}, \frac{\rho_g d_{eq} u_g}{\mu_g}, \frac{\rho_l \delta u_l}{\mu_l}, \frac{\sigma}{u_l \mu_l}, \frac{u_l}{g\delta}, \frac{d_{eq}}{\delta}, \frac{u_g}{u_l}, \frac{\mu_g}{\mu_l}\right) = 0$$

If the last three terms in the general functional form can be assumed to have negligible influence on the mass transfer coefficient, then this functional equation can be written as:

$$0 = f\left(Sh_g, Sc_g, Re_g, Re_l, Ca_l, Fr_l\right)$$

Therefore the mass transfer coefficient can be correlated using the following dimensionless terms:

$$Sh_g = f\left(Sc_g, Re_g, Re_l, Ca_l, Fr_l\right)$$